INFORMATION TO USERS

This reproduction was made from a copy of a document sent to us for microfilming. While the most advanced technology has been used to photograph and reproduce this document, the quality of the reproduction is heavily dependent upon the quality of the material submitted.

The following explanation of techniques is provided to help clarify markings or notations which may appear on this reproduction.

1. The sign or "target" for pages apparently lacking from the document photographed is "Missing Page(s)". If it was possible to obtain the missing page(s) or section, they are spliced into the film along with adjacent pages. This may have necessitated cutting through an image and duplicating adjacent pages to assure complete continuity.

2. When an image on the film is obliterated with a round black mark, it is an indication of either blurred copy because of movement during exposure, duplicate copy, or copyrighted materials that should not have been filmed. For blurred pages, a good image of the page can be found in the adjacent frame. If copyrighted materials were deleted, a target note will appear listing the pages in the adjacent frame.

3. When a map, drawing or chart, etc., is part of the material being photographed, a definite method of "sectioning" the material has been followed. It is customary to begin filming at the upper left hand corner of a large sheet and to continue from left to right in equal sections with small overlaps. If necessary, sectioning is continued again—beginning below the first row and continuing on until complete.

4. For illustrations that cannot be satisfactorily reproduced by xerographic means, photographic prints can be purchased at additional cost and inserted into your xerographic copy. These prints are available upon request from the Dissertations Customer Services Department.

5. Some pages in any document may have indistinct print. In all cases the best available copy has been filmed.

University Microfilms International
300 N. Zeeb Road
Ann Arbor, MI 48106

Gal, Eli

DUST FILTRATION IN GRANULAR BEDS

City University of New York

PH.D. 1984

PLEASE NOTE:

In all cases this material has been filmed in the best possible way from the available copy. Problems encountered with this document have been identified here with a check mark __✓__.

1. Glossy photographs or pages _____
2. Colored illustrations, paper or print _____
3. Photographs with dark background _____
4. Illustrations are poor copy _____
5. Pages with black marks, not original copy _____
6. Print shows through as there is text on both sides of page _____
7. Indistinct, broken or small print on several pages _____
8. Print exceeds margin requirements _____
9. Tightly bound copy with print lost in spine _____
10. Computer printout pages with indistinct print _____
11. Page(s) _____ lacking when material received, and not available from school or author.
12. Page(s) _____ seem to be missing in numbering only as text follows.
13. Two pages numbered _____. Text follows.
14. Curling and wrinkled pages ✓
15. Other _____

University
Microfilms
International

DUST FILTRATION IN GRANULAR BEDS

BY

ELI GAL

A dissertation submitted to the Graduate Faculty in Chemical Engineering in partial fulfillment of the requirements for the degree of Doctor of Philosophy, The City University of New York.

This manuscript has been read and accepted for the Graduate Faculty in Engineering in satisfaction of the dissertation requirement for the Doctor of Philosophy.

May 30, 1984
Date

Professor G. Tardos
G. Tardos
Chairman of Examining Committee

May 31, 1984
Date

Professor P. Karmel
Executive Officer

Dr. R.W.L. Snaddon

Professor R. Pfeffer

Professor R. Graff

Professor R. Shinnar
Supervisory Committee

The City Universirty of New York

ABSTRACT

During the present work an experimental and theoretical study on granular bed filtration was conducted with a thorough examination of the contribution of each of the filtration mechanisms in the filtration of micron and submicron solid dust and liquid aerosol particles. It was found that the major mechanisms involved were inertial impaction and electrostatic deposition and the emphasis was placed on measuring and analysing their effect. Furthermore, to utilize the potential of granular bed filters, a new type of granular bed filter the rotating fluidized bed filter (RFBF) was developed.

A filtration model predicting single sphere and total bed efficiencies based on trajectory calculation of dust particles in the voids of granular bed was developed for the domain where inertia effects are dominant. The model uses the flow field in a bed of spheres arranged in a body centered cubic array for which the filtration efficiency was found to be a function of a modified Stokes number defined by St'=StxF. The function F depends only on the Reynolds number Re and it is the ratio of two dimensionless velocities. The value of the function F can be found experimentally or predicted from the Ergun correlation to be F = 1 + Ø.Ø157Re. The filtration efficiency calculated using the model, agrees well with experimental results obtained in

beds of dense cubic packing of spheres especially at relatively low Reynolds numbers Re<200 and relatively high modified Stokes numbers St'>0.01. The prediction of the theoretical model also agrees well with experimental data for randomly packed beds at low porosities and low Reynolds numbers.

Industrial filtration of fine dust and aerosol particles is difficult and expensive and there is a need for high efficiency inexpensive and easy to operate filter devices; The rotating fluidized bed filter has the potential to be such an industrial device. It was demonstrated during the present research that the device operates continuously at high gas throughputs and using dielectric bed materials it experiences strong electrostatic and inertia effects. Also high collection efficiencies, 99.9% for particles larger than 1.0 micron and 90% for particles 0.3-0.5μm in diameter, were obtained during extensive research and it was shown that the high efficiency is mainly due to the inertia of the particles and to the electrostatic charge generated on the granules. Since high collection efficiencies were obtained using relatively shallow beds, the total pressure drop was found to be low even though the gas velocity through the bed was high. A new pilot size RFBF was designed: the new sysytem is expected to be easy to control and to have efficiency of 99.9% for all particles larger than 0.3μm.

This research was carried out under the supervision of Professor G. Tardos and Professor R. Pfeffer of the Chemical Engineering Department at the City College of the City University of New York.

ACKNOWLEDGMENT

I wish to thank Professor Robert Pfeffer and Professor Gabriel Tardos for suggesting the subject and for their helpful advice, supervision and encouragement during all stages of this work.

Thanks are also due to Mr. Dov Firnberg for his help in constructing the experimental device and for running some experiments and to Ms. Veneta Nikitiades for her help in typing the manuscript.

CONTENTS

List of Figures

List of tables

NOTATION

a - filter element radius

$A_{\emptyset}$ - cross section area of a unit cell

A_c - area in the base of a unit cell from which particles are collected

A_p - open area in the base of a unit cell from which air flow into the cell

a_r - centrifugal acceleration

b - distance of limit trajectory from X_1 axis

c - volumetric concentration of aerosol in air

c_o - initial dust concentration

C - Cunningham correction factor

C_{ji}, C_{pi} - constants in equations (3.6,3.7)

d_c - dimensionless constriction diameter of constricted tube

d_g - filter element diameter

d_p - dust particle diameter

e - radius of unit cell defined in Eq. (3.2)

E - single sphere efficiency in Eq. (2.3)

E' - single sphere efficiency in Eq. (2.4)

E^* - single sphere efficiency defined in Eq. (3.21)

E_R, E_D, E_G, E_k - single sphere efficiency due to interception, diffusion, gravity settling and electrostatic effects respectively

E_{RDG} - single sphere efficiency due to the combined effect of interception, diffusion end gravity

f - collision factor

F - dimensionless parameter defined in Eq. (3.13)

$\vec{F}_{ext}$ - external force acting on particle

Ga - Galileo number

g - accelaration of gravity

$g(\varepsilon)$ - function of porosity in equation (2.5)

k - Boltzman constant

k_1, k_2, k_3 - constants in Eqs. (4.14 and 4.15)

K_1 - constant in eq. (2.3)

Kc - electric force constant, dimesionless

L - bed thickness

m_p - mass of dust particle

n_{out} - concentration of dust particles in filter outlet

n_{in} - concentration of dust particles in filter inlet

P - dimensionless pressure

p - pressure drop across a unit cell in granular bed

P - pressure drop across a granular bed

Pe - Peclet number

$\tilde{q}_c$ - net average charge on collector defined in Eq. (4.8)

$\hat{q}_c$ - absolute average charge on collector defined in Eq. (4.9)

$\hat{Q}_c$ - absolute average charge on collector per unit surface area

$\tilde{q}_p$ - average charge on particle defined in Eq. (4.10)

$\tilde{Q}_p$ - average charge on particle per unit surface area defined in Eq. (4.11)

r - distance from sphere's center

$R=r/a$ - dimensionless distance from sphere's center

Re - Reynolds number

r_i, r_o - inner and outer radii of rotating fluidized bed

r_p - aerosol (dust particle) radius

$R_p=r_p/a$ - interception parameter

St - Stokes number

St' - modified Stokes number defined in Eq. (3.17)

Steff - Effective Stokes number defined in Eq. (3.13)

t - time

$T=tUF/a$ - dimensionless time

$\vec{u}$ - air velocity inside a granular bed

u_p - dust particle velocity

U - superficial gas velocity in the z direction

U_o - superficial gas velocity

$\vec{U}=\vec{u}/UF$ - dimensioless air velocity

U_r - radial velocity

U_{po} - initial dust particle velocity outside the bed

U_t - tangential velocity

$v_j (j=1,2,3)$ - dimensionless air velocity defined in Eq. (3.6)

V - dimensionless superficial velocity defined in Eq. (3.15)

$V_o=Ø.ØØØ258$ - dimensionless average velocity in the z direction for Re=Ø. Experimental value from Martin et al.,(1951)

$V^*(Z)$ - dimensionless superficial velocity in the Z

direction defined in Eq. (3.11)

W - rotating speed of the rotating fluidized bed filter

$\vec{x}$ - position vector

$x,y,z,$ - coordinates

$x_j (j=1,2,3)$ - dimensionless coordinates

$\vec{X}=\vec{x}/a$ - dimensionless position vector

$X=x/a, Y=y/a, Z=z/a$ - dimensionless coordinates

Greek letters

β - flow intensification factor

$\mathcal{D}$ - diffusion coeficient defined in Eq. (2.7)

ε - void fraction of a granular bed

η - total filtration efficiency of a granular bed

μ - gas viscosity

ρ_f - gas density

ρ_p - particle density

ϕ_{pi}, ϕ_{ji} - trigonometric functions that satisfies the periodicity and symmetry conditions of flow in eq.s (3.6) and (3.7)

$\mathcal{X}$ - a function that satisfies the no-slip condition of flow in Eq (3.6)

τ - volume of a unit cell

Subscript

g - granule

p - dust particled

1. INTRODUCTION

Filtration of dusty gases in hot and/or corrosive environments is a difficult technical problem for which classical cleaning devices such as electrostatic precipitators and venturi scrubbers are not well suited. Also difficult is the filtration of small dust and aerosol particles in the micron and submicron range. Small dust particles tend to follow the streamlines of the gas, and like the gas they penetrate through the entire dust collector. Most industrial dust collectors show a sharp drop in collection efficiency as the size of dust particles decreases (Stairmand, 1965). Others, such as bag filters, are very expensive, do not stand well high temperatures and corrosive conditions and cause many problems in industrial operation.

The submicron mode usually represents about Ø.2-2.2% of the total mass of dust particles entering particulate control devices in coal operated power plants (McElroy et al, 1981) but their mass percentage increases significantly in the flue gases at the exit. Because of their small size the fine particles are very slow to settle, thus they remain in the atmosphere for long periods of time. In the absence of wind, fine particles may accumulate in the atmosphere and become an environmental problem. The fine particles are considered hazardous to health because they can penetrate

deeply into the lungs (Amdur and Corn, 1963; Mahar and Zimmerman, 1975). Since the early 1970's federal regulations have increased mass removal requirements from about 90% to 99.7%. EPA is tightening its standards for particulate emission and there is a need for small, simple, inexpensive filter devices with high filtration efficiencies for all ranges of dust particle sizes especially in hot and corrosive environments.

In recent years there is a growing interest in the development of industrial granular bed filters. Granular bed filters have the potential of having high dust collection efficiency, low pressure drop, continuous operation and application to high temperature and high pressure processes.

Understanding the fundamental behavour of filtration in a granular bed is a precondition for the development of reliable and efficient granular bed filters. Capture of the gas-borne particles by a granular collector occurs mainly by the processes of Brownian diffusion, interception, gravity settling, inertial impaction and electrophoretic migration. In a recent review of fundamental processes in gas filtration Clift (1984) notes that, in spite of the extensive theoretical research that has been done, the basic understanding of granular bed filtration is still in an early stage especially as far as the inertial impaction and electrostatic effects are concerned.

In the present work both theoretical and experimental research is done to further the understanding of granular bed filtration mechanisms. A filtration model is developed for predicting filtration efficiency due to inertial impaction. The model predicts filtration efficiencies in a periodic array of spheres at low porosity and low Reynolds numbers fairly well. The model is also suitable for randomly packed bed filters and even for fluidized beds when low porosity and low Reynolds numbers are maintained.

Furthermore, a new type of granular bed filter has been designed and tested. The rotating fluidized bed filter (RFBF) seems to overcome many of the problems of other granular bed filters. It can operate continuously at high gas flow rates per unit area of distributor, thus making the device relatively small with high capacity. The high velocity increases inertial impaction effects which are important in increasing filtration efficiency. Also, triboelectrification effects are strong in the rotating fluidized bed filter which increases the filtration efficiency especially when charged dust particles are being filtered. The results of the experimental research are used for a scale-up design of an improved version of the exisiting apparatus.

2. BACKGROUND AND LITERATURE REVIEW

2.1 Introduction

In granular beds, high filtration efficiency can be achieved for aerosol particles in the micron and submicron size range. Granular bed filters are especially important in the cleaning of high temperature and corrosive gases, where other filters cannot be used. The parameters affecting filtration efficiency in granular beds are well known, yet the prediction of filtration efficiency is very difficult. There is presently no available theoretical model that can accurately predict the filtration efficiency of granular beds from the basic principles of fluid mechanics and mass transfer.

In the granular bed filtration process, the dusty gas flows through a bed of granules on which dust particles are captured. The total filtration efficiency of a granular bed is defined as

$$\eta = 1 - n_{out}/n_{in} \qquad (2.1)$$

where n_{out} represents the number concentration of dust particles that penetrate through the entire bed and are found in the filter outlet, and n_{in} is the number concentration of particles carried into the bed by the

incoming stream. The total bed efficiency η, can be predicted if the trajectories of all dust particles traveling inside the bed are known, and it can be assumed that dust particles do not bounce from the granules' surface once they are deposited. If bouncing occurs a correction must be made for the re-entrained particles. Thus the problem of predicting filtration efficiencies is basically the problem of predicting the trajectories of dust particles in the bed; a dust particle whose center approaches the surface of a granule to within a distance equal to its radius is said to be collected.

The motion of a dust particle in a granular bed depends on its shape and size, its initial velocity, the flow field in which it travels, the external forces acting on it, and the obstacles in its path. When these parameters are known, the trajectories of the particles traveling inside the bed can, in principal, be computed.

The trajectory equation was presented and used previously by many authors (Paretsky et al,1971; Spielman and FitzPatrick, 1973; Payatakes et al, 1974; George and Poelhein, 1974; Pilat and Perm, 1976; Nielsen and Hill, 1976; Rajagopalan and Tien, 1976; Gutfinger and Tardos, 1979; Fan and Gentry, 1979; Snaddon and Dietz, 1980; Pfeffer et al, 1981; Degani and Tardos, 1981; Pendse and Tien, 1982). For filtration of aerosol particles from gases

the equation takes the form

$$\frac{d^2\vec{x}}{dt^2} \quad \frac{6\pi\mu r_p}{m_p C}\left(\vec{u} - \frac{d\vec{x}}{dt}\right) + \frac{\vec{F}ext}{m_p} \qquad (2.2)$$

where $\vec{x}$ is the position vector, $\vec{u}$ is the gas velocity, r_p and m_p are the particle's radius and mass, C is the Cunningham correction factor and $d^2\vec{x}/dt^2$ and dx/dt are the particle's acceleration and velocity, respectively. $\vec{F}_{ext}$ is a vector summing all external forces acting on a particle traveling inside the bed such as gravitational, and electrical forces.

The vectorial equation 2.2 results in a set of three equations. In a cartesian coordinate system the solution gives the x,y,z, location of a particle as a function of time as it flows through the granular bed. There is not yet available a solution to equation 2.2 that includes all the parameters involved in the filtration phenomena. The common approach is to isolate the various mechanisms and to obtain a separate solution for each individual mechanism, i.e., a solution for inertial impaction controlled filtration, a solution for diffusion controlled filtration, a solution for electrostatic forces controlled filtration, etc. If more than one mechanism of particle capture becomes important, it is common to assume that the efficiency of the different mechanisms are additive. This is clearly an oversimplification, which is valid if the individual efficiencies are all small or if one mechanism clearly

dominates the others (Dorman 1960).

The trajectory of a particle through an entire granular bed is still very difficult to compute by equation 2.2 even when only one mechanism is considered at a time. To simplify the problem further it is assumed that every filter element experiences similar filtration phenomena, and therefore a single particle efficiency, E, can be defined so that the filtration efficiency of the entire bed of granules can be computed by summing the effect of all the elements in the filter. Thus, the theoretical computation of the overall filter efficiency usually first requires predicting the single particle efficiency, E.

Other assumptions are that the dust particle concentration in the gas stream is low enough not to influence the gas flow field around the filter elements, and that the filtration process is time independent so that each filter element, as well as the entire filter bed, always has the same efficiency. The assumptions above are valid for low aerosol concentrations in the gas and for operating conditions associated with a clean filter medium. The assumption that a particle which approaches a granule to within a distance comparable to its radius will collide and stick to it is valid for liquid aerosols which in most cases adhere to granules surface but it is questionable for solid particles.

2.2 Total bed and single sphere efficiency

Assuming that all filter elements in a granular bed experience similar filtration phenomena the total bed efficiency, η, can be found by summing the effect of all elements in the bed. The semiempirical expression commonly used for η is

$$\eta = 1 - \exp[-K_1(1-\varepsilon)(L/2a)E] \qquad (2.3)$$

where E is the single sphere efficiency, defined as the ratio of the number of aerosol particles in the gas reaching the granule to the number of aerosol particles approaching it, ε is the bed porosity and K_1 is a constant. The values given for K_1 are: 1.5 (Snaddon and Dietz, 1980; D'Ottavio and Goren, 1983), $1.5/\varepsilon$ (Paretsky et al, 1971; Tardos et al, 1974), 1.5f where f is a collision factor (Patterson and Jackson, 1977), and 1.875 an empirical constant (Schmidt et al, 1978). Another expresion used by Payatakes et al (1973) and Pendse and Tien (1982) to obtain the total efficiency of a granular bed composed of n identical layers is

$$\eta = 1-(1-E')^n \qquad (2.4)$$

Clift et al (1981) shows that the ratio E/E' in equations 2.3 and 2.4 is about 0.86 for a common granular

bed based on the difference in defining the efficiency of a single sphere (equation 2.3) rather than the efficiency of a single unit cell (equation 2.4). This approach is similar to the one taken by Tien (1984). Since there is no single accurate and acceptable solution for E or E', there is no way to confirm the validity of either equation.

Experiments do show (Knettings and Beekman, 1974; Doganuglu et al, 1978; D'Ottavio and Goren, 1983) that for large values of L/2a there is an exponential dependence between L/2a and η. The effect of other parameters on η is not quantitatively clear or agreed upon. In spite of the limitations of the sphere-in-cell models and the single sphere efficiency aproach they are widely used in the literature (Paretsky et al 1971; George and Poehlein, 1974; Tardos et al, 1974; Pilat and Perm 1976; Gutfinger and Tardos, 1979; Nielsen and Hill, 1976; Dietz, 1978; Lee and Gieseke, 1979; Tardos and Pfeffer, 1980; Pfeffer et al, 1981; Degani and Tardos, 1981; Snaddon, 1981; Pendse and Tien, 1982; D'Ottavio and Goren, 1983) mainly because no other theoretical solutions for the filtration efficiency of granular beds are available.

2.3. Aerosol deposition mechanisms

The simplified assumptions discussed above allow a grnular bed filter to be modeled mathematically. The single

sphere collection mechanisms considered to be important are Brownian diffusion, inertial impaction, direct interception, gravitational settling and deposition by electrostatic effects. Each of the mechanisms above is considered separately and it is assumed that one is independent of the other.

2.3.1. Diffusional capture

Diffusional capture results from transport of aerosol to the surface of a collector (granule) by Brownian motion. This process is important in the submicron size range at low gas velocity. If the dust particles are retained on the surface of a collector, a concentration gradient is established and particles diffuse in the direction of the collector.

The single sphere efficiency due to diffusion is usually given in the form

$$E_D = g(\varepsilon)\, Pe^n \qquad (2.5)$$

where ε is the bed porosiry and Pe is the Peclet number given by

$$Pe = d_g U_o / \mathfrak{D} \qquad (2.6)$$

and $\mathcal{D}$ is the diffusion coefficient given by

$$\mathcal{D} = CkT/6\pi\mu r_p \qquad (2.7)$$

and C is the Cunningham slip correction factor, k is the Boltzman constant, T is the absolute temperature, r_p the radius of the dust particle and μ is the viscosity of the gas.

The power on the Peclet number is n=-2/3 for creeping flow, as was shown by Levich (1962) for a single sphere in an infinite fluid and extended by Pfeffer (1964) using the Happel (1958) sphere-in-cell flow model, for a granular bed. In the case of potential flow Chao (1969) obtained the power n=-1/2 for a single sphere, a solution that was extended to apply for a granular bed by Ishii and Johnson (1970). The porosity function $g(\varepsilon)$ was investigated theoretically and experimentally by many authors (Pfeffer, 1964; Wilson and Geankoplis, 1966; Cookson, 1970; Gebhart et al., 1973; Sorensen and Stewart, 1974; Meisen, 1975; Tardos et al., 1976; Thambimuthu, 1980) and each found a slightly different function. Results for the case of interest, low Reynolds and high Peclet numbers, are reviewed by Tardos et al. (1978) and Rajagopalan and Tien (1979).

The cell model is relatively successful in predicting diffusional capture even though the cell model is far from

representative of the real conditions in a granular bed. The main reason being the fact that mass transfer at high Peclet number, when the concentration boundary layer is thin, is not very sensitive to the details of the fluid motion far from the solid surface (Clift et al., 1978). Chiang and Tien (1982) using the constricted tube model of Payatakes et al. (1973) found results similar to those given by equation 2.5 with the power n=-2/3.

2.3.2 Gravity settling

The gravitational settling effect is small unless particles are very large and the velocity is very low. Thomas and Yoder (1956) and Paretsky et al (1971) found experimentally that filtration efficiencies obtained in a packed bed is higher for downward flow than for upward flow and they concluded that the difference is due to gravity effects. Tardos et al. (1974) obtained a trajectory solution for a single sphere combining gravitational separation and inertial effects which confirmed the experimental results. Chen (1955) suggested that single sphere efficiency due to gravity setlling is given by

$$E_G = StGa \qquad (2.8)$$

where the Stokes and the Galileo numbers are defined as $St=2C\rho_p U_o r_p^2/9\mu a$ and $Ga=ga/U_o^2$, respectively. The same

expresion was obtained by Prieve and Ruckensein (1974) and Rajagopalan and Tien (1976) for an isolated collector. Tardos and Pfeffer (198Ø) using the expression for the stream function representing gravity as given by Neilsen and Hill (1976) derived an annalitical solution for the efficiency of gravity settling:

$$E_G = StGa \; / \; (1+ StGa) \qquad (2.9)$$

For small values of the parameters St and Ga equations 2.8 and 2.9 are identical.

Pfeffer and Hill (1978) obtained a solution similar to equation 2.8 for the case of a rotating bed, assuming that the dust particle has the radial velocity of the bed. Their solution differs from equation 2.8 only by the definition of the Galileo number where the gravity term g, is replaced by the radial acceleration, $a_r=W^2r_o$, W being the rotational rate in radians/sec and r_o the radius of the rotating cylinder. At high rotational rates $Ga=W^2r_oa/U_o^2$, may be considerably larger than in equation 2.8, yet gravity settling effects are still small.

2.3.3. Inertia and interception

The collection by inertial impaction is caused by the presence of an obstacle (granule) in the flow. The obstacle

interferes with the flow causing bending of the gas streamlines near the surface. The large particles in the gas stream, because of their inertia, continue in a relatively straight path that leads to collision with the collector while the small particles follow the stream lines of the gas exactly and do not collide with the obstacle. Inertial effects are discussed in detail in section 3.

Collision between a collector and a dust particle occurs when the center of the particle approaches to within a particle radius r_p from the surface of the collector. Even an inertialess particle which follows the stream lines of the gas, can be captured due to the mechanism of pure interception if it is carried by the fluid through the concentric annulus of radii a and $a+r_p$ where a is the radius of the granule. Particles carried by the fluid through this space touch the filter element because of their size, r_p.

Paretsky et al. (1971), using the Happel (1958) flow model obtained an analytical solution for pure interception. Their expresion is

$$E_R = 3/2\ g^3(\varepsilon)\ R_p^2 \qquad (2.1\emptyset)$$

where R_p is the ratio of particle to granule radius. A similar expresion was obtained by Rajagopalan and Tien (1976) and Tardos (1977). Using the flow model for potential

flow, Lamb (1932), E_R becomes

$$E_R = 3\ R_p/\varepsilon \qquad (2.11)$$

Thus, even though interception in both cases is independent of the velocity, the efficiency is a strong function of the flow field. In most granular beds the parameter R_p is of the order of Ø.ØØØ5-Ø.ØØ1 making direct interception small and practically unimportant especially if creeping flow conditions exist.

2.3.4. The effect of electrical forces

The filtration mechanisms mentioned above are purely mechanical. There exists another class of capture processes which results from the attraction or repulsion between electrostatic charges or image of charges on the bed granules and dust particles. Neilsen and Hill (1976) classify the forces involved into five categories as shown in Table 2.1. A similar approach to electrostatic forces involved in the filtration process was used also by other authors (Ranz and Wang, 1952; Kramer and Johnstone, 1955; Tardos, 1977; Pfeffer et al., 1981; Kallio and Dietz, 1981; Shapiro et al., 1983; Coury, 1983).

When no external electric field is applied the main electrical forces are a) Coulombic force, when both

Table 2.1: Electrical Force Expresions (Neilsen & Hill, 1976)

Force	Description	Parameter
a. Coulombic force	Collector and particle are both charged	$K_c=Cq_cq_p/K^*$
b. Charged particle image force	Particle only is charged. Charge separation induced in collector.	$K_{ic}=\gamma_c Cq_p^2/K^*$
c. Charged collector image force	Collector only is charged. Charged separation induced in particle.	$K_{ip}=2\gamma_p Cq_c^2 r_p^2/K^* a^3$
d. External electric field force	Particle only is charged. Charge separation in collector induced by external electric field.	$K_{ex}=Cq_pEo/6\pi r_p \mu Uo$
e. Electric dipole interaction force	Neither body is Charged. Charge separation in both bodies induced by external electric field.	$K_{icp}=2\gamma_c\gamma_p\ {}_fCr_p^2Eo/a\mu Uo$

$K^*=24\pi^2\epsilon_f r_p a^2 \mu Uo$

collector and particle are electrically charged and b) charged particle image force when the particle only is charged and an induced charge exists on the collector. The charge collector image force (c) is relatively weak because the size of the aerosol is always much smaller than the size of the granule $r_p << a$ so that the induced dipole is weak.

Neilsen and Hill (1976), Pfeffer et al. (1981) and Kallio and Dietz (1981) solved the tarjectory equation with the force term in equation 2.2 replaced by one or more of the mechanisms shown in Table 2.1. The solutions are based on different flow models for a single isolated sphere or a single sphere in a granular bed. Results of different investigators differs significantly but all indicate a large increase in filtration efficiency attributed to the electrical forces.

Kramer and Johnston (1956) and Neilsen and Hill (1976) found the collection efficiency of a single sphere due to Coulombic interaction to be

$$E_k = 4K_c \qquad (2.12)$$

a result which does not depend on the flow field. Pfeffer et al. (1981) using the Neal and Nader (1974) flow field found values for the efficiency E_k for a packed bed with porosity $\varepsilon = 0.4$. Their results are about a factor of two higher than

the values determined from equation 2.12.

In a fluidized bed, where different granules may be charged with opposite charges the picture becomes much more complicated as charged dust particles experience attraction and repulsion forces as they approach different collectors. There is no available theortical solution to this problem.

2.4. Pilot size and industrial granular bed filters

Reviews of industrially applied granular bed filters were presented by Stone & Webster (1974) Clift and Thambimuthu (1976) and by Tardos and Pfeffer (1978). The granular bed filter design can be classified into fixed, moving and fluidized beds.

2.4.1. Fixed bed filters

Fixed bed granular filters usually have high filtration efficiency. Their main disadvantage is their cyclic operation of filtering and then cleaning to remove the collected particles.The cleaning step involves substantial operational problems. The main industrial filters in the fixed bed category are the Ducon filter developed by the Ducon company and the Panwel Bed Filter developed by A. M. Squires and R. Pfeffer at CCNY.

The Ducon filter consists of a vertical array of granular beds held between two concentric metal cylinders. Dusty gas enters the multiple array of beds through perforated screens and filtration is accomplished by downward flow through the granular bed. When the resistance to flow reaches a predetermined value the beds are fluidized by a backflush pulse of gas and the dust is ejected to a collection hopper. The bed material used in pilot scale experiments was sand and collection efficiency was in the order of 85-90%.

A different kind of a fixed bed filter is the panel type developed by Squires and Pfeffer (1970). In the pannel bed filter the dusty gas flows horizontaly across a number of beds of sand acting in parallel. The filter is designed in such a way that a cake can form on the upper surface of the bed containing fine sand particles. Once a thick cake is formed and the pressure drop increases beyond a certain limit the cake is removed by a high pressure air "puffback" which flows in the opposite direction of the dirty air. When the cake is removed the pressure drops back to its initial value and the filtration cycle can start again. The puffback, while removing the filter cake also supplys clean particles to the bed to keep the bed thickness constant. Efficiencies as high as 99.9% can be achieved at room temperature. At higher temperature the filtration efficiency drops somewhat.

2.4.2. Moving bed filters

As opposed to fixed bed filters which are periodically cleaned, in moving beds the bed material is in constant motion. Typical moving beds are those developed by Guillory (1977) and Geffken et al (1978) at Combustion Power Co., Inc for the DOE. Dust filtration is accomplished by causing the dusty gas to flow radially outward in cross flow through an annulus of granular bed material. The bed material is flowing downwards at a rate determined to operate at steady state and at reasonably low pressure drops.

Another type of moving bed filter is the one developed by EFB (Electrified Filter Bed) (1979) where the bed material flows downward. The dusty gas flows horizontally in cross flow through two stages. In the first stage the large particles are mainly collected. The fine particles not collected in the first stage are electrically charged and flow through the second stage where a high colection efficiency is obtained. Filtration efficiencies reported for the EFB are 99% for particles as small as Ø.1μm and 99.9% for 1.Øμm particles.

2.4.3. Fluidized bed filters

Fluidized bed filters operate continuously as clean

particles are fed to the bed and dirty granules are removed. The dusty gas flows through the filter in an upward direction resulting in fluidization of the granules. Operating just above minimum fluidization to avoid bubble formation, the bed can operate at steady state and at high filtration efficiency. Extensive work on fluidized bed filters was done by Tardos (1977) and Gutfinger and Tardos (1979). The performence of the fluidized bed may be increased by lubricating the granules to reduce bouncing of dust particles, Jugel et al (197Ø), and by using an elerctrofluidized bed, Zahedi and Melcher (1976), where an external electric field is applied to the bed. The main disadvantage of the fluidized bed filter is the relatively low gas velocity allowed in the bed. If the velocity exceeds minimum fluidization bubbles are formed and the filtration efficiency reduces significantly because dust particles bypass the bed in the bubble phase. Stabilization of the fluidized bed at higher velocities may be obtained by applying a magnetic field to the bed as suggested by Rosensweig et al (1979) and Colberg and Liu (1982) or by using a rotating fluidized bed as was suggested by Pfeffer and Hill (1978) and Gal et al. (1982).

3. A NEW MODEL FOR INERTIAL DEPOSITION IN A GRANULAR BED

(Part of this section was accepted for publication in the AIChE J. (March 1984))

3.1. Introduction

In investigating the effect of inertial impaction on filtration efficiency, one should assume that all other forces influencing the trajectory of a particle in a granular bed are small compared to the inertia. This assumption is valid in a granular bed where granules and dust particle are electrically neutral, gas velocity is high, dust particles diameter is larger than 1.Ø micron and granule size is relatively small. When bed and dust particles are electrically neutral and diffusional and gravitational effects are negligible, inertia becomes the dominant mechanism of filtration and equation 2.2 is reduced to

$$\frac{d^2\vec{x}}{dt^2} = \frac{6\pi\mu r_p}{m_p C}\left(\vec{u} - \frac{d\vec{x}}{dt}\right) \qquad (3.1)$$

By nondimensionalizing equation 3.1, it can be eassily shown that the filtration efficiency of a granule in the bed is characterized by only one dimensionless group called the Stokes number, $St=2\rho_p r_p^2 UC/9\mu a$.

Filtration efficiency due to inertial effects, can be

predicted once the solution of equation 3.1 is known; such a solution is given in the present work. The equation is solved in cartesian coordinates for a dense cubic packing of spheres (body centered cubic) at low Reynolds numbers. The theoretical solution is then compared with experimental results obtained in a similar arrangement of spherical particles. The validity of the solution for higher Reynolds numbers and randomly packed beds with different porosities is also examined.

3.2. Previous models

3.2.1 Flow models in granular bed

The actual flow of fluid in a bed of granules is usually so complicated that simplified models have to be used. These models are usually classified as either internal flows where the fluid is assumed to flow in pores of different geometry inside the granular bed, or external flows where the fluid is assumed to flow around the granules (Rajagopalan and Tien, 1979).

In internal flow models the pore is usually taken as a cylindrical capillary or a constricted tube; the pores' walls act as collectors for the dust. Particles reach the surface by various filtration mechanisms. The capillary model was initially used by Jackson and Calvert (1966) for

particle collection in a packed bed of spheres. The unit bed element is assumed to have N capillaries per unit area of bed. The main mechanism of filtration in those capillaries, for particles larger than Ø.5 micron, is inertial impaction which occurs due to centrifugal forces acting on the particles as the capillary turns.

More complicated capillary models such as constricted tube models were developed by Petersen (1958) and more recently by Payatakes et al (1973), and Niera and Payatakes (1978). The unit cell is characterized by three physical parameters, the maximum and minimum diameter of the constricted tube and its height. The tube wall is assumed to be parabolic (Payatakes et al, 1973), sinusoidal (Fedkiew and Newman, 1977) or hyperbolaidal (Petersen, 1958; Venhateson and Rajagopalan, 198Ø). Pendse and Tien (1982), found that trajectory calculations using a combination of all three cases mentioned above agree better with experimental data than each of the models alone. The filtration of particles is accomplished by the deposition of particles on the surface of the tube and the efficiency increases as the constriction minimum to maximum diameters ratio decreases. Due to its geometry, the constricted tube flow model predicts much higher filtration efficiencies than those predicted by the capillary flow model.

Most known external solutions for velocity profiles in

granular beds assume the bed to be a homogeneous swarm of spherical granules of uniform size. Each sphere has a free surface (no sphere is touching another), and it is located in a center of a cell surrounded by the flowing fluid. The cells are all identical, experiencing the same flow in their voidage. The radius of the cell e, is defined so that the void fraction of a unit cell is equal to the local void fraction of the bed

$$e = a(1- \varepsilon)^{-1/3} \qquad (3.2)$$

where a is the radius of the sphere and ε is the void fraction in the bed. The flow fields are given in terms of a stream function (Gutfinger and Tardos, 1979) and they differ from each other only by the boundary conditions imposed at the cell boundary. The sphere-in-cell models, such as the ones suggested by Lamb(1932), Happel(1958), Kuwabara(1959), Tam (1969) and Neal and Nader (1974), assume the flow to be two dimensional and the Reynolds number to be either very small (creeping flow) or very large (potential flow).

3.2.2 Limitations of existing flow models in the computation of dust particle trajectory.

Using two dimensional flow models for trajectory calculations in a granular bed, reduces the vectorial Eq. 3.1 to a set of two differential equations describing

the motion of a dust particle towards a single sphere in the bed. Once the limiting or critical trajectory, i.e. the trajectory that just missed the collector is found (see Fig. 3.1) the single sphere efficiency can be defined as

$$E = (b/a)^2 \qquad (3.3)$$

where b is the radius of the limiting trajectory. Single sphere efficiencies due to inertia, E, for different flow models, as computed by Tardos (1978), are given in Figure 3.2. The curves in the figure are based on equation 3.3 where b is calculated from the trajectory equations.

The commonly used flow field models (Lamb, 1932; Happel, 1958; Kuabara, 1959; Tam, 1969; Payatakes et al, 1973; Neal and Nader, 1974) for trajectory calculations in packed beds, are far from representative of a real bed. The pressure drop predicted using these models usually agrees reasonably well with experimental data. However, the calculated velocity profiles differ significantly from the actual velocity profiles, since the sphere-in-cell models assume that none of the spheres are touching each other. The existance of contact points between spheres can not be ignored when calculating the dust particles' trajectories. Their existance increases the tortuosity of the stream lines which strongly effects the motion of a dust particle flowing through the bed. Moreover, many dust particles are captured

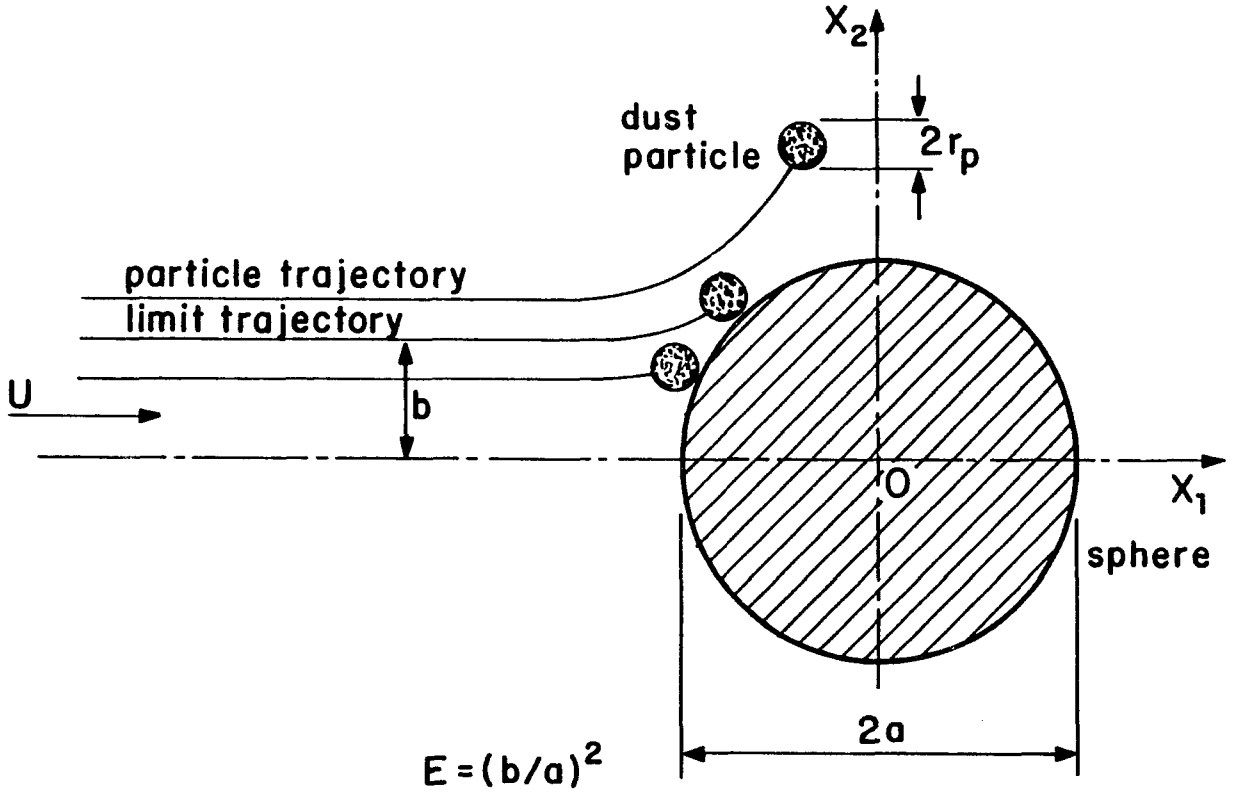

Figure 3.1: Inertial deposition of particles on a sphere.

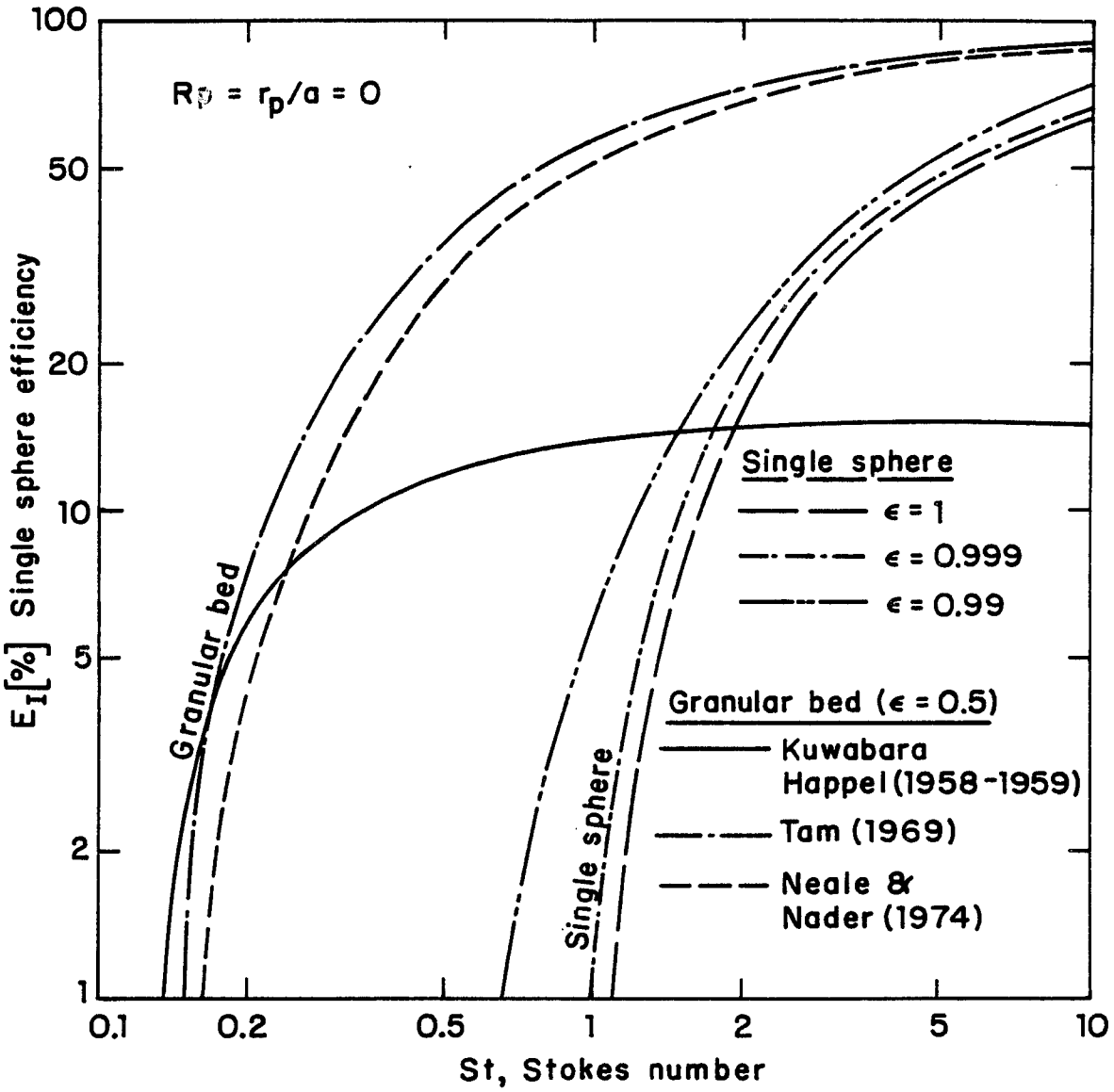

Figure 3.2: Inertial deposition on a sphere ($\mathcal{E} = 1$) and in a granular bed ($\mathcal{E} = 0.5$). Comparison between different flow models.

due to the existance of these contact points. Figure 3.3 demonstrates this fact; in the plane of the paper the collection efficiency of each of the two nontouching spheres is E=b/a while the collection efficiency of each of the two touching spheres is E=(a+b)/2a. The impact of the touching points between spheres becomes increasingly important for low inertial effects as the distance b becomes very small. Many dust particles traveling in the plane of the paper will escape through the opening between the spheres if they are nontouching whereas they would be captured when the two spheres are in contact. Thus, filtration efficiency computations based on sphere-in-cell flow models can be expected to predict a lower filtration efficiency than is actually found in a real fixed bed.

The higher filtration efficiency observed experimentally when compared to the theoretical predictions described above, is explained by Snaddon and Dietz (1980) to be the result of flow intensification. This intensification is caused by the acceleration of the flow through the constrictions in the voids and is accompanied by flow separation at high Reynolds numbers. The intensified flow impinges onto the upstream face of the bed granules with a velocity greater than the superficial velocity, and results in increasing inertial impaction effects. The flow model used by Snaddon and Dietz is the unit-cell potential flow model (Lamb, 1932) where the original boundary conditions on

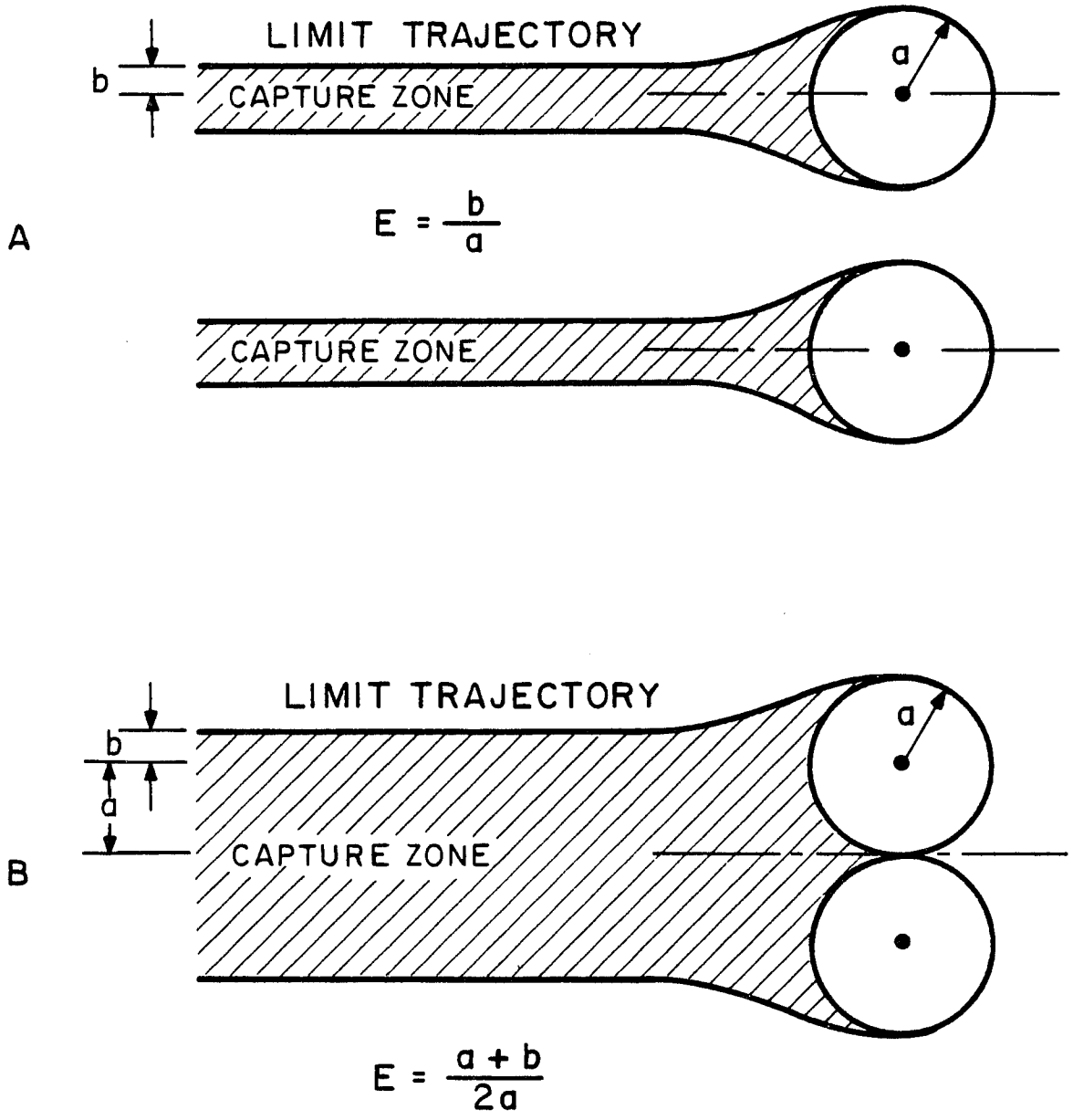

Figure 3.3: Inertial deposition of particles:
A - two nontouching spheres
B - two touching spheres

the cell surface are replaced by

$$U_r(r=1) = -\beta U\cos\theta \qquad 0 \leq \theta \leq \phi \qquad (3.4)$$
$$= 0 \qquad \phi < \theta \leq \pi/2$$

where

$$\phi = 1/2\ \cos^{-1}(1 - \beta/2) \qquad (3.5)$$

β is called the intensification factor and is unity for very low Reynolds numbers and increases with increasing Reynolds number. As β increases ϕ decreases and the flow is constrained to enter the cell in a narrowing jet centered around the axis. This model, however, is semi-empirical since β must be evaluated experimentally.

Lately, a number of researchers have developed empirical correlations for the single sphere efficiency especially for the region were inertial effects are dominant; some of these correlations are given in Table 3.1. These correlations and theoretical predictions of filtration efficiency based on the sphere-in-cell model for creeping and potential flow are compared in Figure 3.4. The large discrepency between the results indicates that the flow models described above are not sufficiently representative for use in trajectory calculations. A similar conclusion was reached regarding the constricted tube models from the comparison of experimental and theoretical data by Pendse and Tien (1982).

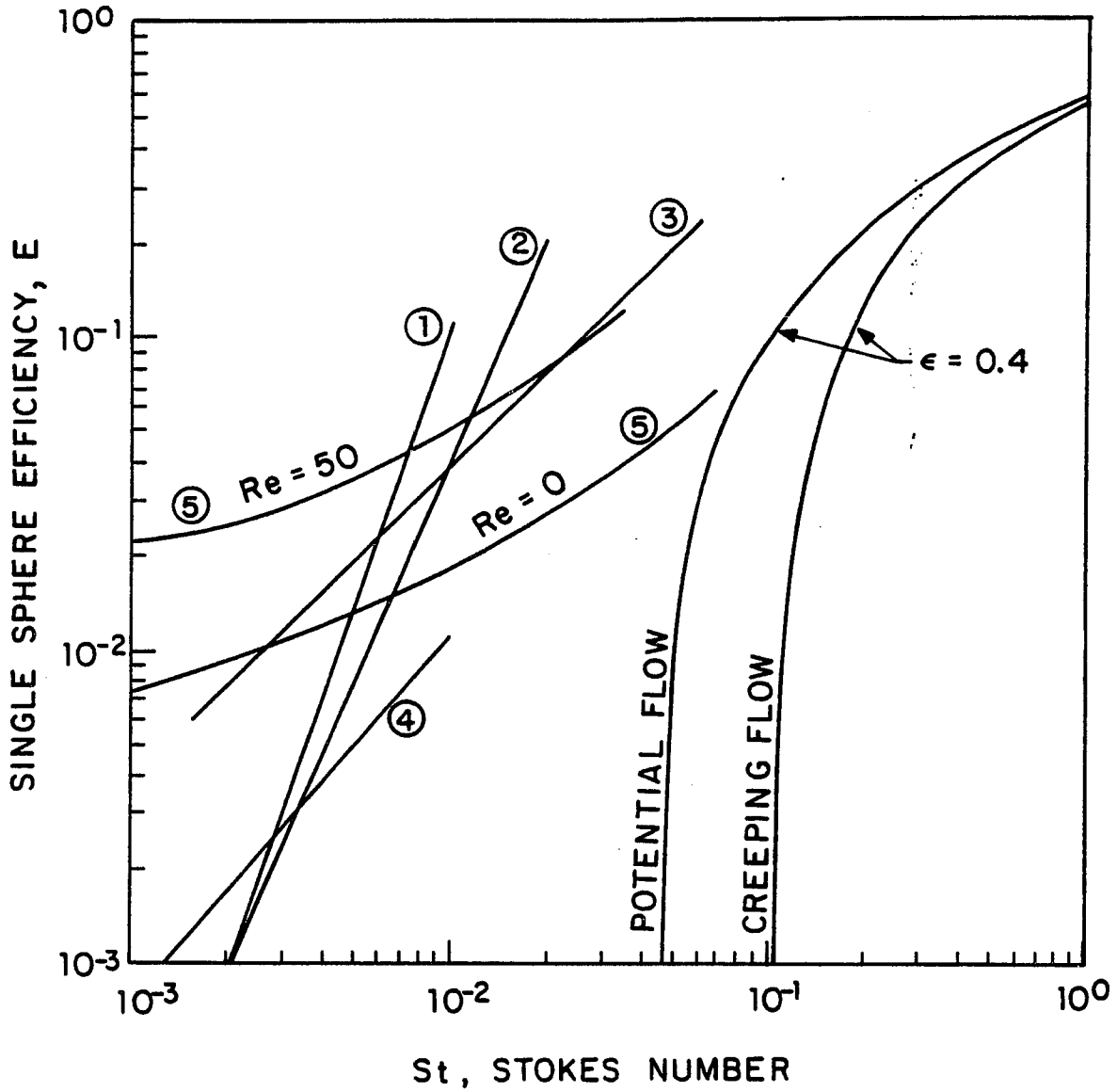

Figure 3.4: Theoretical predictions of single sphere efficiency in a granular bed (Tardos, 1978) compared with empirical correlations; (1) Thambimuthu (1978), (2) Goren (1978), (3) Schmidt et al. (1978), (4) Paretsky (1972), (5) Pendse and Tien (1982).

Table 3.1: Empirical correlations for single sphere efficiency

Author	E	Range
Paretsky (1972)	$2xSt^{1.13}$	St<Ø.Ø1
Meisen and Mathur (1974)	Ø.ØØ75+2.6xSt	St<Ø.Ø1
Doganoglu (1975)	2.89xSt	Ga=Ø d_g=1ØØ microns
	Ø.Ø583xRexSt	Ga=Ø d_g=6ØØ microns
Melcher et al. (1978)	St	Re<1ØØ
	Ø.Ø1xRexSt	1ØØ<Re<1ØØØ
	1ØxSt	Re>1ØØØ
Thambimuthu et al.(1978)	$1Ø^5xSt^3$	Ø.ØØ1<St<Ø.Ø1
Schmidt et al. (1978)	3.75xSt	St<Ø.Ø5
Goren (1978)	$127ØxSt^{9/4}$	Ø.ØØ1<St<Ø.Ø2
Pendse and Tien (1982)*	(1+Ø.Ø4Re)[St+f(Rp)]	
D'Ottavio and Goren (1983)#	$\frac{St_{eff}^{3.55}}{1.67 + St_{eff}^{3.55}}$	13<Re<165Ø Ø.33<ε<Ø.38

* $f(Rp)=Ø.48(4-\frac{4Rp}{d_c}-\frac{Rp^2}{d_c})^{1/2}\frac{Rp^{1.Ø41}}{d_c}$

\# $St_{eff}=f(Re,\varepsilon)St$

$f(Re,\varepsilon)=(1-h^{5/3})/(1-1.5h^{1/3}+1.5h^{5/3}-h^2) + 1.14Re^{1/2}/\varepsilon^{2/3}$

where $h=1-\varepsilon$

3.3. Aerosol filtration in a dense cubic bed of spheres

3.3.1 Flow model

In order to predict the trajectory of dust particles in packed beds, a more realistic flow model is needed. Flow models for arbitrarily arranged spheres in packed beds are not yet available in the literature. There are, however, three dimensional models of flow through periodic arrays of spheres in special arrangements such as dense cubic, simple cubic and face centered cubic packings. These models which are valid for low Reynolds numbers were developed by Snyder and Stewart (1966), Sorensen and Stewart (1974) and more recently by Sangani and Acrivos (1982) and Zick and Homsy (1982). In this work Snyder's flow field model for flow in a dense cubic bed is used for trajectory calculations. The model has the advantage of describing the flow in a bed which can readily be constructed; thus, theoretical predictions of filtration efficiency based on trajectory calculations can be readily compared to experimental data.

The fluid velocity profile and the pressure distribution at low Reynolds number for the dense cubic packing (Figure 3.5) was obtained by Snyder and Stewart (1966) and is given by

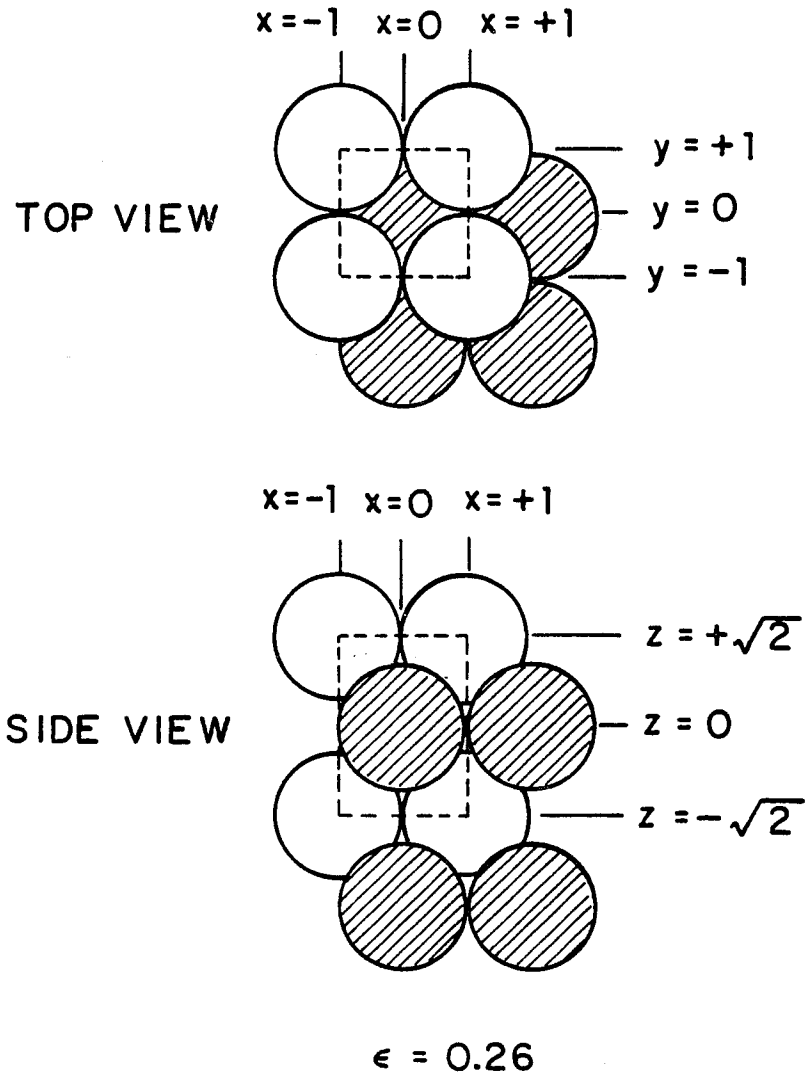

$\epsilon = 0.26$

Figure 3.5: A schematical representation of a dense cubic packing of spheres.

$$v_j = \sum_{i=1}^{M} C_{ji} \alpha \phi_{ji} \qquad j = 1, 2, 3 \qquad (3.6)$$

$$P = (Z+\sqrt{2})/2\sqrt{2} + \sum_{i=1}^{M} C_{pi} \phi_{pi} \qquad (3.7)$$

where j are the three cartesian coordinates, C_{ji} and C_{pi} are constants, α is a function that satisfies the no-slip condition on M neighboring spherical surfaces and ϕ_{ji} and ϕ_{pi} are combination of trigonometric functions satisfying the periodicity and symmetry conditions. Here v_j is a dimensionless fluid velocity defined by

$$v_j = u_j \mu / a \Delta p \qquad (3.8)$$

where u_j is the velocity in the j direction, μ is the viscosity of the fluid, a is the radius of a sphere and Δp is the pressure drop over a unit cell which extends from $Z=-\sqrt{2}$ to $Z=\sqrt{2}$. The dimensionless superficial velocity in the z direction is similarly defined as $V=(\mu/a)(U/\Delta p)$ where U is the superficial velocity in the z direction. The value of V extrapolated to Reynolds number Re->Ø

$$V_{Re->Ø} = V_o = (\mu/a)(U/\Delta p)_{Re->Ø} = Ø.ØØØ258$$

can be found from the experimental work by Martin et al. (1951) or from the Ergun correlation as given in eqution 3.15.

The constants C_{ji} and C_{pi} in equations 3.6 and 3.7 can be evaluated by using Galerkin's method. The trial solutions are substituted into the continuity and momentum equations for Re - Ø and integrated over the volume τ of a unit cell

$$\int_{\tau} \sum_{j=1}^{3} \frac{\partial V_j}{\partial X_j} \; w_i' d\tau = \emptyset \qquad i=1,2,\ldots N \qquad (3.9)$$

$$\int_{\tau} \left(\nabla^2 V_j + \frac{\partial P}{\partial X_j}\right) w_i d\tau = \emptyset \qquad i=1,2,\ldots N \quad j=1,2,3 \quad (3.10)$$

Here w_i and w_i' are weight functions defined in Snyder and Stewart (1966) and the integration is done numerically using M-triple Gausian points. Introducing the trial functions, given in equations 3.6 and 3.7 into equations 3.9 and 3.10 and integrating over the volume of the cell, reduces the system into 4N linear equations with C_{ji} and C_{pi} as unknowns. The velocity profile satisfies the conservation equations approximately, and the boundary and symmetry conditions exactly. The solution is given in detail in Appendix A.

The dense cubic packing of spheres is shown in Figure 3.5. The unit cell enclosed by dotted lines contains the sphere centered at (Ø,Ø,Ø) and one eighth portion of eight adjacent spheres. The void fraction of this arrangement is Ø.26 and the flow is assumed to be in the positive z direction. A necessary condition for the solution to be accurate is that $V^*(Z)$, which is the average normalized

dimensionless velocity (normalized by V_o=Ø.ØØØ258) in the z direction in the range $-\sqrt{2}<Z<\sqrt{2}$ given by

$$V^*(Z)=1/4\int_{-1}^{1}\int_{-1}^{1}(v_z/V_o)dXdY \qquad (3.11)$$

should be unity. The dimensionless velocity $V^*(Z)$, as obtained using Snyder's 22 term solution in the range $Ø<Z<\sqrt{2}$ is shown in Figure 3.6; the solution deviates by +11.8% to -21.4% from the required value of unity. This error is clearly too large for trajectory calculations. Improvement in accuracy was achieved in the present work by increasing the number of terms in the series from 22 terms to 68. Using this solution with 2Ø-triple Gausian points (compared to the 16 used by Snyder), $V^*(Z)$ converges to 1.Ø with a deviation of only 5.9% to -7.9%, as shown in Figure 3.6. This solution for the velocities v_x, v_y, v_z and the pressure P requires the solution of a 272x272 matrix to determine the coefficients C_{xi}, C_{yi}, C_{zi} and C_{pi}. The convergence of the series is very slow and in order to increase the accuracy even further, one has to solve for many more constants, a procedure which requires an enormously large computer capacity. For the trajectory calculations presented in this work however, the 68 terms solution seems to be reasonably accurate. A typical velocity profile v_z in the plane $Z=-\sqrt{2}$ as obtained by using the 68 term solution is given in Figure 3.7.

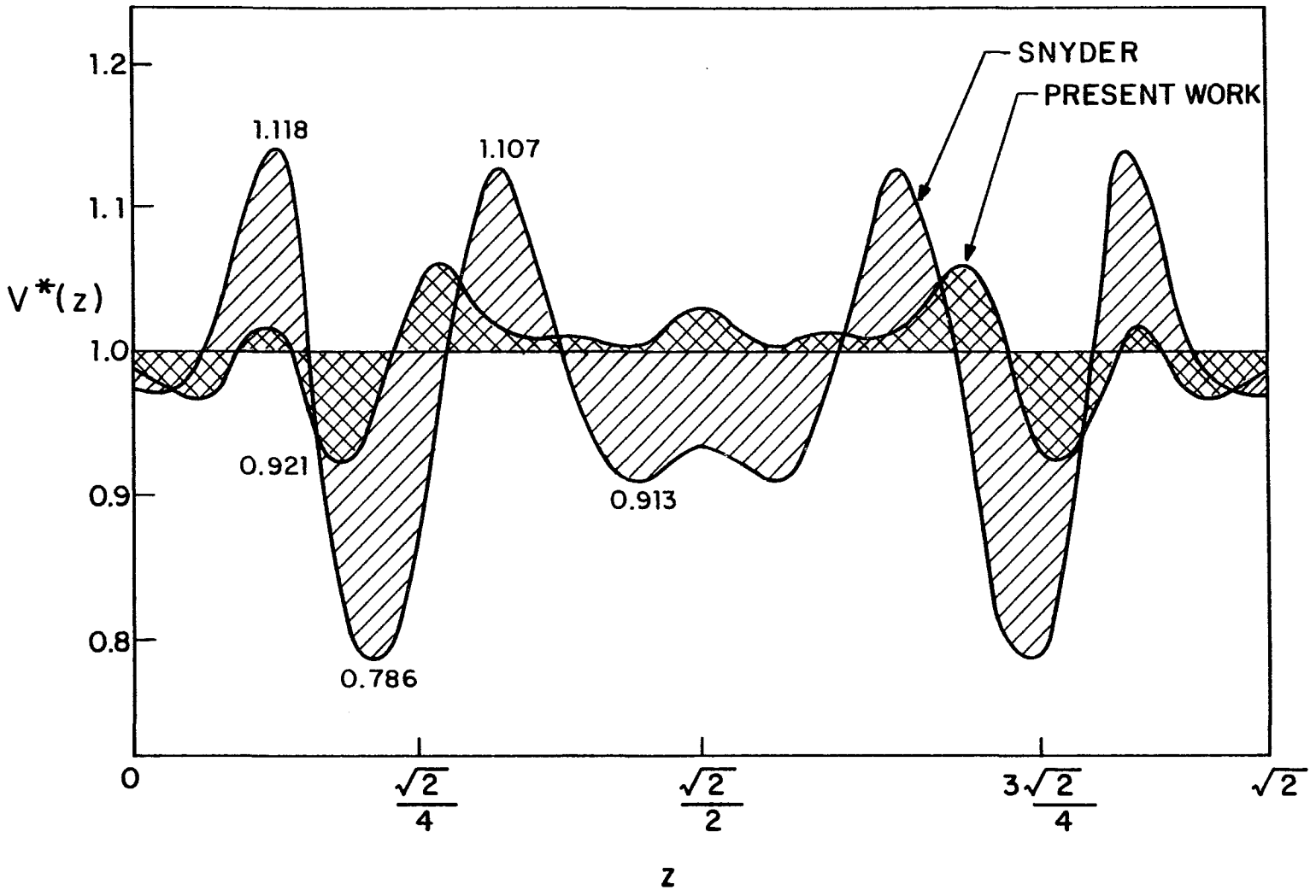

Figure 3.6: The velocity $V^*(Z)$ as defined by equation 3.11 Comparison between Snyder's solution and the present work.

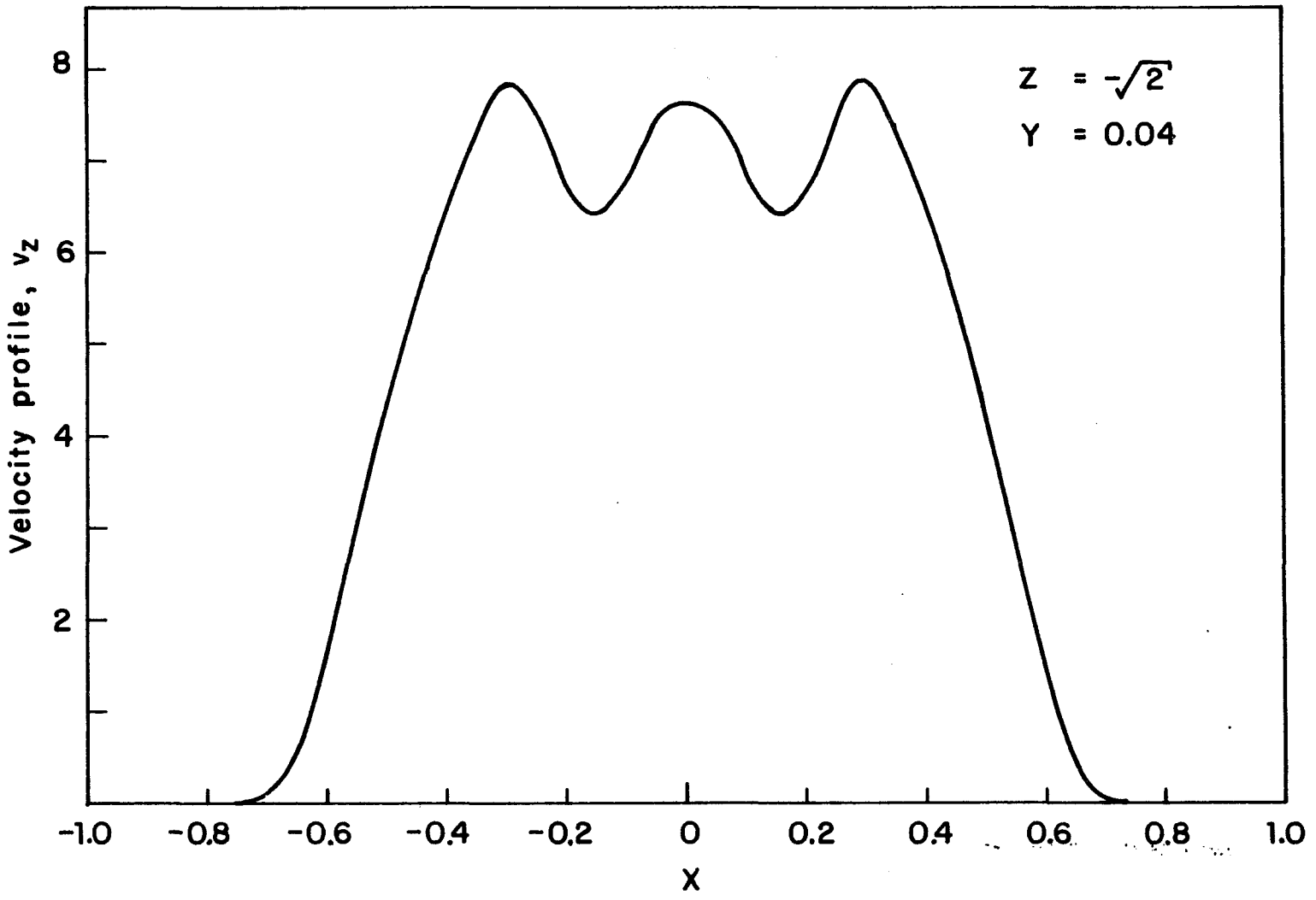

Figure 3.7: The velocity v_z as a function of X at $Z = -\sqrt{2}$, Y =Ø.Ø4 in the range -1.Ø<X <1.Ø .

3.2 Three dimensional trajectories calculations in a dense packed bed

The flow model described above can be used in the trajectory equation (Eq. 3.1) to predict filtration efficiencies in a dense cubic packing of spheres. In dimensionless form equation (3.1) has the form

$$\frac{d^2\vec{X}}{dT^2} = \frac{1}{StF}\left(\vec{U} - \frac{d\vec{X}}{dT}\right) \qquad (3.12)$$

where the dimensionless parameters are:

$\vec{X}=\vec{x}/a$, $T=tUF/a$, $\vec{U}=\vec{u}/UF=\vec{v}/V_o$

$St=2\rho_p r_p^2 UC/9\mu a$

The factor F is defined as the ratio of the dimensionless superficial velocity at Re->Ø, V_o, to the superficial velocity at any Reynolds number

$$F = V_o/V = (U/\Delta P)_{Re->\emptyset} \;/\; (U/\Delta P)_{Re\neq\emptyset} \qquad (3.13)$$

The velocities V and V_o can be found experimentally or by using the experimental results by Martin et al (1951). The factor F can also be determined for any granular arrangment using the well known Ergun correlation

$$\frac{\Delta P}{L} = \frac{150\mu U(1-\varepsilon)^2}{d_g^2\,\varepsilon^3} \quad \frac{1.75\rho U^2(1-\varepsilon)}{d_g}\frac{}{\varepsilon^3} \qquad (3.14)$$

where P is the total prssure drop across the bed, $L=d_g(kn+1)$ is the thickness of the bed, n is the number of unit cells in the z direction and k is a factor correlating the height of a unit cell to the diameter of the spheres, e.g., $k=\sqrt{2}$ in a dense packed bed, k=1 for a simple cubic arrangement and so on. Using equation (3.14) one can find the value of V to be

$$V = \frac{U\mu}{\Delta pa} = \frac{2\varepsilon^3}{[150(1-\varepsilon)+1.75Re](k+1/n)(1-\varepsilon)} \qquad (3.15)$$

and

$$F = V_o/V = 1.0+1.75Re/150(1-\varepsilon) \qquad (3.16)$$

Using the Ergun correlation, the velocity V_o for the dense cubic packing (with $k=\sqrt{2}$, $\varepsilon=0.26$, Re->0, n->large) is 0.0003 which is by about 16% higher than the experimental value of Martin et al (1951). The value of F is unity for Re->0 but becomes larger for higher values of the Reynolds number. The product StxF in equation 3.12 is defined as a modified Stokes number St' and is given by

$$St' = StxF = St[1.0+1.75Re/150(1-\varepsilon)] \qquad (3.17)$$

Introducing the modified Stokes number St' into equation (3.12) yields

$$\frac{d^2\vec{X}}{dT^2} = \frac{1}{St'}\left(\vec{U} - \frac{d\vec{X}}{dT}\right) \qquad (3.18)$$

Equation 3.18 is used for trajectory computations with the initial conditions

$$\vec{X}(T=\emptyset)=(X_{\emptyset},Y_{\emptyset},-\sqrt{2}) \qquad (3.18a)$$

$$d\vec{X}/dT(T=\emptyset)=\vec{U} \qquad (3.18b)$$

which assumes that the velocity of the particle is identical to the velocity of the gas at T=Ø. The actual initial velocity of the dust particles, at $Z=-\sqrt{2}$ depends on the Stokes number: it is exactly equal to the gas velocity U for St=Ø and lower for larger Stokes numbers. Thus, using the initial conditions as shown above introduces a small error in the trajectory calculation for small Stokes numbers which increases however with increasing Stokes number.

3.3.3 Single sphere and total bed efficiency

As a first step, single sphere efficiencies in the unit cell were computed using equation (3.18). The procedure of the solution is given in Appendix B. The flow in the cell is taken to be in the positive z direction and all dust particles are assumed to be entering the first layer of cells through the plane at $Z=-\sqrt{2}$. The single sphere collection efficiency, E, is defined as the ratio of the flux of dust particles through the area from which they are collected, Ac, (see Figure 3.8) to the flux of particles flowing towards the cell through the area $A_{\emptyset}$ equal to the

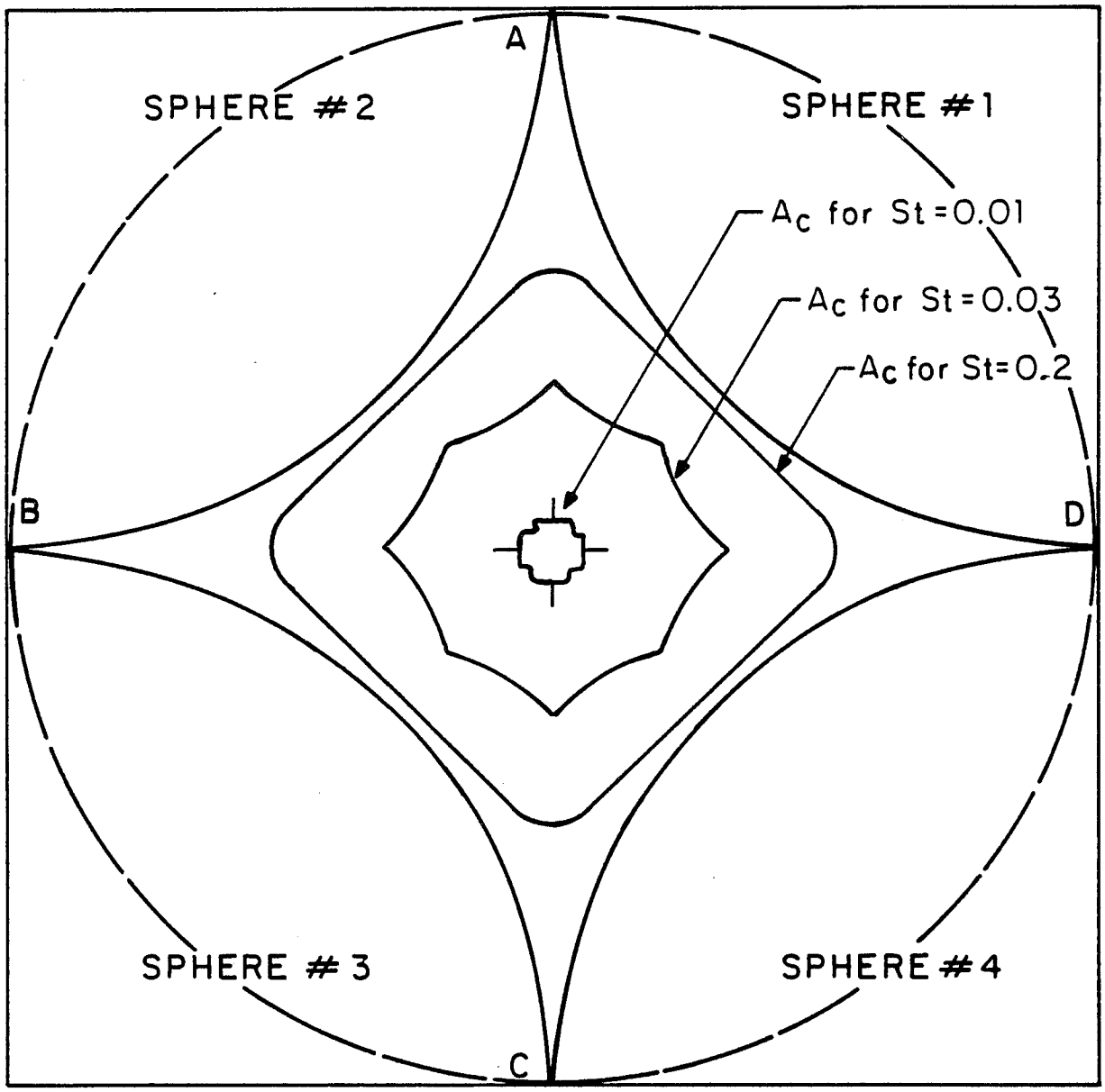

Figure 3.8: The area A_c at $Z = -\sqrt{2}$ from which dust particles are collected on the central sphere of the cell for different Stokes numbers. The area A_p is the free cross section area of the cell surrounded by four spheres (curve A,B,C,D).

cross section area of the cell

$$E = \frac{1}{c_o U_{po} A_\emptyset} \int_{A_c} c\vec{u}_p dA \qquad Z=-\sqrt{2} \qquad (3.19)$$

Here c and $\vec{u}_p$ are the dust concentration and the dust velocity, respectively, at $Z = -\sqrt{2}$ and c_o and U_{po} are the uniform dust concentration and velocity far outside the bed. The filtration efficiency of the first half layer of spheres, the half facing the stream, is assumed to be insignificant so that all dust particles flowing towards the cell are present at the plane $Z = -\sqrt{2}$ where the trajectory computation starts. The error involved in this assumption was demonstrated by experiment to be small. The assumption also stands to reason based on the fact that these half spheres can be considered as single spheres in an almost infinite fluid (ε is very large) where the collection efficiency for Stokes numbers St<Ø.1 is very small.

Assuming the velocity $U_{po}=U$, the velocity $\vec{u}_p=\vec{u}$ at $Z=-\sqrt{2}$ and the concentration $c=c_\emptyset$ at $Z=-\sqrt{2}$ equation (3.19) reduces to

$$E = \frac{1}{A_c} \int_{A_c} \vec{U} dA \qquad (3.2Ø)$$

The area A_c for which the integration is performed, is found from the solution of the limiting trajectories. The size of the area A_c depends on the Stokes number, and the initial

conditions of the dust particles entering the bed. Computation of a trajectory is stopped when the center of a dust particle approaches to within a dimensionless distance Rp from the surface of a sphere where it is said to be collected or when a particle leaves the cell. In such computations, interception, determined by the value of the parameter Rp, is usually small compared to inertial effects unless the Stokes number, St, is very small. The area Ac for the central sphere in the cell for Stokes numbers, St=Ø.2,Ø.Ø3,Ø.Ø1 is given in Figure 3.8 and the efficiency E for different Stokes numbers is given in Figure 3.9. On the same figure single sphere efficiencies computed by Tardos (1978) using the Neal and Nader (1974) flow model (for ε =Ø.25, Ø.35, Ø.5) are also given. As expected the efficiency found in the present work is much higher then that predicted by the sphere-in-cell models. The two main reasons for the higher efficiency are:

1. The effect of contact points between spheres is taken into account and the contact points (12 for each sphere in the cubic dense bed) increase the tortuosity of the flow and hence the inertial effects.
2. Flow intensification effects which arise in the present model because of the assumed structure of the bed. The flow enters the cell through the cross section area Ap (ABCD) shown in Figure 3.8. The main flux is in the center of this area where the average velocity is much higher than the superficial velocity in the bed (see

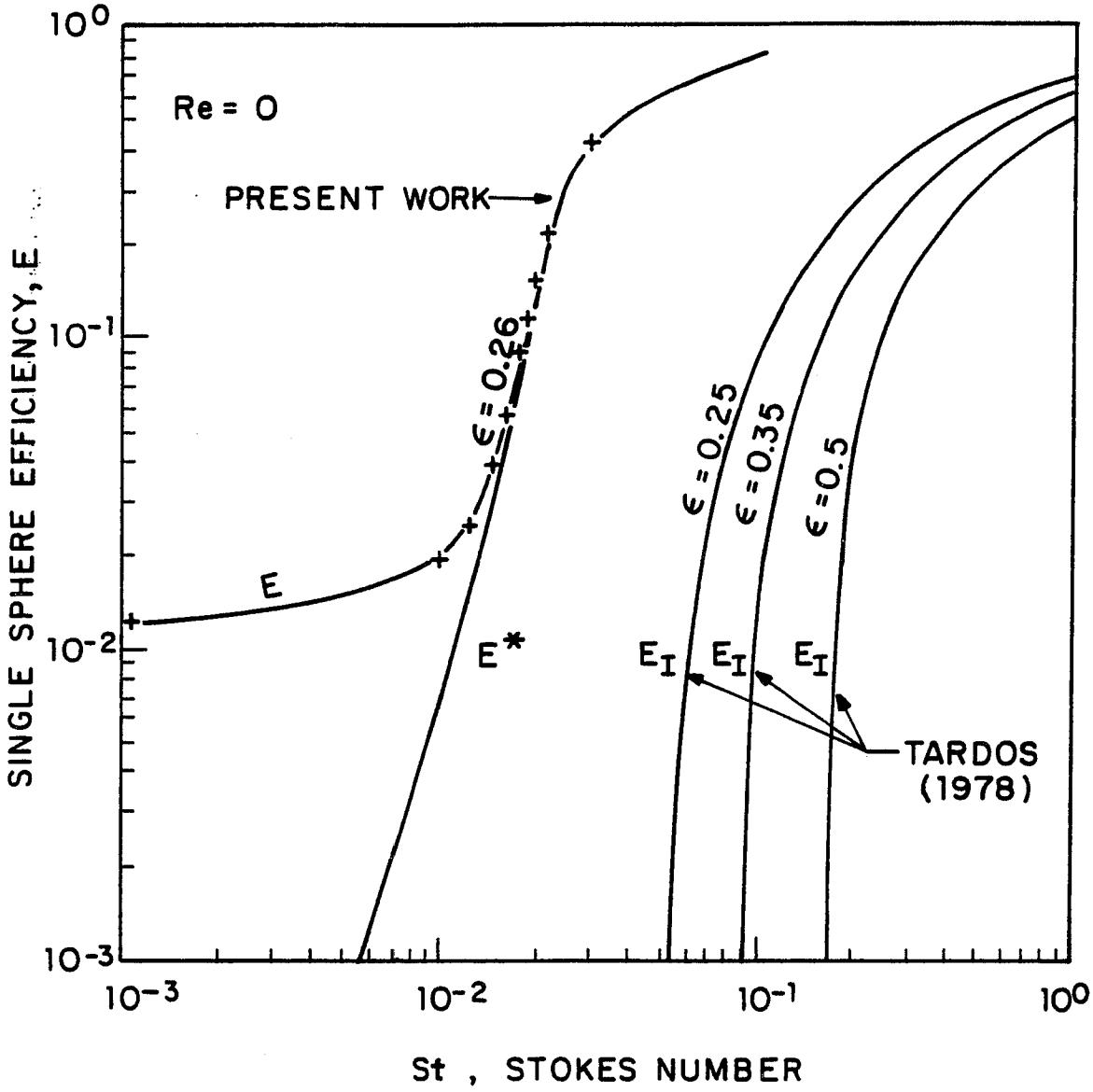

Figure 3.9: Comparison of single sphere efficiencies due to inetia as obtained in the present work and by Tardos (1978).

figure 3.7). The flux is thus targeted towards the central sphere of the cell and impinges on its upstream face.

The velocity profile given by Equation (3.6) satisfies the boundary and symmetry conditions exactly and the conservation equations approximately. The error in the flow field introduces an error in the trajectory computations. A simple way to estimate the error was to compute the filtration efficiency at zero Stokes number, St=Ø, for particles of dimensionless radius $R_p=1Ø^{-5}$. The actual efficiency for these conditions should be very small since at St=Ø particles travel exactly along stream lines and at $R_p=1Ø^{-5}$ the interception effect is negligible. The calculated efficiency, however, is 1.1% for the sphere situated in the center of the cell as well as for an entire bed composed of 9 layers of spheres. This result indicates that some stream lines originating from around the point $(Ø,Ø,-\sqrt{2})$ are on a path of collision with the sphere centered at (Ø,Ø,Ø). This error is small for large Stokes numbers where the efficiency is high compared to 1.1% but it becomes large and even dominant for very low Stokes numbers where the filtration efficiency is very small. To overcome this problem we define the efficiency E^* as

$$E^*=E-E_{St=Ø} \qquad (3.21)$$

to insure zero efficiency at zero Stokes number. The efficiency E^* is shown as the dashed line in Figures 3.9. A correlation $E^*=f(St')$ was found by linear regression of the computed values in Figure 3.9 and is given by

$$E^* = 2xSt'^{3.9}/(4.3x10^{-6}+St'^{3.9}) \qquad (3.22)$$

$$\text{for} \quad 0.01<St'<0.03$$

The correlation fits the computed data within 7% and it gives very similar values to the experimental correlation of D'Ottavio and Goren (1983) (Table 3.1) for $0.01<St<0.03$ and low values of the Reynolds number.

The total bed efficiency, η, can be computed using a similar procedure as described above for any number of unit cells situated on top of each other. A schematic of a bed made out of 9 layers (4 unit cells) is shown in Figure 3.10. The trajectory starts at $Z=-\sqrt{2}$ and the origin of the system is at $(0,0,0)$ which is the center of the central sphere in the first cell. A particle not collected by the first cell (layers 0-2) leaves it at $Z=\sqrt{2}$. For computation purposes the origin of the coordinate system is then transfered to $(0,0,2\sqrt{2})$ and the trajectory computation continues. From the particle's point of view it is entering the second unit cell. For the computer program the particle is back at the plane $Z=-\sqrt{2}$. The initial conditions at the inlet to the

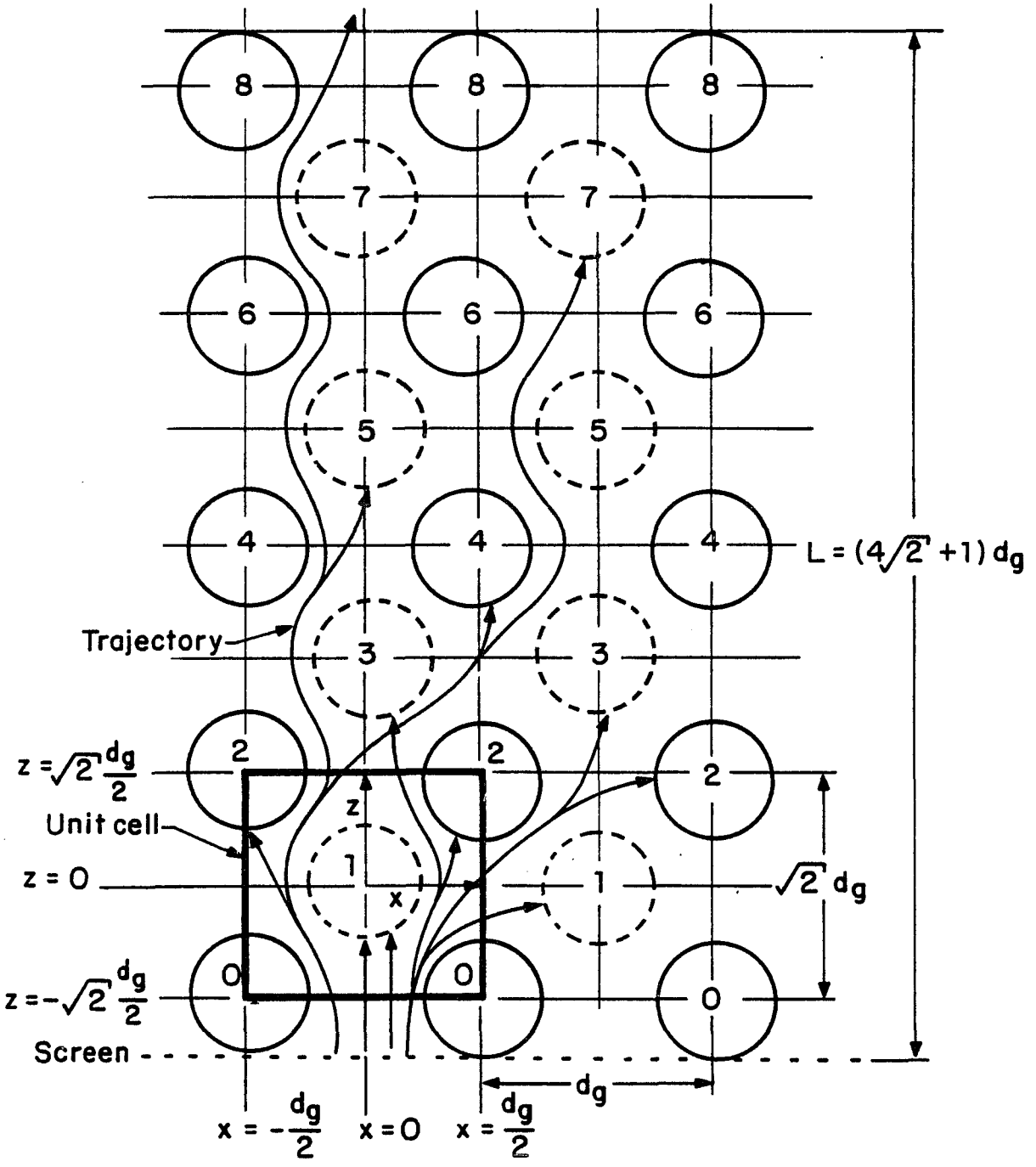

Figure 3.10: Schematic representation of the dense cubic bed containing 9 layers of spheres (4 layers of unit cells). Side view.

second cell are the outlet conditions from the first cell. Hence, for a large number of layers the error introduced by the assumed initial conditions in equation (3.18) at $Z=-\sqrt{2}$ becomes small. If the particle leaves the cell at X=1 the origin is then tranfered to (2,Ø,Ø) and the computation is continued as mentioned above. The computation is stopped when the dust particle is collected on one of the spheres or when it pass through a predetermined number of layers.

The area A_c used in equation (3.2Ø) to obtain the filtration efficiency of an entire bed (E is changed to η) is composed of many subregions in the initial $Z=-\sqrt{2}$ plane corresponding to the many spheres on which the dust particles are collected and this area is shown for St=Ø.Ø18 in Figure 3.11. The nodal points of the grid shown in Figure 3.11 are used as starting points for trajectory computations. From symmetry considerations only 1/8 of the total area A_p has to be searched for particles that are not collected. The computational error depends on the distance between nodal points. The total efficiency, η, for the bed shown in Figure 3.1Ø for Stokes numbers St=Ø.Ø1,Ø.Ø15,Ø.Ø18, Ø.Ø2 using node increments dX=dY=Ø.Ø1 is shown in Figure 3.12. The numerical error in evaluating the integral in equation (3.19) is estimated at less than 5% of the total efficiency based on reducing the increments dX and dY from dX=dY=Ø.Ø2 to dX=dY=Ø.Ø1. On the same figure, the single sphere efficiency calculated from the values of the total

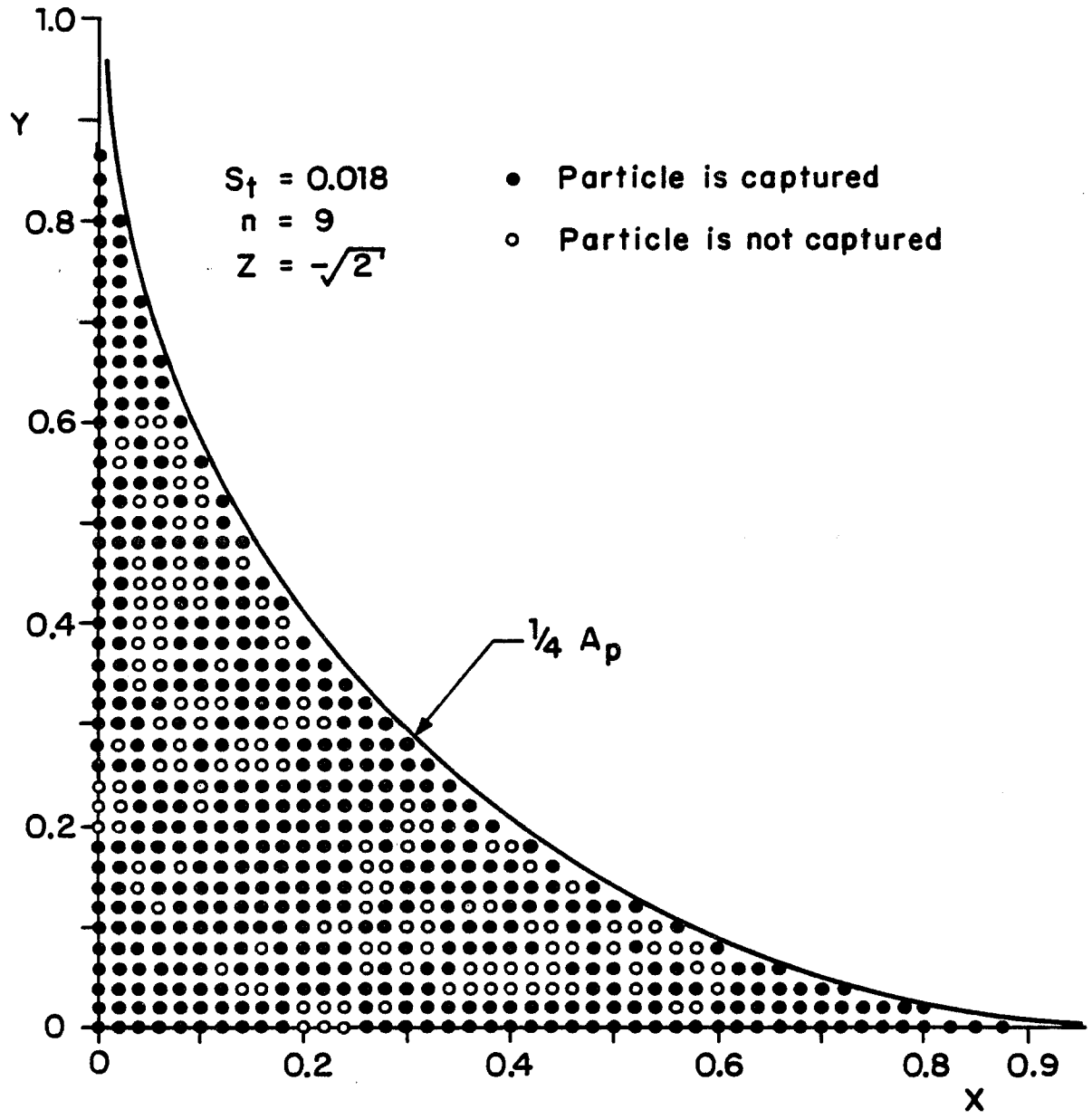

Figure 3.11: Computational grid in the area A_p with $\Delta X = \Delta Y$ = Ø.Ø2 for a 9-layer bed at St=Ø.Ø18.

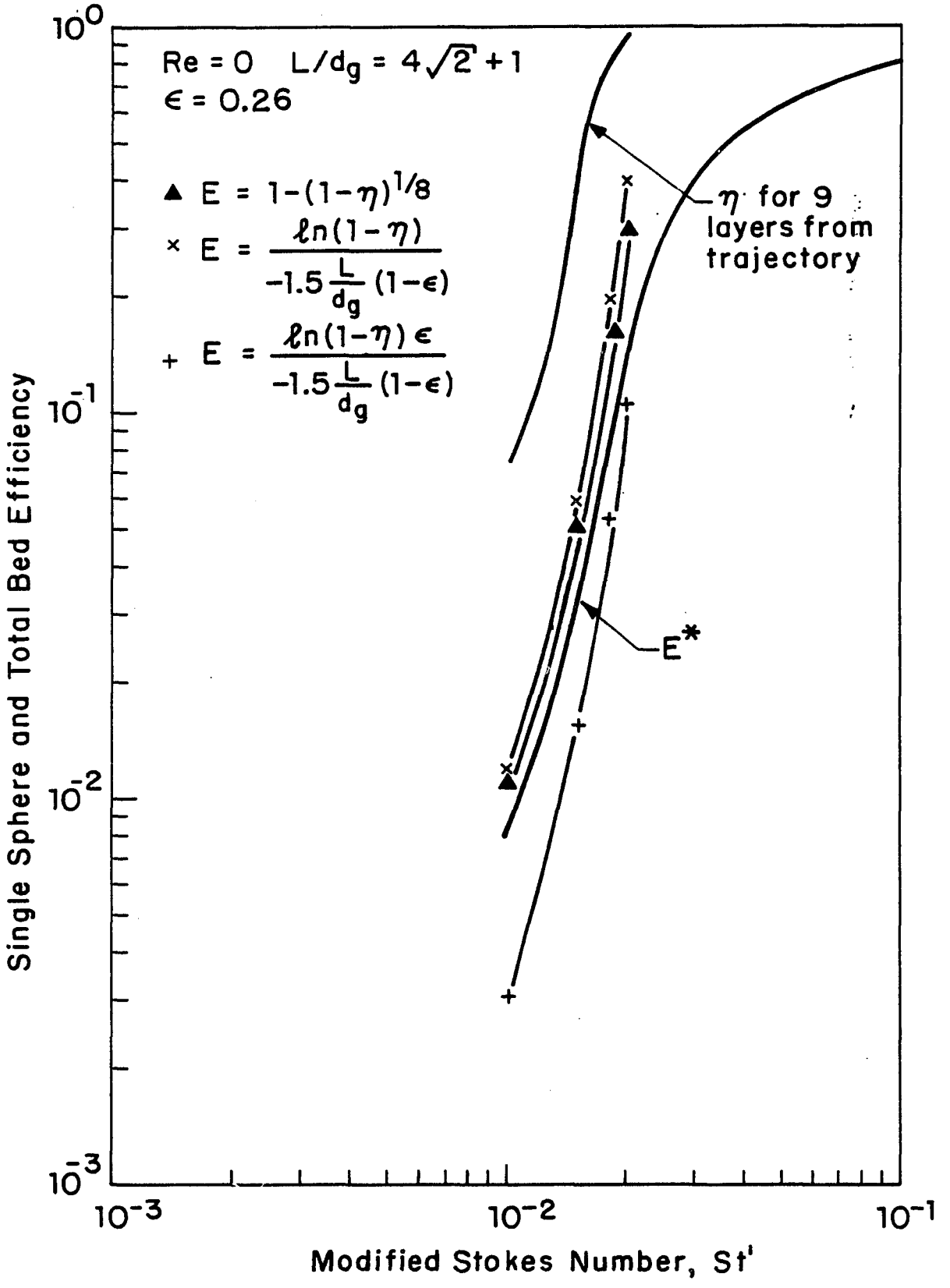

Figure 3.12: Total bed and single sphere efficiencies vs. the modified Stokes number St'.

bed efficiency, η, for 9 layers using equations (2.3) and (2.4) are compared to single sphere efficiencies obtained directly from trajectory computations for the central sphere in a unit cell. Using the assumption that the first layer of spheres contributes very little to the bed efficiency, n-1 should be used as the exponent in equation (2.4). As seen in the figure, equation (2.4) seems to give values which are in slightly better agreement with the values of E^* than equation (2.3) with K_1=1.5. Equation (2.3) with $K_1=1.5/\varepsilon$ is in a good agreement with E^* for St=Ø.Ø18-Ø.Ø2; for lower Stokes numbers, however, the single sphere efficiency is too low. It is not clear from these results whether Eq. (2.3) or Eq.(2.4) is the more appropriate for total bed efficiency calculations and therefore this question will be answered by a comparison with experimental data in the next section.

3.4. Experimental work in dense packed beds

3.4.1. Apparatus and procedure

To examine the validity of the filtration model, experimental research was conducted in which a densly packed cubic bed was used to filter solid latex particles from both an air and a Helium stream. A schematic drawing of the aparatus used in these experiments is shown in Figure 3.13. The bed used was constructed of metallic uniform spheres contained in a rectangular duct where the spheres could be

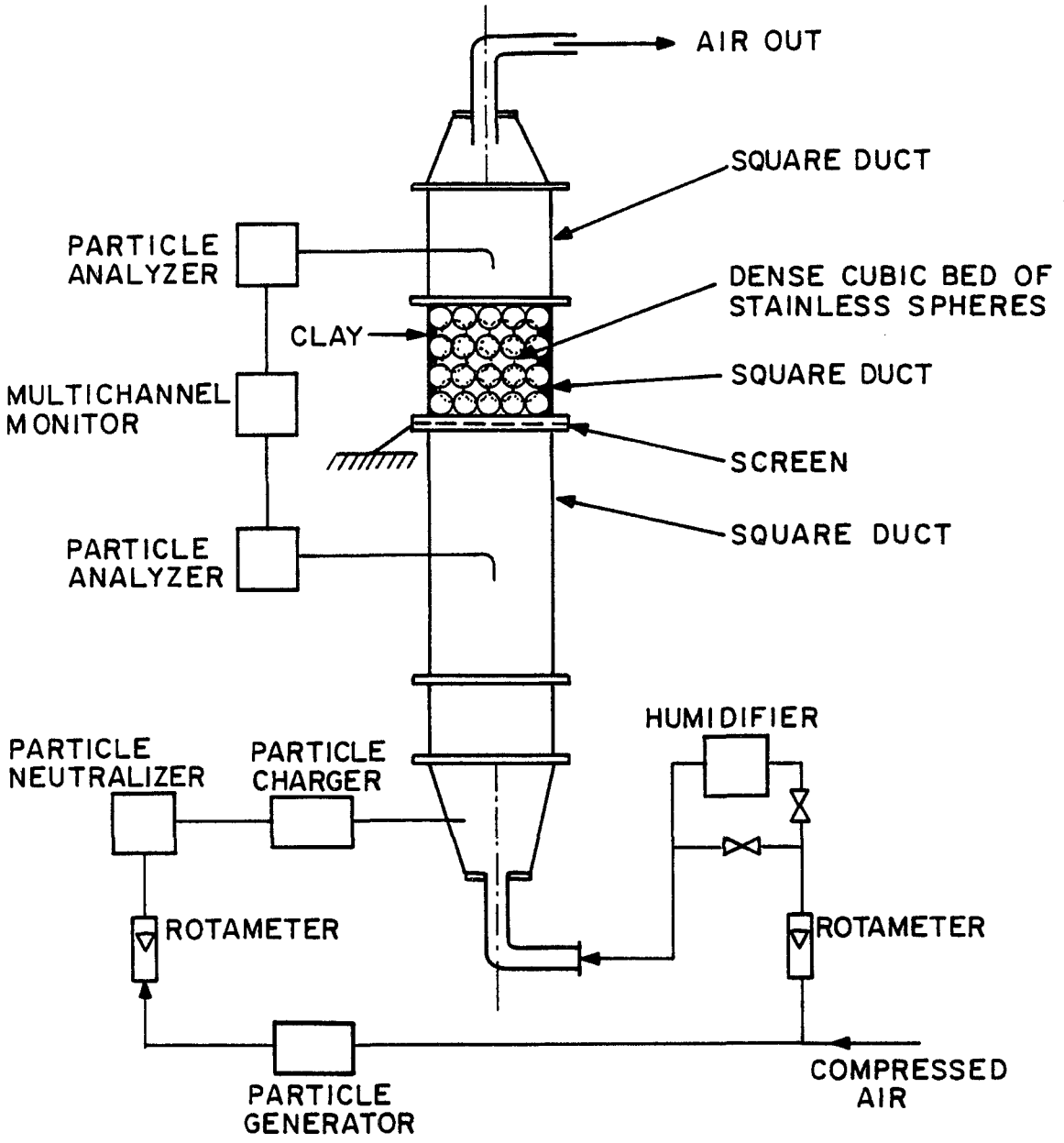

Figure 3.13: Schematic representation of the experimental set-up.

arranged exactly as described by the model (see figure 3.10). The granule diameter d_g was 0.476cm and the cross section area of the duct 5.23x5.23cm^2 to allow for exactly 11x11 spheres in all odd layers. There were 10x10 spheres in even layers and the excess voidage near the wall was blocked by clay to avoid flow along the walls. The actual cross sectional area of the bed was therefore 4.76x4.76cm^2. Experiments with a bed thickness equivalent to 3,9 and 15 layers of spheres (1,4 and 7 unit cells) were conducted. The bed was grounded to avoid buildup of electrostatic charge on the spheres. The granules surface was coated, in most experiments with a DOP layer to reduce bouncing.

Monodispersed latex particles were generated from a solution of pure methanol and their concentration was measured simultaniously at the inlet and outlet of the bed using Climet CI-225 and CI-208S as sensors and a Climet CI-210 as a multichannel monitor. The filtration efficiency was also measured using a Royco-1200 sensor with a Royco-4100 monitor. The data scattered within less than 5%. The gas humidity in the system was controlled and measured and experiments at a relative humidity varying from 0-80% were performed.

The total length of the square duct was 50cm below the bed and 30cm above the bed to allow for fully developed flow in the duct and a good mixing of the aerosol in the gas.

Experiments with gas flowing upwards (as shown in Figure 3.13) and with gas flowing downwards were performed with no apparent difference in filtration efficiency indicating that capture by gravity settling was negligible. The gas velocity was controlled using rotameters and ranged between 40-110 cm/sec for air (Re=120-330) and between 90-270 cm/sec for Helium (Re=35-110).

Filtration experiments for randomly packed bed of glass spheres were also performed to examine the validity of our results for random packings. The experimental conditions were: diameter of the glass spheres d_g=0.125 cm, porosity ε=0.37, air velocities between 25-125 cm/sec (Re=20-100) and a bed thickness of 3.17 cm.

3.4.2. Experimental results and discussion

The total bed efficiency as defined in equation (2.1) was found experimentally and is plotted against Reynolds number in Figures 3.14 and 3.15 and against Stokes number in Figure 3.16. No apparent differences in filtration efficiency were observed for different relative humidities in the range between 0-80% at room temperature. These results indicate that no electrostatic effects were involved and that inertia was the dominant mechanism of filtration during the experiments.

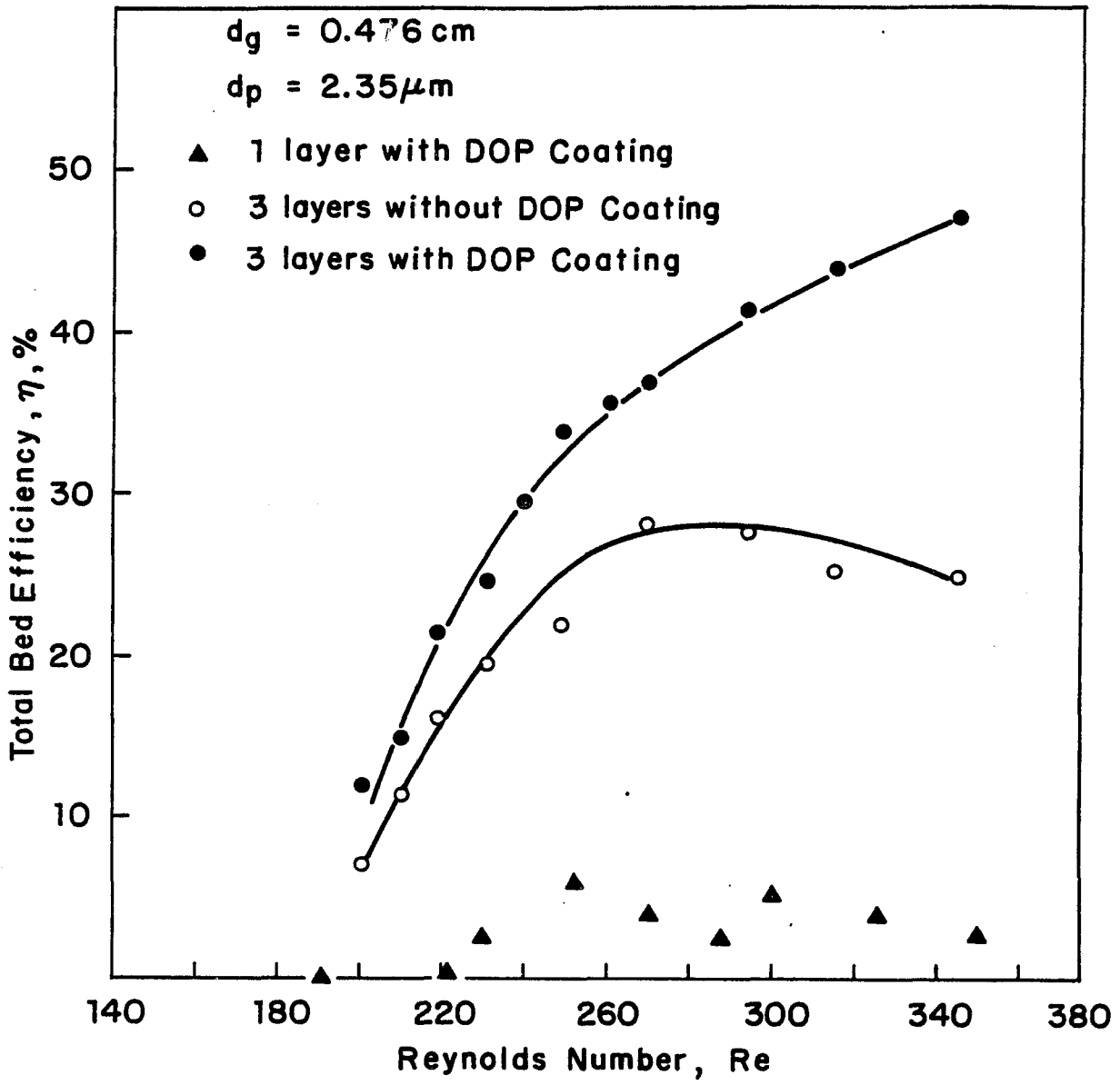

Figure 3.14: Total bed efficiency as a function of Reynolds number for a dense cubic bed of spheres with and without DOP coating.

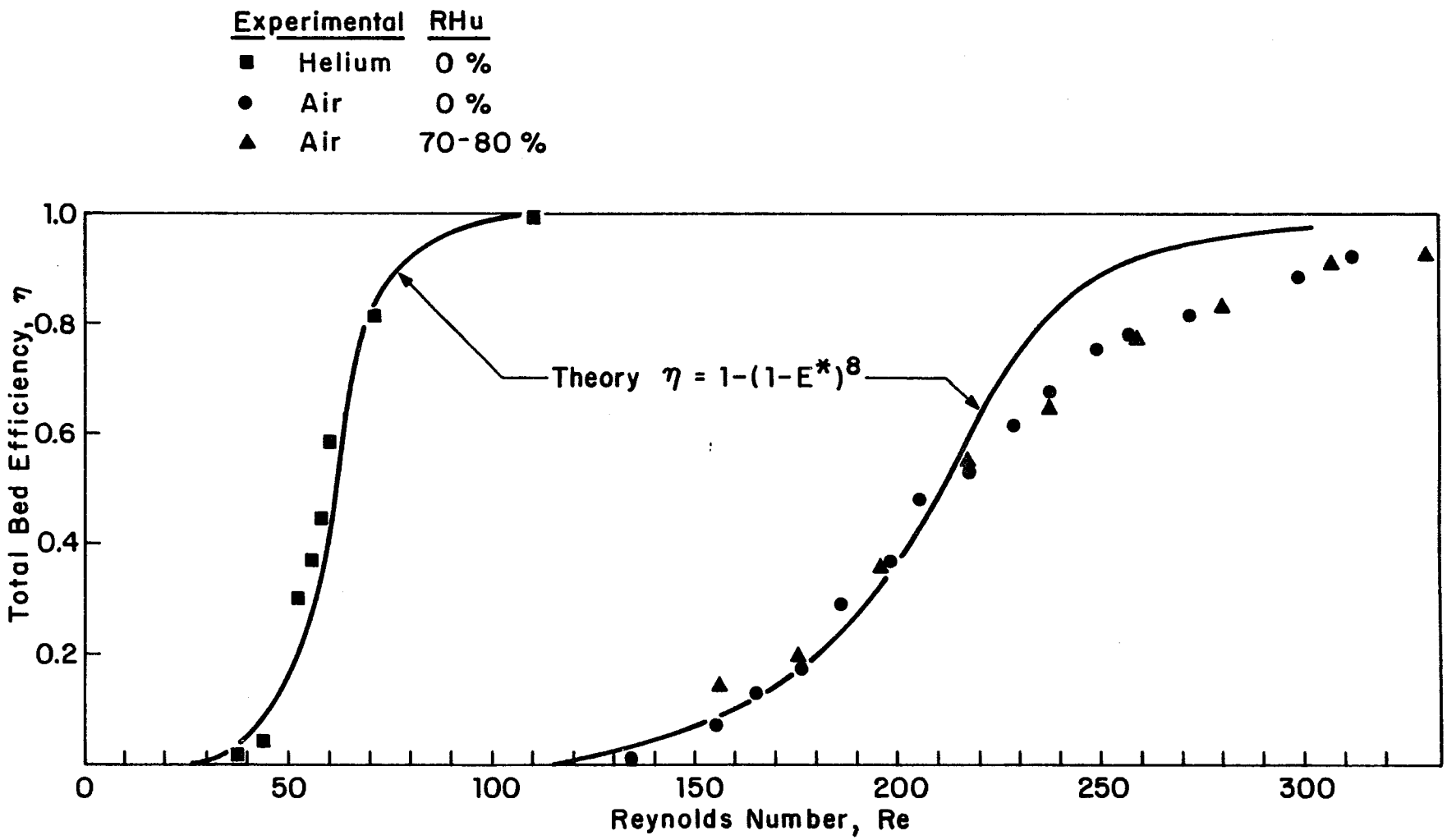

Figure 3.15: Total bed efficiency as a function of Reynolds number for a 9-layer dense cubic bed of spheres. The curves represent trajectory solutions.

In most experiments the spheres were coated with DOP to reduce bouncing. The effect of the coating is shown in figure 3.14. The efficiency of the clean bed (spheres were washed with ethanol) is much lower than that of a bed sprayed with DOP. While the efficiency of the latter bed increases continuously with velocity, the clean bed efficiency reaches a maximum and than drops as the velocity increases. Although coating the granules surface with DOP reduces bouncing significantly it is not clear if bouncing is eliminated completely.

The efficiency of the screen and the first layer of spheres is assumed negligibly small. This assumption was examined by an experiment where only the screen and one layer of spheres were used to filter solid latex particles. The results shown in Figure 3.14 indicate that the assumption is indeed correct; the maximum efficiency of the screen and the one layer of spheres was 6% with most of the results around 4% and lower which is well within the error of the measuring device.

Air and Helium were used in the experiments. Helium has a viscosity similiar to that of air but a density of only about 1/7 that of air. Thus for the same Stokes number, the Reynolds numbers for the experiments with Helium are much smaller than that of air. As shown in Figure 3.15, high

filtration efficiency is obtained using Helium at much lower Reynolds numbers as compared to air. On the other hand, as shown in figure 3.16, higher efficiency was obtained using air at much lower Stokes numbers as compared to Helium. The filtration efficiency therefore must clearly be a function of both the Stokes and the Reynolds numbers. The parameter St', which was defined in eq. (3.17), is the proper variable which combines these two parameters. The filtration efficiency plotted against the Stokes number, St, and the modified Stokes number, St', are both shown in Figure 3.16. The experimental results as a function of St' are compared to the theoretically predicted curve using trajectory computations for the total bed composed of 9 layers of spheres. Also shown in the figure is the curve predicted by trajectory computations for the single sphere efficiency which has been converted to total bed efficiency using equation (2.4). As seen the experimental results agree well with those predicted by both models for the range of Stokes numbers between $Ø.ØlSt'Ø.Ø2$. For $St'>Ø.Ø2$ the model seems to overestimate the efficiency. The difference may possibly be explained by the fact that at higher Stokes numbers the Reynolds numbers are also higher due to the larger gas velocities and the flow field becomes less accurate.

Clearly, the Helium experiments which were performed at lower Reynolds numbers agree better with the model (the upper curve in Figure 3.16) than the experiments performed

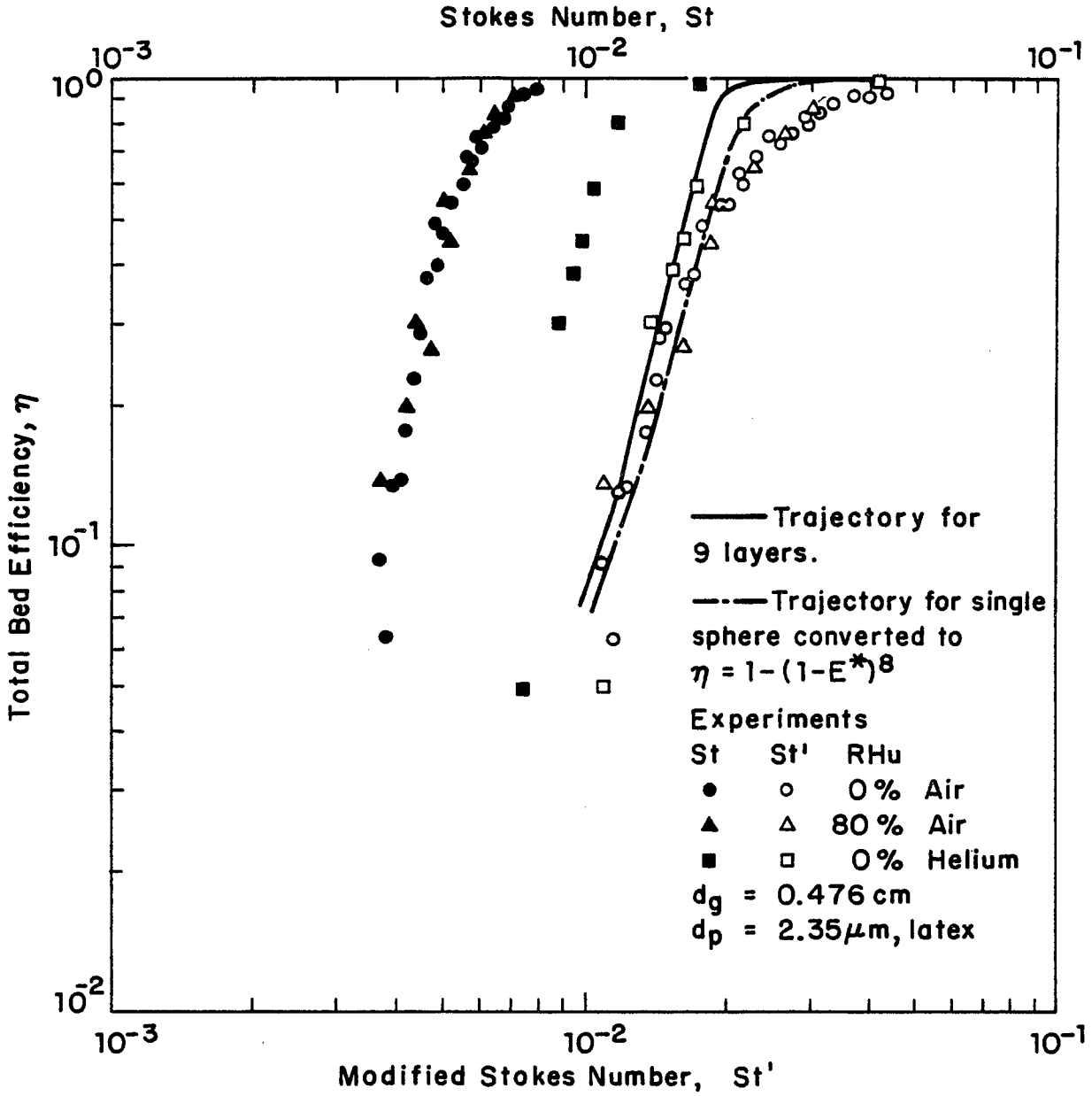

Figure 3.16: Total bed efficiency as a function of Stokes number and modified Stokes number for a 9-layer dense cubic bed of spheres. The curves represent trajectory solutions.

with air. Bouncing may also be a factor in the lower experimental efficiencies observed. The coating of the surfaces of the spheres by spraying DOP before the experiment reduces bouncing significantly (see Figure 3.14) but may not eliminate bouncing completely. Bouncing increases as the kinetic energy of the solid dust particle increases (D'Ottavio and Goren 1983). The bouncing is also more apparent when the filtration efficiency is high. Thus, at higher values of the parameter St', where the kinetic energy of the dust particle is high, the deviation of the experimental results from the model predictions should be more significant.

A comparison between the experimental results and the single sphere efficiency, E^*, as predicted by trajectory computations is given in Figures 3.17-3.19. Experimental results using 3,9 and 15-layer beds are shown. The single sphere efficiency for constant St' is independent of the number of layers in the bed. In Figures 3.17 and 3.18 equations (2.4) and (2.3) with K_1=1.5 are used. Both show a very good agreement with the predicted values up to St=Ø.Ø2. For St>Ø.Ø2 the experimental results are lower than predicted as discussed above. In figure 3.19, equation (2.3) with $K_1=1.5/\varepsilon$ is used. The large difference between the predicted and experimental results suggests a significant inaccuracy in using $K_1=1.5/\varepsilon$ in Equation (2.3).

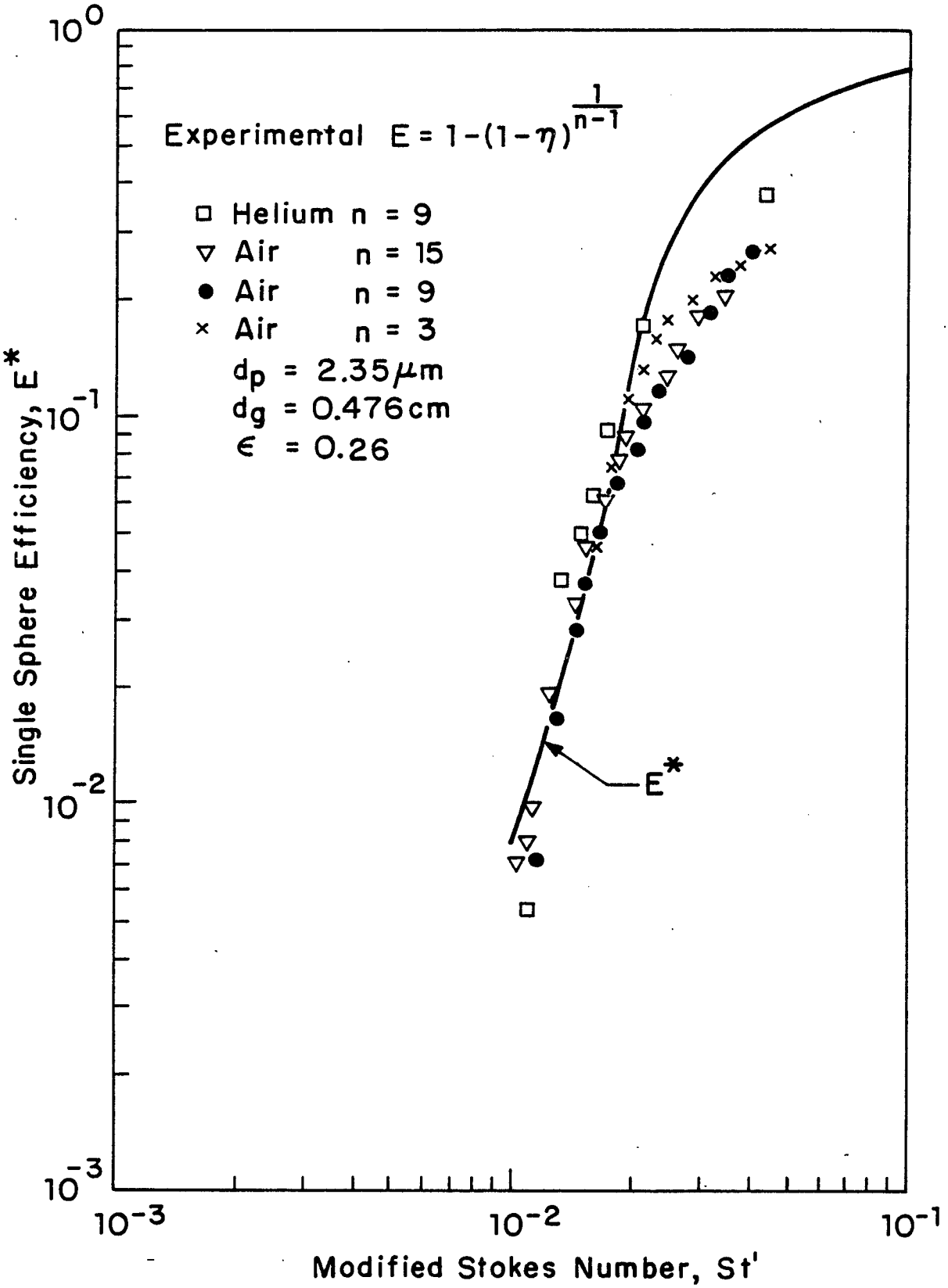

Figure 3.17: Single sphere efficiency as a function of the modified Stokes number; theoretcal prediction and experimental data.

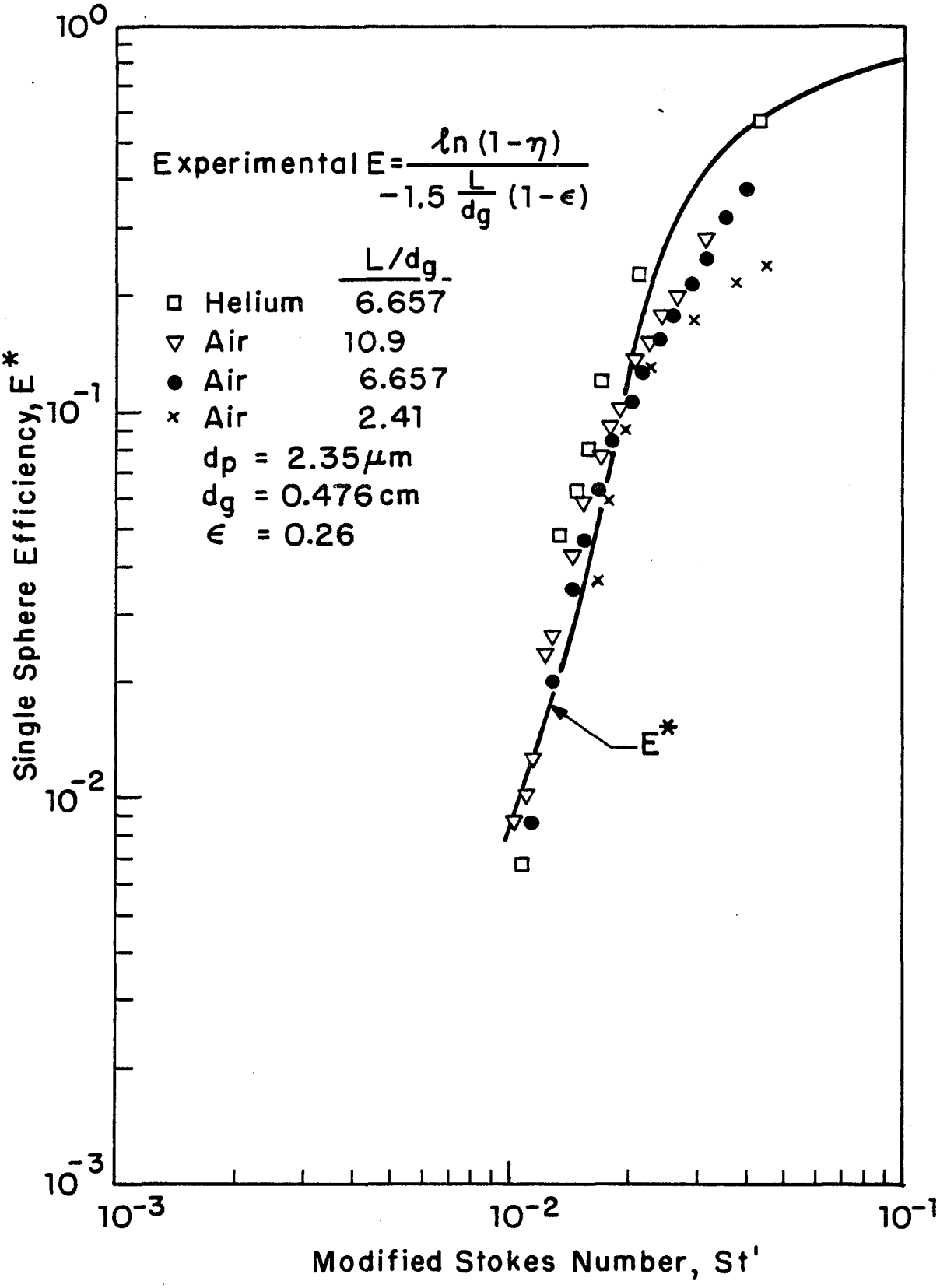

Figure 3.18: Single sphere efficiency as a function of the modified Stokes number; theoretical prediction and experimental data.

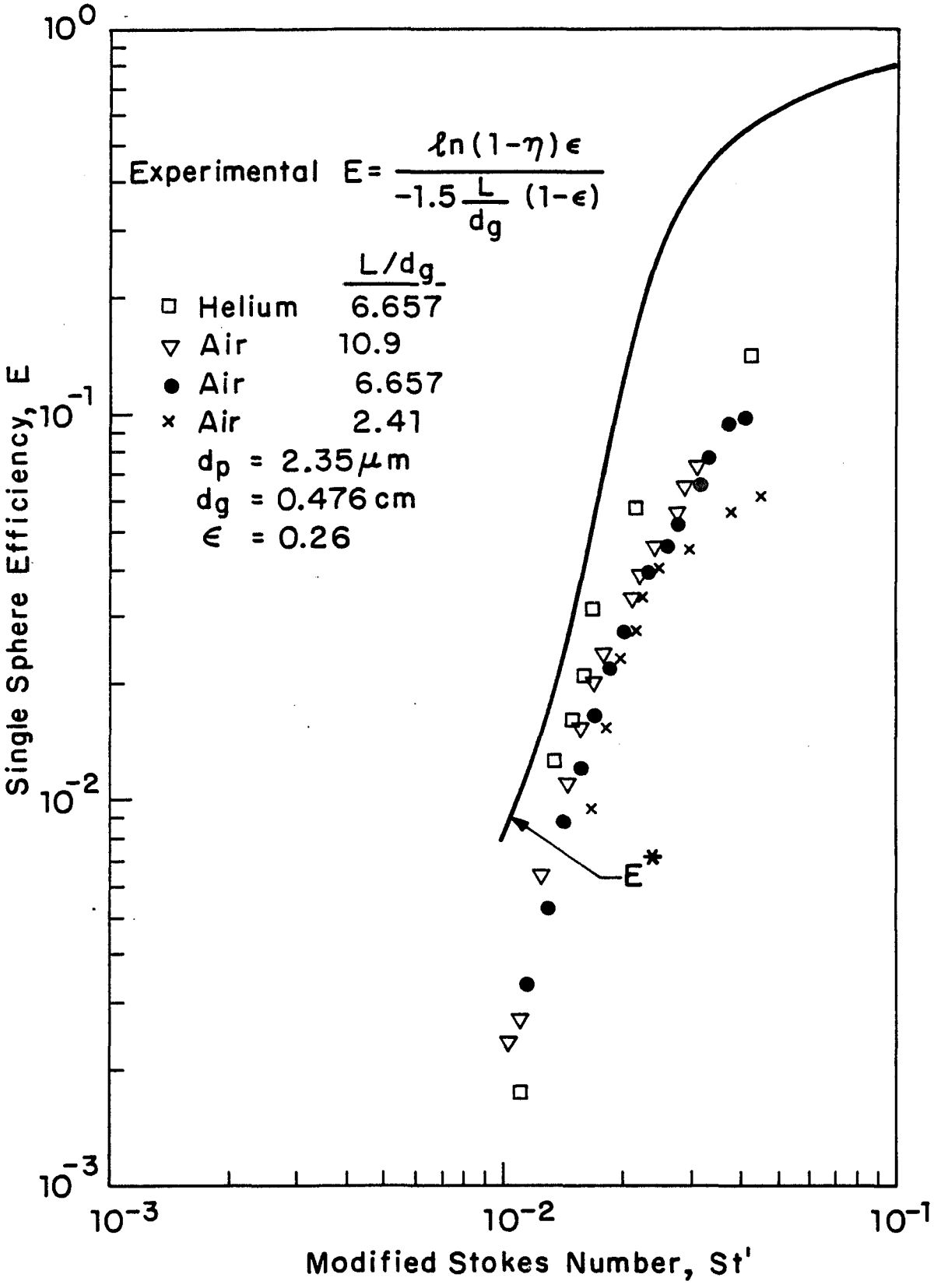

Figure 3.19: Single sphere efficiency as a function of the modified Stokes number; theoretical prediction and experimental data.

Lastly the theoretical model is compared to filtration efficiencies obtained in randomly packed beds with different granule sizes and porosities. In a recent paper, D'Ottavio and Goren (1983), found an experimental correlation between the effective Stokes number St_{eff} defined as

$$St_{eff}=f(Re, \varepsilon)xSt/2 \qquad (3.23)$$

and the filtration efficiency. Their experiments were performed using randomly packed beds with Re=13-162Ø and porosities ε=Ø.33-Ø.38. A comparison between D'Ottavio and Goren's correlation (given in Table 3.1) for ε=Ø.33 (the lowest porosity in their experiments) and our theoretical predictions for the single sphere efficiency in a dense cubic packing is shown in figure 3.2Ø. As seen, there is a good fit between the two correlations for Reynolds numbers as high as Re=6Ø; as the Reynolds number increases to 14Ø, however, there is an appreciable discrepency between the two.

Results for experiments using randomly packed beds of glass spheres (ε=Ø.37,d_g=Ø.125 cm) to filter 1.1μm and 2.35μm latex particles are shown in Figure 3.21. There is a reasonably good agreement between the experimental data and the theory for both particles sizes. The somewhat lower filtration efficiencies observed for the larger particles may be due to bouncing since their mass and hence their

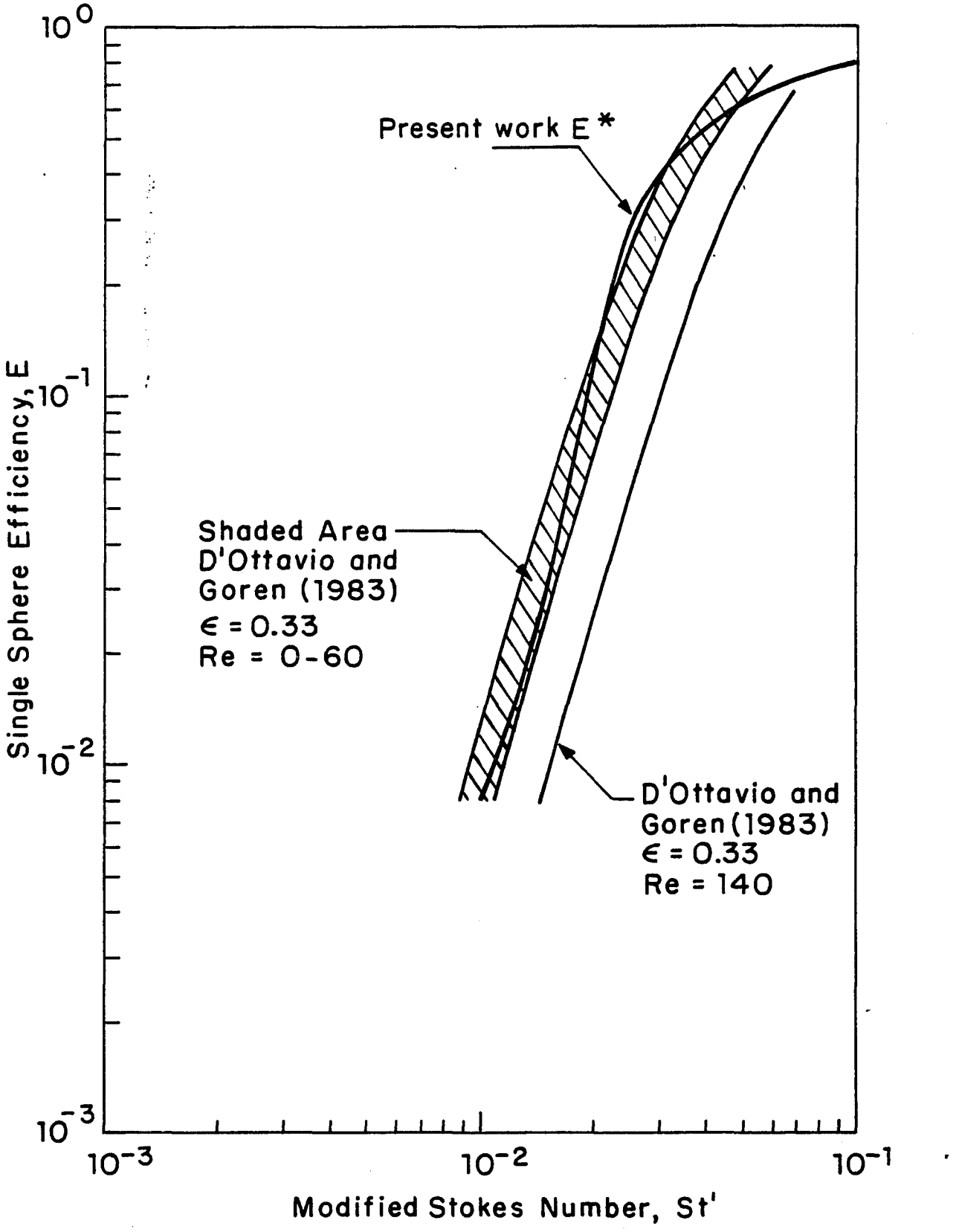

Figure 3.20: Single sphere efficiency as predicted for a dense cubic packing compared to an empirical correlation for a randomly packed bed ε=0.33, Re=0-60, 140, from D'Ottavio and Goren (1983).

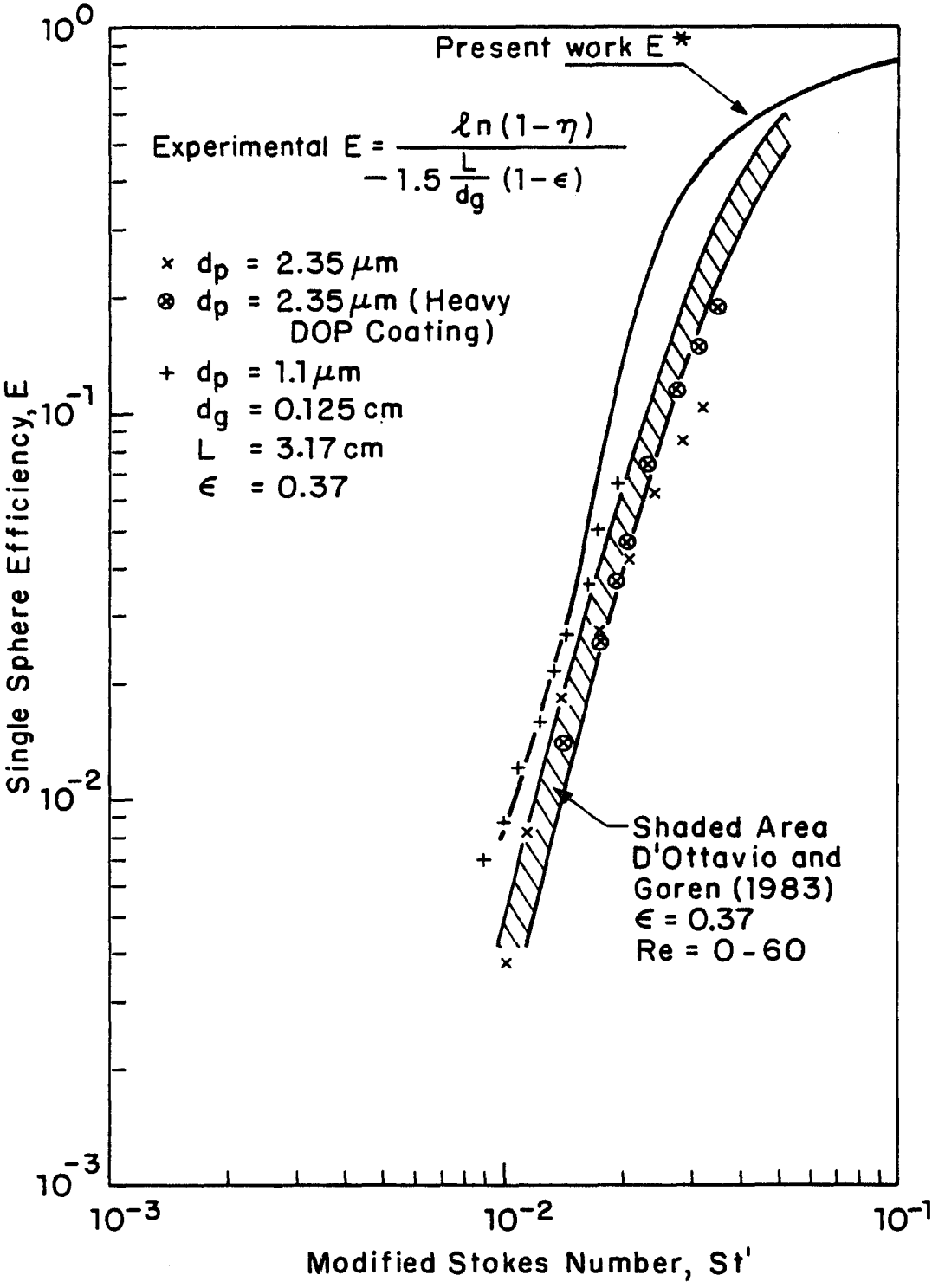

Figure 3.21: Single sphere efficiency as predicted for a dense cubic packing compared to an empirical correlation for a randomly packed bed ε=Ø.37, Re=Ø-6Ø, from D'Ottavio and Goren (1983), and experimental data.

kinetic energy is about 10 times that of the smaller particles.

3.5. Conclusions

A filtration model predicting both single sphere and total bed efficiency was developed for a dense cubic packing using the flow field developed by Snyder and Stewart (1966). The model is based on the trajectories of dust particles inside the granular bed and assumes no bouncing of dust particles from the surface of the granules. The filtration efficiency was found to be a function of both the Stokes and Reynolds numbers through a modified Stokes number St' defined as St'=StxF where the factor F=1+0.0157Re is derived from the well accepted Ergun correlation.

The present work is the first in which a three dimensional flow field is used for the evaluation of filtration efficiency in granular bed. Trajectory calculations were performed for both a single sphere in the bed and an entire bed. The trajectory calculations for the total bed are compared to the trajectory calculations for a single sphere through the use of equation (2.3) and equation (2.4) and show a good agreement indicating that the single sphere approach for predicting the total bed efficiency is valid.

The model predictions agree very well with

experimental results obtained using a dense packed bed of spheres at Re<200 and 0.01<St'<0.02 and reasonably well at Re<200 and 0.02<St'<0.03. The model predictions also agree well with the experimental correlation by D'Ottavio and Goren (1983) and with our own experimental data for randomly packed beds at low porosities and low Reynolds numbers.

As the kinetic energy of a dust particle increases, either by increasing its velocity or its mass, the deviation of the experimental data from the curve predicted by the model increases and the experimental results are always lower suggesting that bouncing occurs. This phenomena was not considered in the theoretical model.

3.6. Recomendations for including electrostatic effects

It was shown that inertial effects are strong for modified Stokes numbers St'>0.01. For smaller Stokes numbers inertial effects are weak. To increase the filtration efficiency for the lower range of Stokes numbers, electrostatic effects have to be utilized. Charging the dust particles in a corona charger and using dielectric spheres (ceramics, sand, glass or plastics) will result in a higher filtration efficiency. The expected higher filtration efficency is the result of the forces between a charged particle and the charges induced on the spheres in the bed.

The theoretical solution procedure for such a system is similar to the one obtained for inertial effects in section 3.2. To account for the electrostatic effects equation 3.12 should include the electric parameter:

$$\frac{d^2\vec{X}}{dT^2} = \frac{1}{StF}\left(\vec{U} - \frac{d\vec{X}}{dT}\right) + \sum_{j=1}^{m} K_{icj}\,\vec{e}_j \qquad (3.24)$$

where K_{icj} is the parameter for the charged particle image force when the particle only is charged and charge separation is induced in the collector (see table 2.1).The parameter j relates to the jth sphere in the cell on which charge is induced. The charged particle entering a unit cell induces image charges on all spheres in the cell and the the effect of all the resultant forces should be accounted for. It is most likely that the dominant force is that of the closest sphere and that the other forces are insignificant. The direction of each force, $\vec{e}_j$, is towards the center of each of the spheres causing it.

4. A STUDY OF THE ROTATING FLUIDIZED BED FILTER

4.1 Introduction

In recent years, with increasing emphasis on reducing particulate emission especially that of small submicron particles from hot and corosive atmospheres, there is a growing interest in the possible use of granular bed filters for the filtration of micron and submicron particles.

In granular bed filters (fixed, moving and fluidized beds) the granules are used as the filter media. The contaminated gas stream containing small solid or liquid particles is passed through the bed granules on which the dust particles are collected.

The fixed bed filter is the simplest, best understood and the mostly studied. Many studies have been reported in the literature in which a fixed granular bed is used to filter fine particles from a gas or liquid stream. Some of these studies have been summarized by Paretsky(1972), Jackson(1974), Payatakes et al(1974), McCarthy et al(1976), Clift and Thambimuthu (1977), Tardos and Pfeffer (1979) and Tien and Payatakes (1979) and recently by Clift (1984). The main problem in using a fixed granular bed is the removal of collected particles from the filter bed. If the dirty granules are not removed periodically the bed becomes

saturated, filtration efficiency drops and pressure drop increases. The regeneration problem has been overcome by use of continuously operating filtration systems such as the panel bed filter (Squires and Pfeffer, 1970; Paretsky et al, 1971; Paretsky, 1972; Lee, 1975) and the Ducon filter (Zenz and Krockta, 1972; Kalen and Zenz, 1973). As pressure drop in these systems increases, as a result of dust accumulation, the beds are cleaned by a backflush pulse of gas. The dust, combined with some bed material, is removed and collected in a collection hopper. The system can operate continuously with only few of the stages backflushed at a time.

Other types of continuously operating granular beds are fluidized beds (Black and Boubel, 1969; Doganoglu and Clift, 1974; Krupp-Kopper, 1974; Patterson and Jackson, 1977; Tardos et al, 1978), moving beds (Geffken et al, 1978) spouted beds (Meisen and Mathur, 1974; Balusubramanian et al, 1978) and the fluidized bed cross-flow filter (Tardos, 1977; Gutfinger et al, 1977). In these systems the bed material is removed continuously and a steady state can be maintained with respect to dust accumulation.

In fluidized bed filters the gas to be filtered is used as the fluidization medium. The fluidized collector particles can be removed and replaced continuously with no operating difficulties. Improvements in filtration

efficiency can be obtained by using a multistage fluidized bed (McCarthy et al, 1976; Patterson and Jackson, 1977), a lubricated fluidized bed that reduces bouncing of dust particles (Jugel et al,1970) and electro-fluidized bed that has a higher efficiency due to electrical forces between the granules and particles (Johnson and Melcher, 1975; Zahedi and Melcher, 1976, 1977; Melcher et al, 1977; Snaddon 1981). A similar effect of increasing filtration efficiency can be obtained by triboelectrification using fluidized beds of dielectric material as the filtering media (Gutfinger and Tardos, 1979; Tardos et al, 1979).

Although it has been found that high collection efficiency could be obtained in a continuously operating fluidized bed filter (Knetting and Beekman, 1974; McCarthy et al, 1976; Patterson and Jackson, 1977; Gutfinger and Tardos, 1979) the fluidized bed dust filter has failed to gain industrial acceptance. This is mainly because fluidized bed filters are limited to operation at velocities no higher than 1.2 to 1.5 times the minimum fluidization velocity and, therefore, require very large surface areas to handle the high gas throughputs typically found in industrial applications. Operating at velocities higher than the minimum fluidization velocity leads to by-passing of gas in the form of bubbles, and consequently to poor collection efficiency (Scott and Guthrie, 1959; Black and Boubel, 1969; Tardos, 1977; Patterson and Jackson, 1977).

To overcome the limitations of operating the fluidized bed filter at velocities of the order of the minimum fluidization velocity and thus achieving higher gas throughputs, Pfeffer and Hill (1978) and Gal et al (1982) suggested the use of the rotating fluidized bed as a filter device. In a rotating fluidized bed the drag force of the gas acting on the bed particles is balanced by the centrifugal forces caused by the rotation. Formation of bubbles can be avoided in pricipal at any gas flow rate by increasing the rotating speed of the bed. High filtration efficiency in the rotating fluidized bed is obtained mainly due to inertial impaction which is a result of the high velocity through the bed and electrostatic effects which is the result of triboelectrification. The rotating fluidized bed filter (RFBF) has the advantages of high filtration efficiency, continuous operation and high flow rates of gas per unit area of distributor; thus it appears very attractive for industrial application.

4.2 Description of apparatus and procedure

A rotating fluidized bed similar to the ones described by Lindauer et al (1966), Levy and Chen (1977) Metcalfe and Howard (1977) and Levy et al (1981) was used to perform experiments in our laboratory to determine the feasibility of using such a device to seperate small micron and

submicron particles from a contaminated gas stream. The RFBF is essentially a vertical cylinder with porous walls which rotates around its axis of symmetry. Filter material in the form of granules is introduced into the cylinder and is forced to the wall due to the large centrifugal forces produced by the rotation. The wall serves as the gas distributor and the gas flows radially inward through it and through the bed of granules. When the drag forces on the granules balance the centrifugal forces, the bed becomes fluidized. Minimum fluidization can be achieved at any gas flow rate by changing the rotating speed of the bed. The rotating fluidized bed permits much higher flow rates per unit area of the distributor than are possible in conventional fluidized beds which operate only against the force of gravity.

4.2.1 The semi-batch system

The rotating fluidized bed is shown schematically in Figure 4.1 and in detail in Figure 4.2. The apparatus consists of a Ø.2m diameter, Ø.3m high distributor contained in a cylindrical plenum. The cylinder's lateral wall is perforated (43% open area) and has 456 holes each 3/8 inches in diameter. The wall is covered from the inside by 16 to 4Ø mesh screens depending on the size of granules used. The distributor (cylinder and screen) can be rotated at rotational speeds which can vary from 34Ø to 75Ø RPM. This

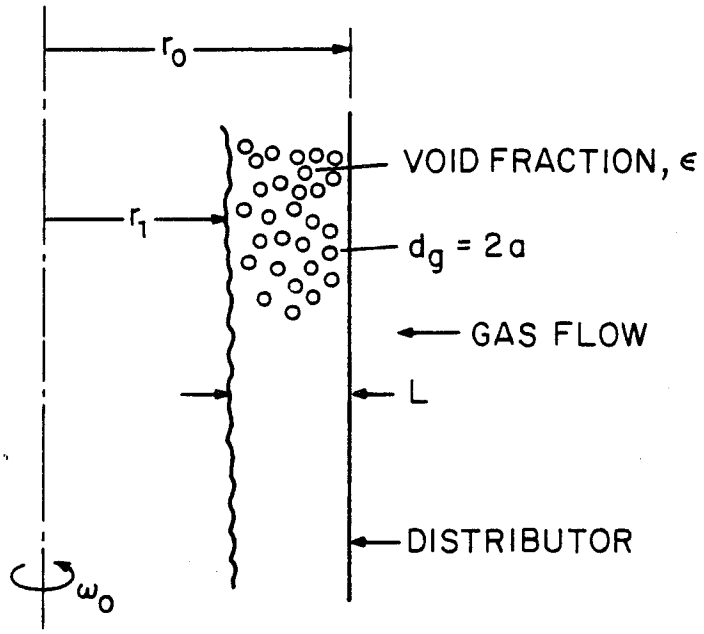

Figure 4.1: Schematic of the bed in the rotating fluidized bed filter.

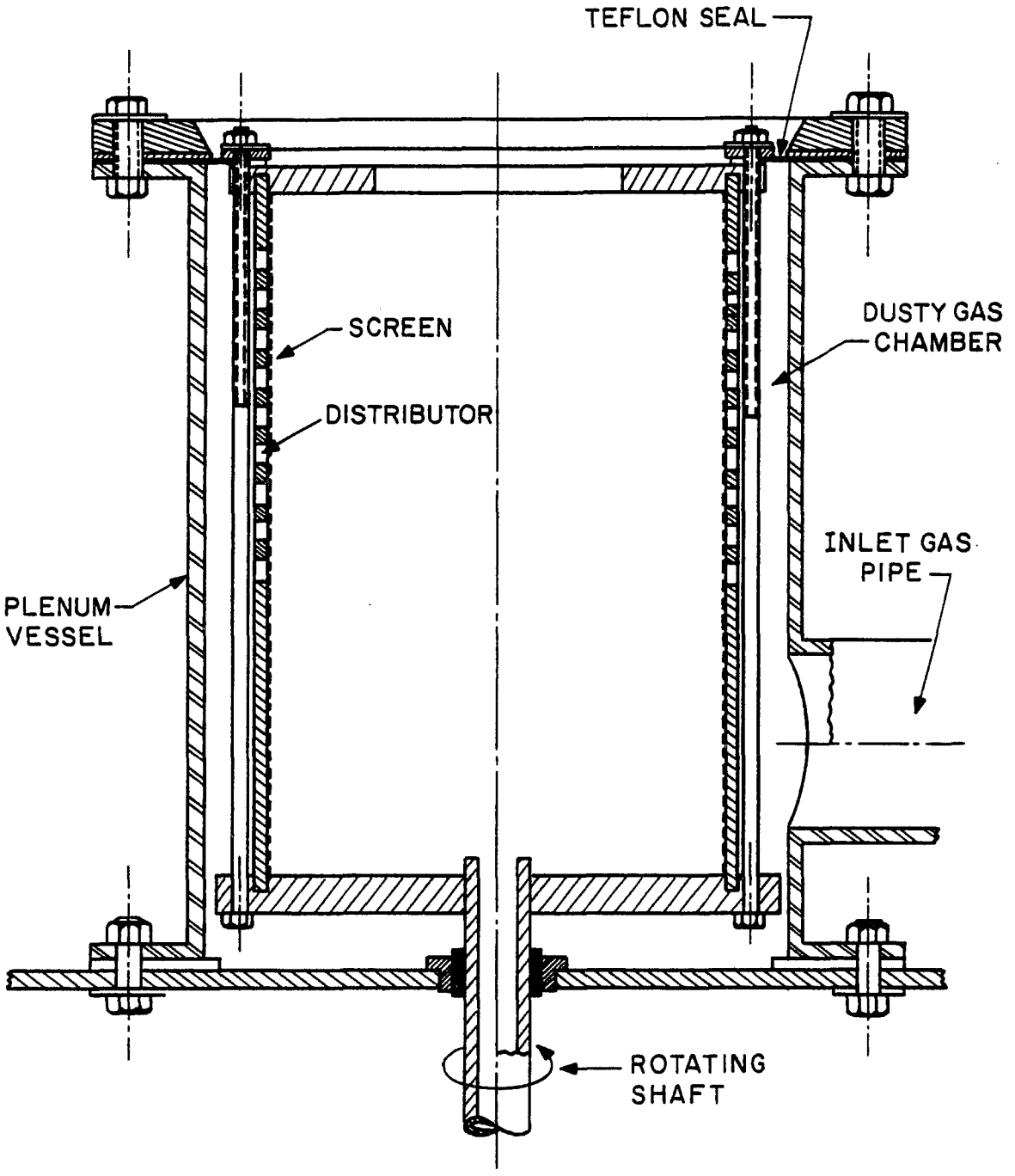

Figure 4.2: The rotating fluidized bed filter.

corresponds to radial accelarations of 13 to 63 g's. Room air is supplied to the plenum from a compressor and the flow rate is determined both by a rotameter and by measuring the centerline velocity in a long four inch pipe using a pitot tube. Liquid aerosol of dioctylphtalate (DOP) is introduced into the inlet air using a Royco 258 smoke generator and particle concentration is measured using a Climet particle size and concentration monitoring system; 99% of all liquid aerosol particles (the DOP) is in the Ø.3-3.Ø micrometer range. Solid aluminum silicate particles in the size range between Ø.3-1Ø.Ø micrometers, are also used. The solid dust is injected pneumatically into the air stream using a homebuilt generator containig a screw feeder and an ejector. A typical number distribution and particle surface area distribution of the liquid and solid aerosols used in the experiments are shown in Figure 4.3. The number distribution is measured by the Climet particle counter and the surface area distribution is found by multiplying the fraction of particles in each size range above by the average surface area of a particle for the same size range.

The set of experiments described here are batch with respect to the collector granules (the granules were not replaced during each experiment), while the air is flowing continuously. The following procedure is used for the experiments:

1. A given charge of bed material or granules is loaded into

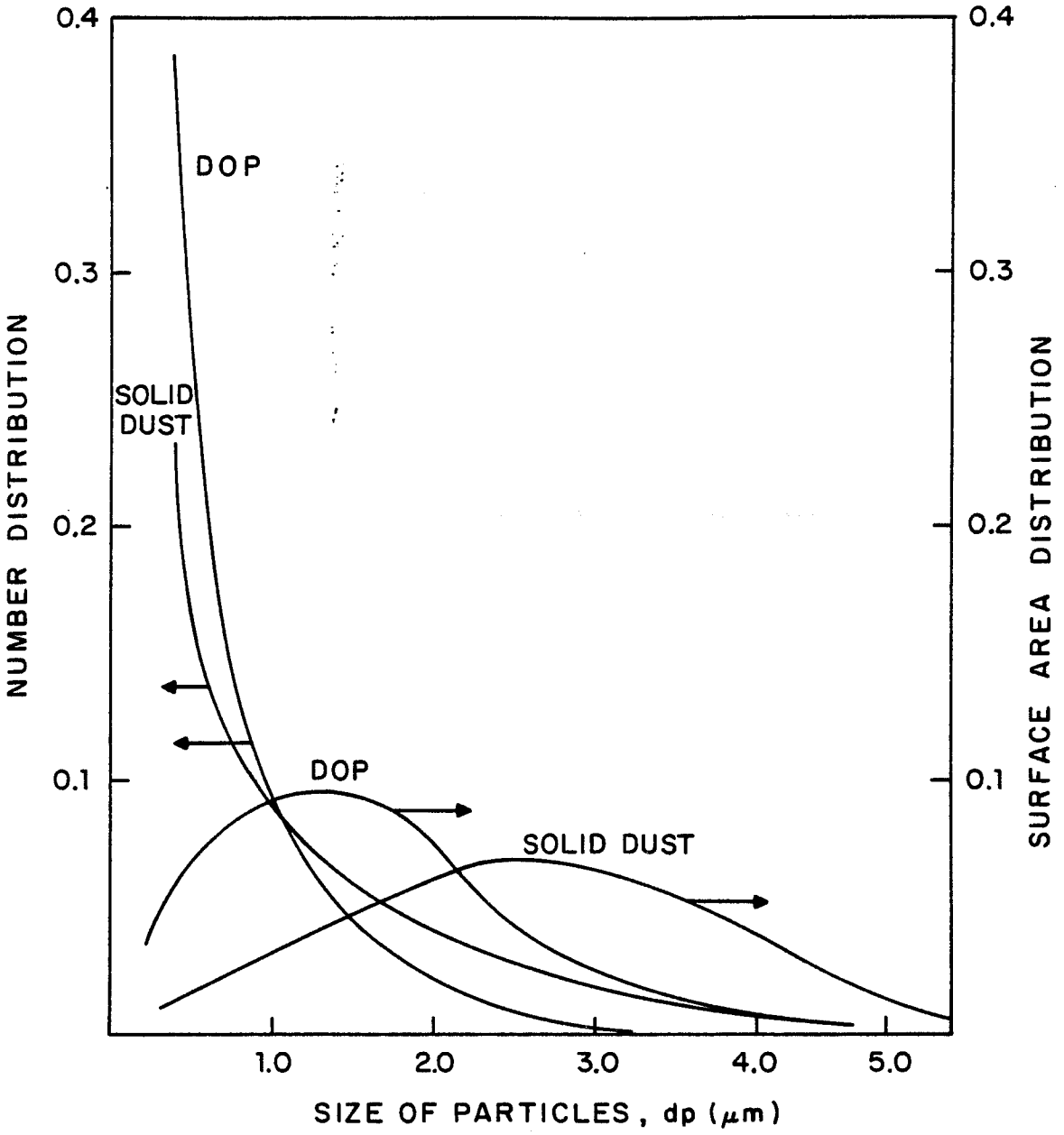

Figure 4.3: Typical number and surface area distribution of DOP aerosol and solid dust used.

the system.

2. The distributor is accelarated from rest to the lowest angular velocity (350 RPM). The free surface of the bed assumes the shape of a paraboloid of revolution.
3. The compressor is turned on and air flows through the system and through the bed material. The flow rate is increased to a level where the velocity is above minimum fluidization. Particles climb up the wall, assuming a cylindrical annular shape. In all experiments, including those performed in the fixed bed region, fluidization is obtained first to insure uniform bed thickness.
4. The angular velocity is set to the desired level.
5. Filtration starts with the introduction of liquid aerosol or solid dust to the air stream. The number and size of dust particles at the bed inlet and outlet are measured to obtain the bed filtration efficiency.

Relative humidity of the air flowing through the system is measured by a Phys Chem Hygrocon 1. The relative humidity is not controlled and it depends on the weather. During the period of the experiments described here the relative humidity varied in the range of 0-48%.

4.2.2. The continuous system

The batch system described in the section above is also used in the continuous experiments with the addition of a

granule feeding and discharge system. The contiuously operating rotating fluidized bed system is shown in Figure 4.4. The feeding system includes a hopper, a screw feeder and a source of compressed air. The clean particles are forced pneumatically to the surface of the bed by the high pressure air stream (about 15 psig), at a rate determined by the screw feeder at the bottom of the hopper.

The discharge system is composed of a baffle in the bed and an inertial separator. As the radial velocity of the gas through the granules increases above minimum fluidization, particles are forced to the center of the cylinder and from there out of the filter in the gas stream. Carry-over of particles from the bed is usually very small but can be increased by the baffle (see Figure 4.4) which stops the rotation of some granules. The centrifugal force on these granules is small and the drag force can easily carry them downstream to the impactor seperator were they are seperated from the clean air. The distance between the edge of the baffle and the screen is adjustable and determines the thickness of the bed. Thus changing the feed rate of granules does not effect the bed thickness but it reduces the average residence time of the granules in the bed.

The rotating fluidized bed operating above minimum fluidization velocity is well mixed so that new incoming clean particles are mixed in the bed and have the same

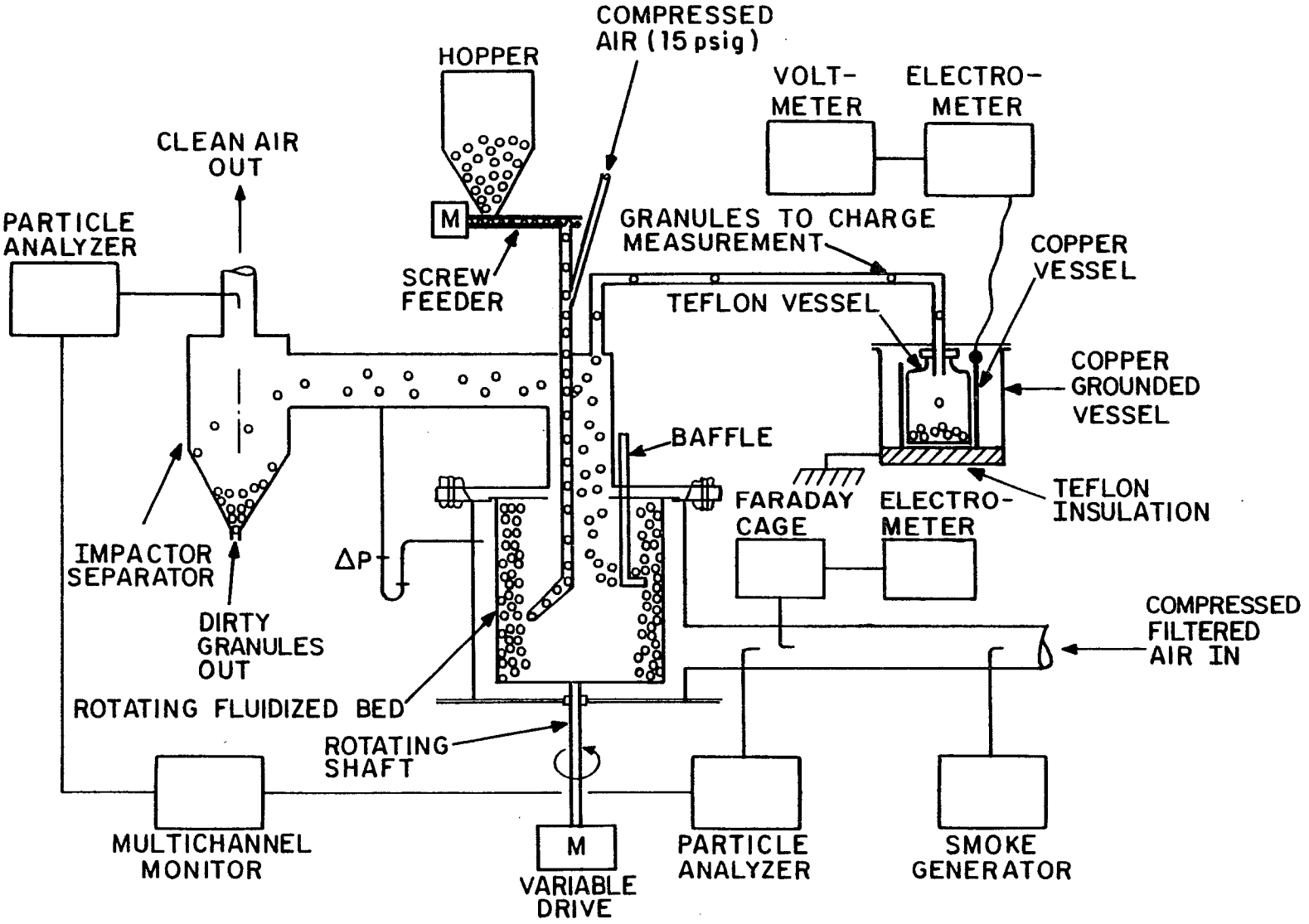

Figure 4.4: The rotating fluidized bed filter experimental set-up.

average residence time as the rest of the granules. The rate of mixing was not determined quantitatively during this study but observation shows that as a bed of initially all white polyethylene granules (diameter Ø.3 cm, density Ø.97 gr/cm^3) is fed with black polyphenylene granules (diameter Ø.3 cm, density 1.Ø3 gr/cm^3), the content of the bed changes rapidly. As about three bed volumes of granules are replaced the bed material becomes mainly black polyphenylene particles.

4.3. Pressure drop and minimum fluidization velocity

In a rotating fluidized bed operated at high enough rotational speed the bed assumes the shape of a cylindrical annulus (Levy et al, 1978). The pressure drop and minimum fluidization velocity in such a bed can be obtained by using classical relationships found in literature for ordinary fluidized beds by replacing the acceleration of gravity, g, in these relationships by the radial acceleration, a_r, produced by the rotation of the distributor. The local pressure drop across an ordinary fluidized bed is given by:

$$dp/dr = (1 - \varepsilon)(\rho_g - \rho_f)g = (1 - \varepsilon)\rho_g g \qquad (4.1)$$

where ε is the void fraction, ρ_g is the density of the fluidized granules and ρ_f is the density of the fluidizing gas. Replacing g by the radial acceleration, a_r, in equation

4.1 gives:

$$dp/dr = (1 - \varepsilon)\rho_g a_r = (1 - \varepsilon)\rho_g U_t^2 / r \qquad (4.2)$$

where U_t is the local tangential velocity. Equation 4.2 can be integrated in two different ways:

a. Assuming the tangential velocity to be constant throughout the bed and taking its value to be $U_t = W\ r_o$ yields:

$$dp/dr = (1 - \varepsilon)\rho g W^2\ r_o^2 / r \qquad (4.3)$$

$$\Delta p = (1 - \varepsilon)\rho_g W^2\ r_o^2\ \ln(\ r_o/r_i\ ) \qquad (4.4)$$

In equations 4.3 and 4.4, W is the angular velocity of the distributor, r_o and r_i are the outer and inner radii of the bed, respectively, as shown in Figure 4.1.

b. Assuming the tangetial velocity to vary throughout the bed (U_t=W r), which upon introduction into equation 4.2 yields:

$$dp/dr = (1 - \varepsilon)\rho_g\ W^2 r \qquad (4.5)$$

$$\Delta p = (1 - \varepsilon)\rho_g W^2 (r_o^2 - r_i^2)/\ 2 \qquad (4.6)$$

Equations 4.4 and 4.6 predict similar pressur drops when the bed thickness r_o-r_i is small. When the bed operates

at fixed bed conditions the pressure drop is independent of the rotating speed and is given by the Ergun correlation (Kunii and Levenspiel, 1969) modified by Levy and Chen (1978) to account for the fact that the cross section area changes as a function of the radius:

$$p = \frac{150(1-\varepsilon)^2 \mu U_o r_o \ln(r_o/r_i)}{\varepsilon^3 d_g} + \frac{1.75(1-\varepsilon)\rho_f U_o^2 r_o^2 [1/r_i - 1/r_o]}{\varepsilon^3 d_g^2} \qquad (4.7)$$

where U_o, μ and ρ_f are the gas linear velocity, viscosity and density, respectivly, d_g is the granule's diameter and r_o and r_i are the outer and inner radii of the bed. The minimum fluidization velocity, U_{mf}, can be found by equating the pressure drop in equations 4.7 with the expression given in Eq. 4.4 or 4.6 and depends on rotational speed, W.

Experimental values of the pressure drop and gas velocity for different rotational speeds of the distributor (in RPM) are shown in Figure 4.5 together with the theoretical predicted pressure drop at minimum fluidization, equations 4.4 and 4.6, the pressure drop in the fixed bed, equation 4.7 and the minimum fluidization velocity given by equation 4.6 and 4.7. The experiments were performed using polystyrene granules as the bed material in a bed with an outer radius of r_o = 10 cm and inner radius of r_i = 8 cm. The granules' diameter, density and bed porosity were

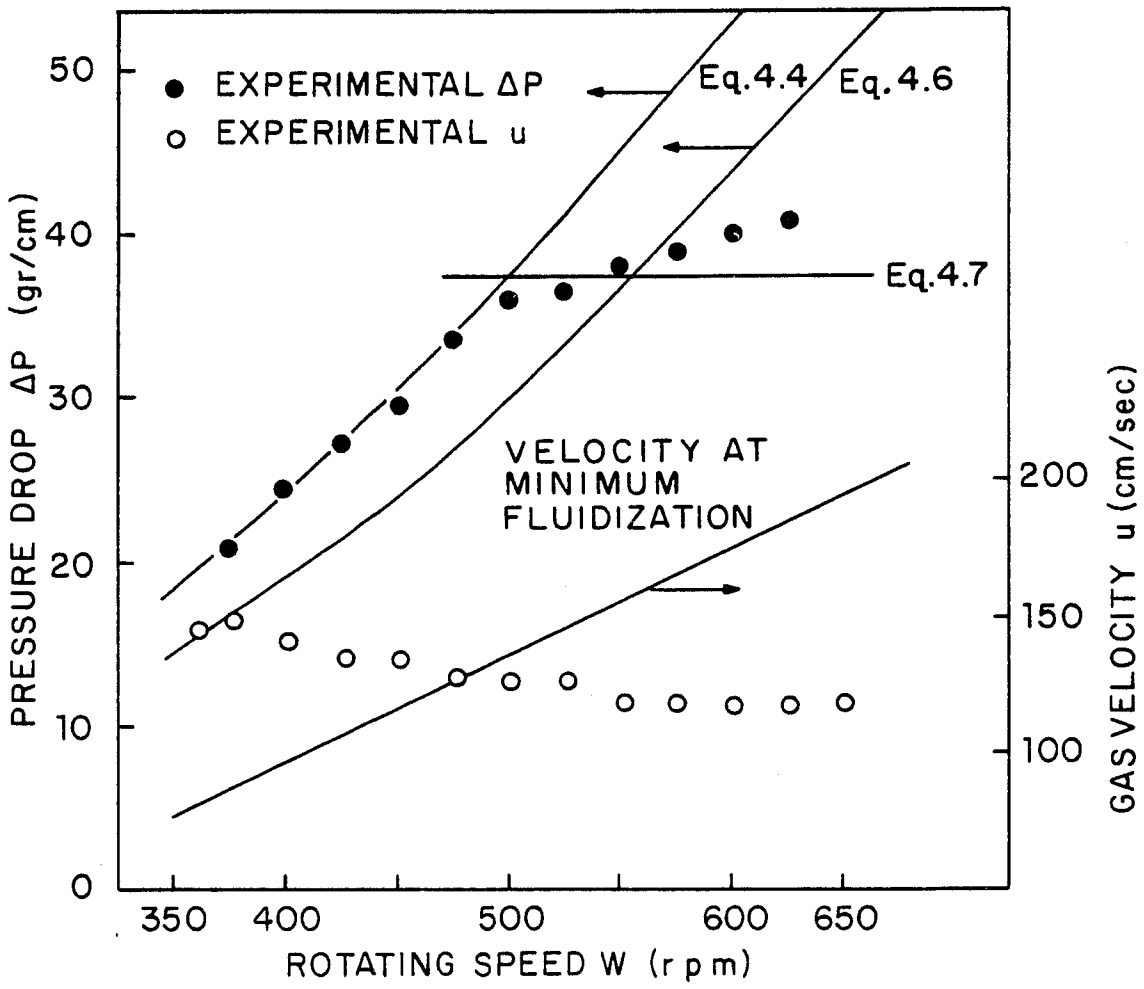

Figure 4.5: Pressure drop and minimum fluidization velocity in the RFBF containing 0.07 cm in diameter polystyrene granules as a function of rotational speed.
Bed thickness, L = 2.0 cm; Bed Porosity, ε = 0.37

d_g=Ø.Ø5 cm, ρ_g=1.Ø2 gr/cm^3 and ε=Ø.38, respectively. Under these conditions, at a velocity of around 125 cm/sec, minimum fluidization was achieved at about 475-5ØØ RPM (correspond to 25-28 g's), and is shown in Figure 4.5. The pressure drop at rotating speeds below 5ØØ RPM fits very well the theoretical curve predicted by equation 4.4 while equation 4.6 underestimates the pressure drop for this region. Above 5ØØ RPM the bed is in a fixed bed region where the pressure drop is below that of fluidization and is given approximately by equation 4.7. All experimental velocities which are below the line given by equations 4.4 and 4.7 indicate fixed bed conditions while those above this line indicate fluidization. The point of intersection gives minimum fluidization conditions at 475 RPM, a value that corresponds to that predicted by equations 4.4 and 4.7 from pressure drop considerations. As seen in figure 4.5 the measured pressure drop through the bed shows a pronounced change in slope at 475 RPM when the bed changes from the fluidized to the fixed bed mode.

Pressure drop as a function of air velocity for Ø.3 cm polyethylene granules is given in figure 4.6 for bed hights L=Ø.52, 1.67, 3.Ø cm and rotational speeds of 35Ø and 45Ø RPM. The experimental results agree well with the prediction of equation 4.7 for the fixed bed region and with those of equation 4.6 for the fluidized bed region. As the bed thickness increases the minimum fluidization velocity

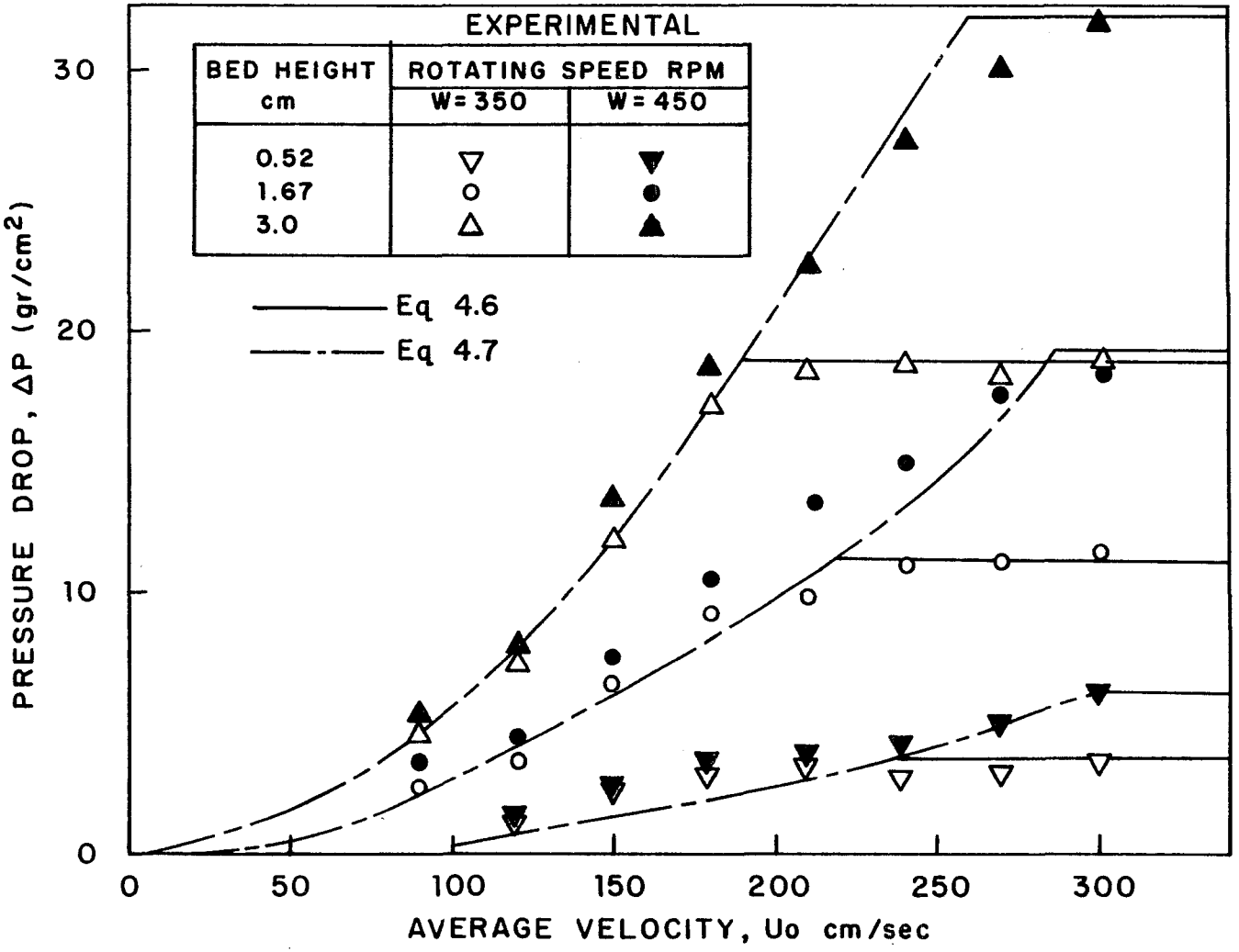

Figure 4.6: Pressure drop in the RFBF containing Ø.3 cm in diameter polyethylene granules as a function of air velocity for different bed heights.
Bed Porosity, ε = Ø.4

decreases from about 240 cm/sec (L=0.52 cm and W=350 RPM) to about 190 cm/sec (L=3.0 cm and W=350 RPM) and from 300 cm/sec (L=0.52 and W=450 RPM) to about 250 cm/sec (L=3.0 and W=450 RPM).

4.4 Filtration Efficiency Measurements

An aerosol particle is captured in a granular bed if it collides with the granule's surface and if it sticks to it. A particulate reaches the granule's surface due to one or more of the filtration mechanisms discussed in detail in section 2.3. Once a particle hits the surface of the collector granule, it may either stick to it or bounce and be re-entrained. It also may split into smaller particles (or droplets in the case of liquid aerosole filtration) especially when the velocity is high the particle diameter is large and the kinetic energy is sufficient for the creation of the new added surface. Part of the droplet may remain on the surface of the granule while smaller droplets generated by the collision may be carried downstream by the gas. Breakdown of liquid aerosol droplets may be a problem if high concentration of relatively large droplets exist in the inlet sream, as discussed by Gal et al. (1982). However, when droplets diameter is smaller than 3μm as in the experiments described here (see Figure 4.3), breakdown of droplets is not observed.

In the rotating fluidized bed filter which operates at high gas velocity the main filtration mechanism is inertial impaction. Also, if aerosol and granules are electrically charged, electrostatic effects may become important. The effect of diffusion and gravitation in the RFBF is small except for very small particles were diffusion may become important or very large particles where gravitation may become significant.

The measured experimental total bed efficiency for a certain size of dust particle is defined as:

$$\eta = 1 - n_{out} / n_{in} \qquad (2.1)$$

where n_{in} and n_{out} are the number concentration of dust particles of a certain size in a unit volume of gas before and after passing through the filter, respectively.

The concentrations n_{in} and n_{out} are measured simultanously by Climet CI-225 and CI-208S dust particle counters. The Climet dust particle counter is an optical device measuring the number and size of dust particles by light scattering. The results are given in terms of number of particles of certain size range per unit volume of gas. The instrument can detect particles with diameters larger than 0.3μm and it has 7 channels for particles in the size range of 0.3-10μm. The two particle counters where tested

by sampling from the same source. Measurement error of the Climet reading is about 5% for particles larger than Ø.5 μm and about 15% for particles in the size range of Ø.3-Ø.5 μm. The measurement error is somewhat larger at low dust concentration. The simultanous reading of inlet and outlet concentrations enable accurate measurments of filtration efficiency even when the dust concentration varies as a function of time which is the case, in the present system, with solid dust experiments. The data are collected and analyzed by a microcomputer. The computer programs used for reading and analyzing the results and a typical output are given in appendix C.

4.4.1 Inertial Effects

The modified Stokes number $St'=[2Cr_p^2\rho_p U_o/9\mu a]xf(Re,\varepsilon)$ is the inertia parameter discussed in detail in Section 3.3. When the Stokes number is small St'<Ø.Ø1 inertial effects are small and changing the value of its parameters does not affect the filtration efficiency. Filtration efficiency becomes very sensitive to changes in the value of the modified Stokes number especially for Ø.Ø1 < St' < Ø.Ø3 when small changes in St' may change the filtration efficiency dramatically. Inertial effects in a regular fluidized bed are similar to those in a fixed bed and the same parameters control filtration efficiency in both type of filters. The following experiments were performed to examine the effect

of those same parameters on filtration efficiency in the rotating fluidized bed filter. Each of the parameters: gas velocity, granule size, Reynolds number, aerosol density and size of aerosol particles is investigated seperately. To isolate the effect of inertia, all the experiments described in this section were performed at a relative humidity larger than 30% where electrostatic effects are small. Also DOP is used in most of the experiments shown in Figures 4.7-14 so that bouncing is not a major factor in determining filtration efficiency in these experiments.

The effect of velocity on filtration efficiency in the rotating fluidized bed filter is shown in Figures 4.7 and 4.8. As velocity increases from 60 cm/sec to 240 cm/sec, in Figure 4.7, filtration efficiency increases from 34% to 98% for the 1-2 μm DOP particles. There is hardly any change in filtration efficiency, which is practically zero, for the 0.5-0.8 μm particles at velocities lower then 180 cm/sec. At higher velocity filtration efficiency increased sharply to 49% at 300 cm/sec. A similar trend is shown in Figure 4.8. Filtration efficiency increases from 75% at 30 cm/sec to 99.9% at 170 cm/sec for 1-2 μm DOP particles. For the 0.5-0.8 μm DOP particles efficiency is almost constant at around 15%-25% as velocity increases from 30 to 120 cm/sec then increases sharply to 58% at velocity of 180 cm/sec. As velocity increases by about 20-30% above minimum fluidization carry over starts and filtration efficiency drops.

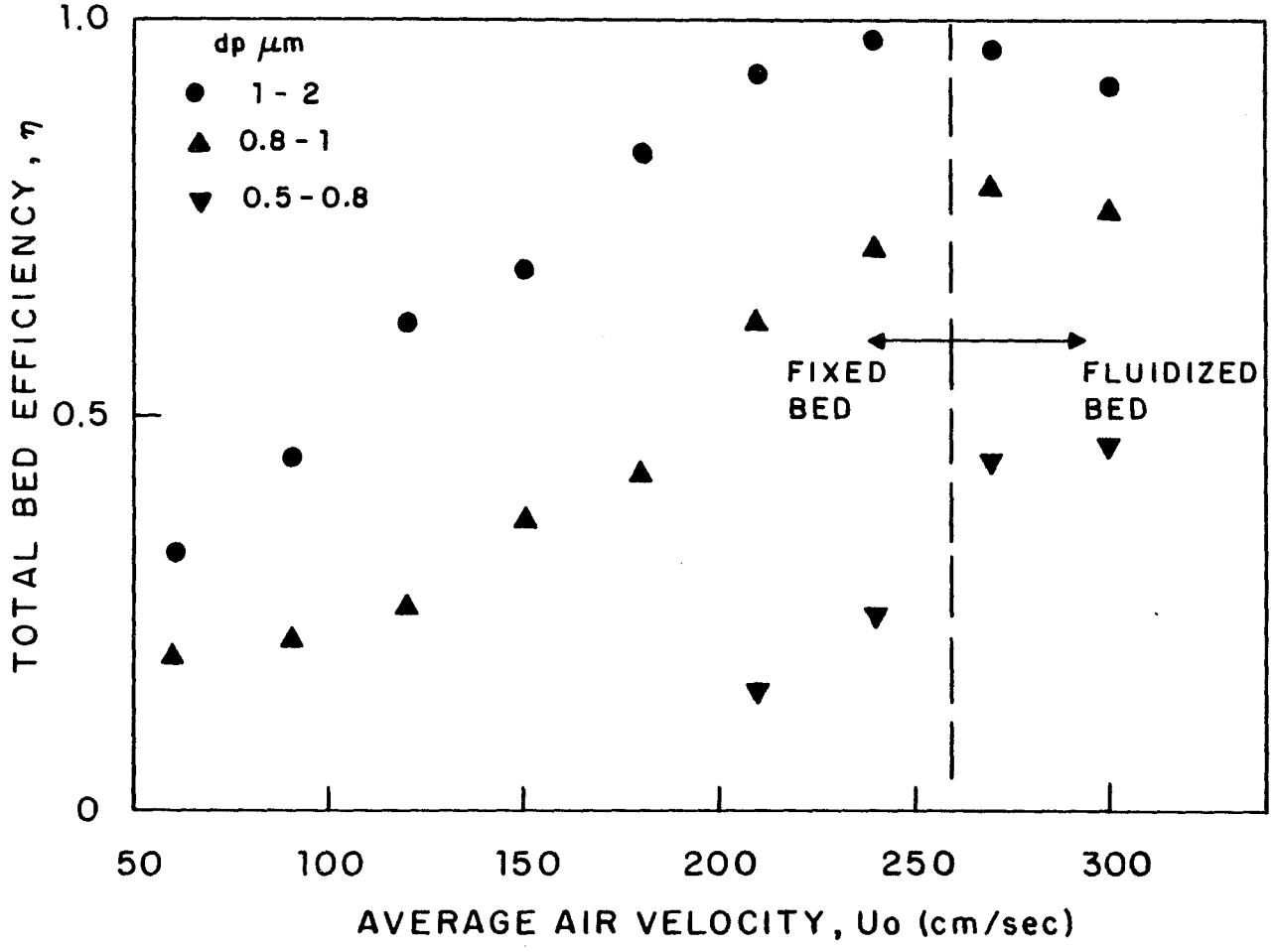

Figure 4.7: Filtration efficiency of a bed containing Ø.3 cm diameter polyethylene granules as a function of average air velocity for different sizes of DOP particles. Relative humidity, RHu = 3Ø%; Bed thickness, L = 3.Ø cm; Bed porosity, ε = Ø.4; Rotating speed, W = 45Ø RPM

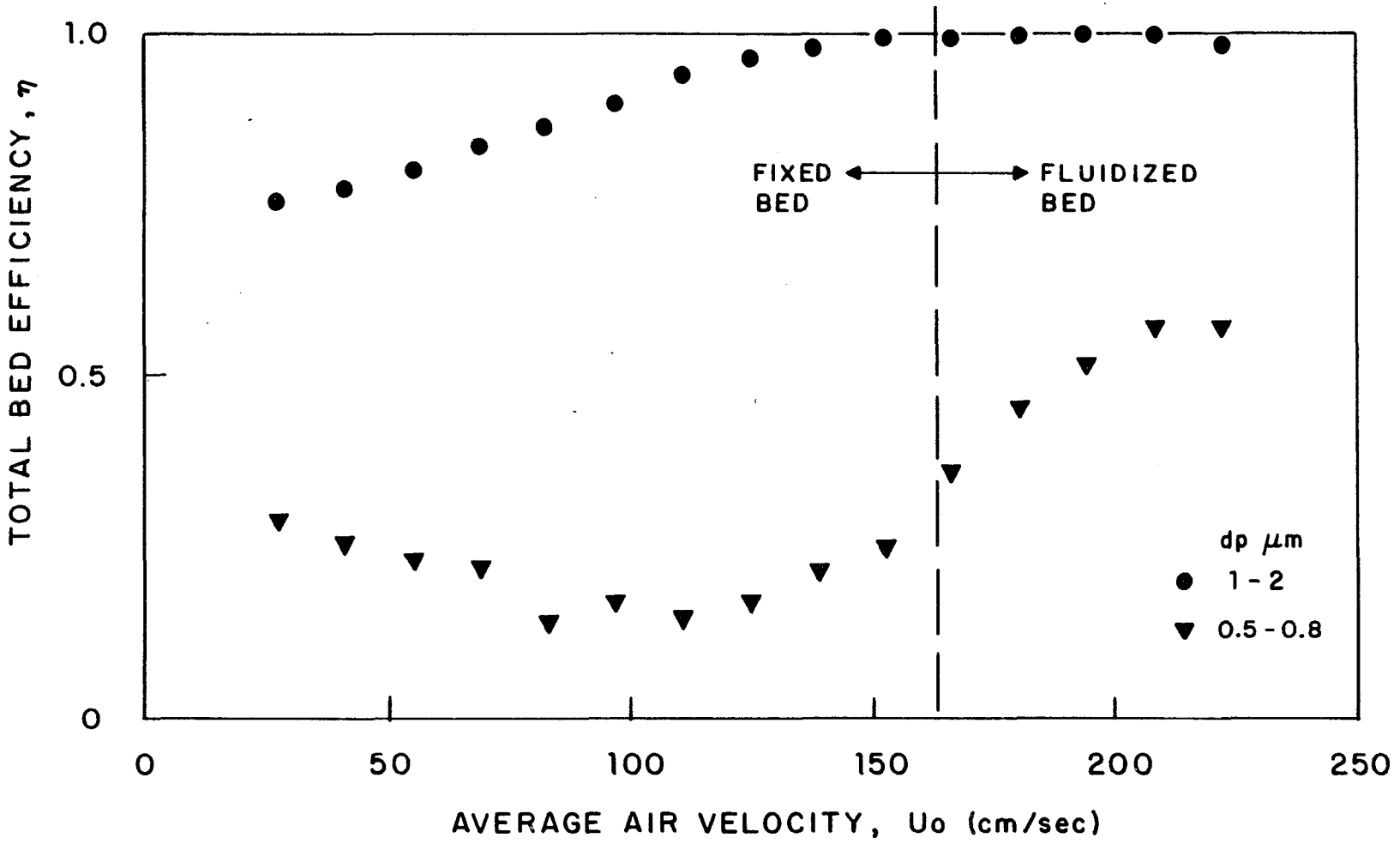

Figure 4.8: Filtration efficiency of a bed containing 0.07 cm diameter polystyrene granules as a function of average air velocity for different sizes of DOP paerticles. Relative humidity, RHu = 33%; Bed thickness, L = 1.0 cm; Bed porosity, ε = 0.37; Rotating speed, W = 600 RPM

The bed material may significantly effect filtration efficiency due to surface phenomena and attraction and repulsion forces that different granules may exert on the aerosol particles. However under conditions of high relative humidity (low electrostatic charge on bed and granules) and low rate of bouncing (which is usually the case when liquid aerosol is used or gas velocity is not too high) one can isolate the effect of granule's size even if different bed materials are used.

The effect of granule size on filtration efficiency is shown in Figure 4.9 for 0.8-1.0 μm DOP particles at 150 and 180 cm/sec. The filtration efficiency is very high 98-99% (at U_o=180 cm/sec) for the 0.03-0.04 cm granules and drops sharply to 92% and further to 48% as granule's size increases to 0.07 cm and 0.3 cm respectively.

The combined effect of gas velocity and granule size is shown in figure 4.10 where filtration efficiency is given as a function of the granule's Reynolds number, $Re=U_o d_g/\nu$. The inertial impaction mechnism is dominant at Reynolds numbers of about 50-100 when the granules size, d_g, is 0.07 cm. When d_g=0.3 cm inertia becomes dominant only for Reynolds number larger than 300. Filtration efficiency increases sharply with increasing Re for small d_g and moderately for large d_g.

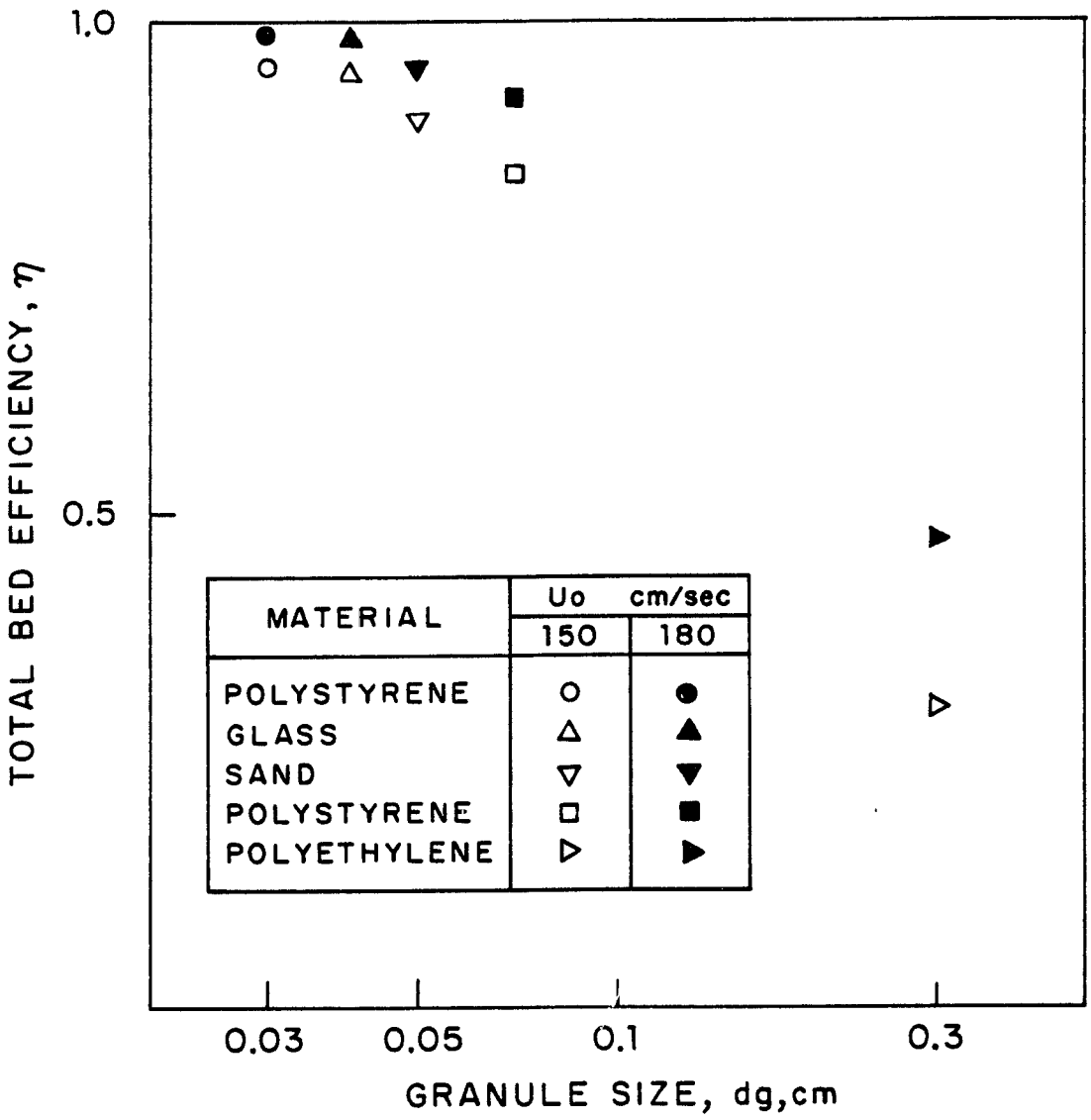

Figure 4.9: Total bed efficiency in the filtration of Ø.8-1.Ø μm in diameter DOP particles as a function of granules size and material.
Bed thickness, L = 1.Ø cm; Bed porosity, ε= Ø.37-Ø.4;
Rotating speed, W = 45Ø-6ØØ RPM

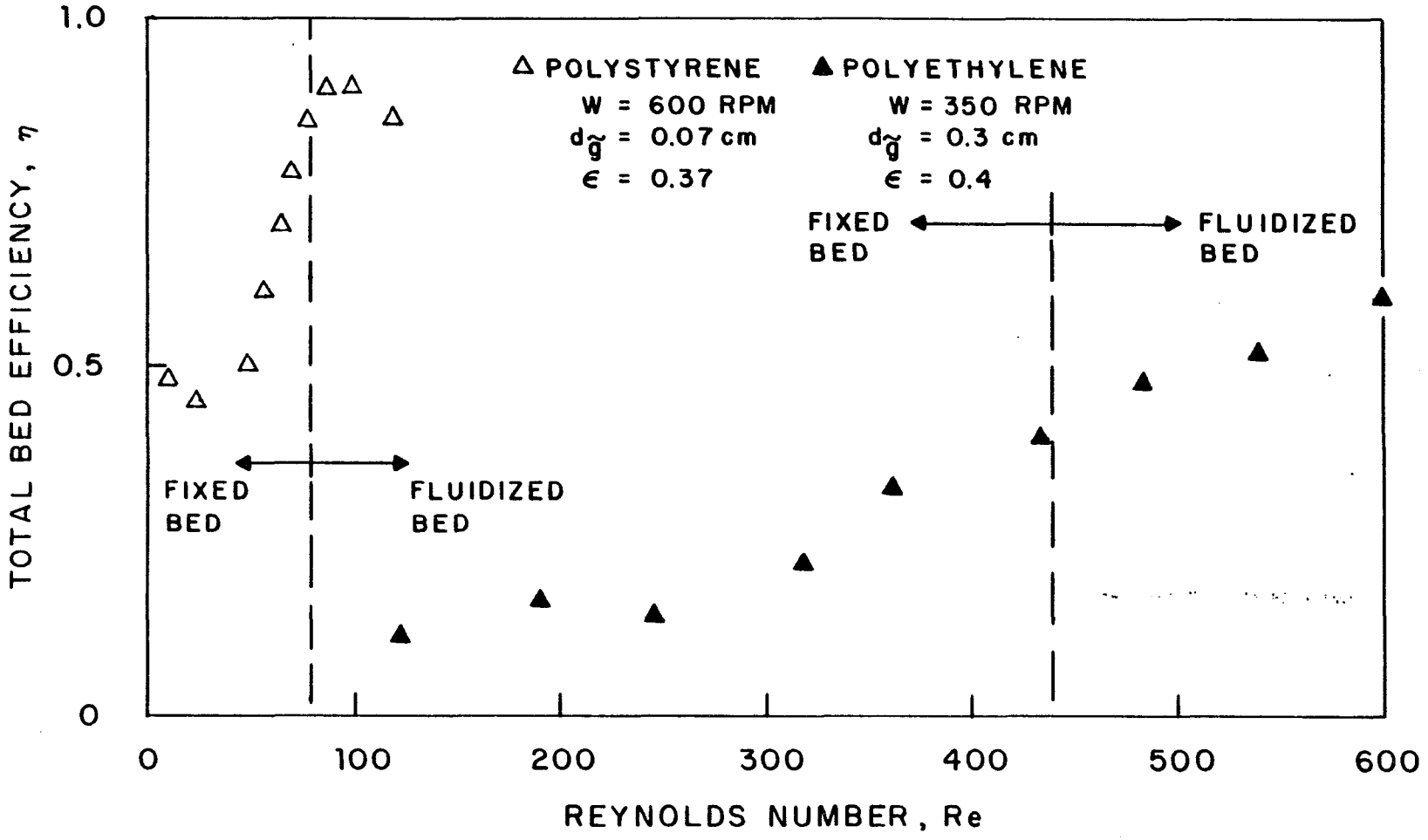

Figure 4.10: Total bed efficiency in the filtration of 0.8-1.0 μm diameter DOP particles as a function of the Reynolds number, Re.
Bed thickness, L = 1.0 cm
Relative humidity, RHu = 30-40%

The inertia of an aerosol particle depends on its density ρ_p. As the density increases the inertial effect becomes stronger and the efficiency increases. In Figure 4.11 filtration efficiency as a function of velocity for liquid DOP aerosol, ρ_p=1.Ø gr/cm^3, and for solid aluminum silicate dust, ρ_p=1.9 gr/cm^3, is compared. The filtration efficiency of the solid aerosol is higher than that of the DOP at constant velocity, 61% vs. 33% at 6Ø cm/sec and 85% vs. 63% at 12Ø cm/sec. Using DOP aerosol it takes a 1.5-2.Ø times higher velocity to obtain the same filtration efficiency as obtained for the solid dust in this range of velocities. However, as the velocity increases, bouncing of solid dust particles occur and filtration efficency drops slightly from 95% at 24Ø cm/sec to 9Ø% at 3ØØ cm/sec. At velocities higher than 2ØØ cm/sec the filtration efficiency of the DOP and the solid dust is almost the same.

A granular bed can be an almost absolute filter for aerosol particles larger than 2μm if bouncing can be avoided. However when the particles are smaller penetration occurs and the filtration efficiency drops. The decrease in efficiency is very sharp as shown in Figure 4.12 where the filtration efficiency is seem to drops from 93% for d_p = Ø.Ø9μm and d_g = Ø.Ø7 cm to a mere 12% for d_p = Ø.Ø4μm. The efficiency is even lower when using larger bed granules.

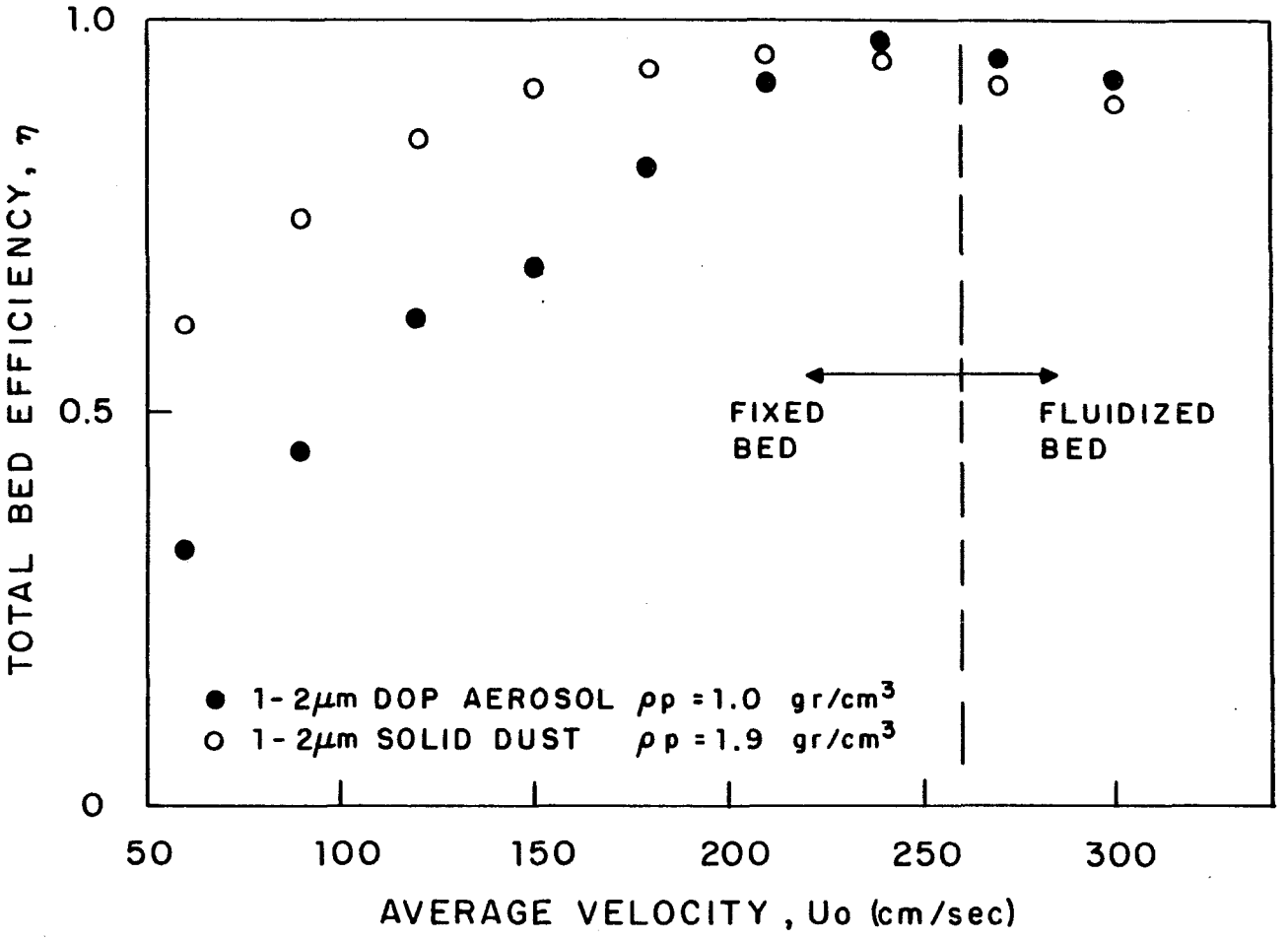

Figure 4.11: Total bed efficiency as a function of air velocity for DOP and solid dust particles in a RFBF containing Ø.3 cm diameter polyethylene granules.
Bed thickness, L = 3.Ø cm; Bed porosity, ε = Ø.4;
Rotating speed, W = 45Ø RPM;
Relative Humidity, RHu = 35-4Ø%

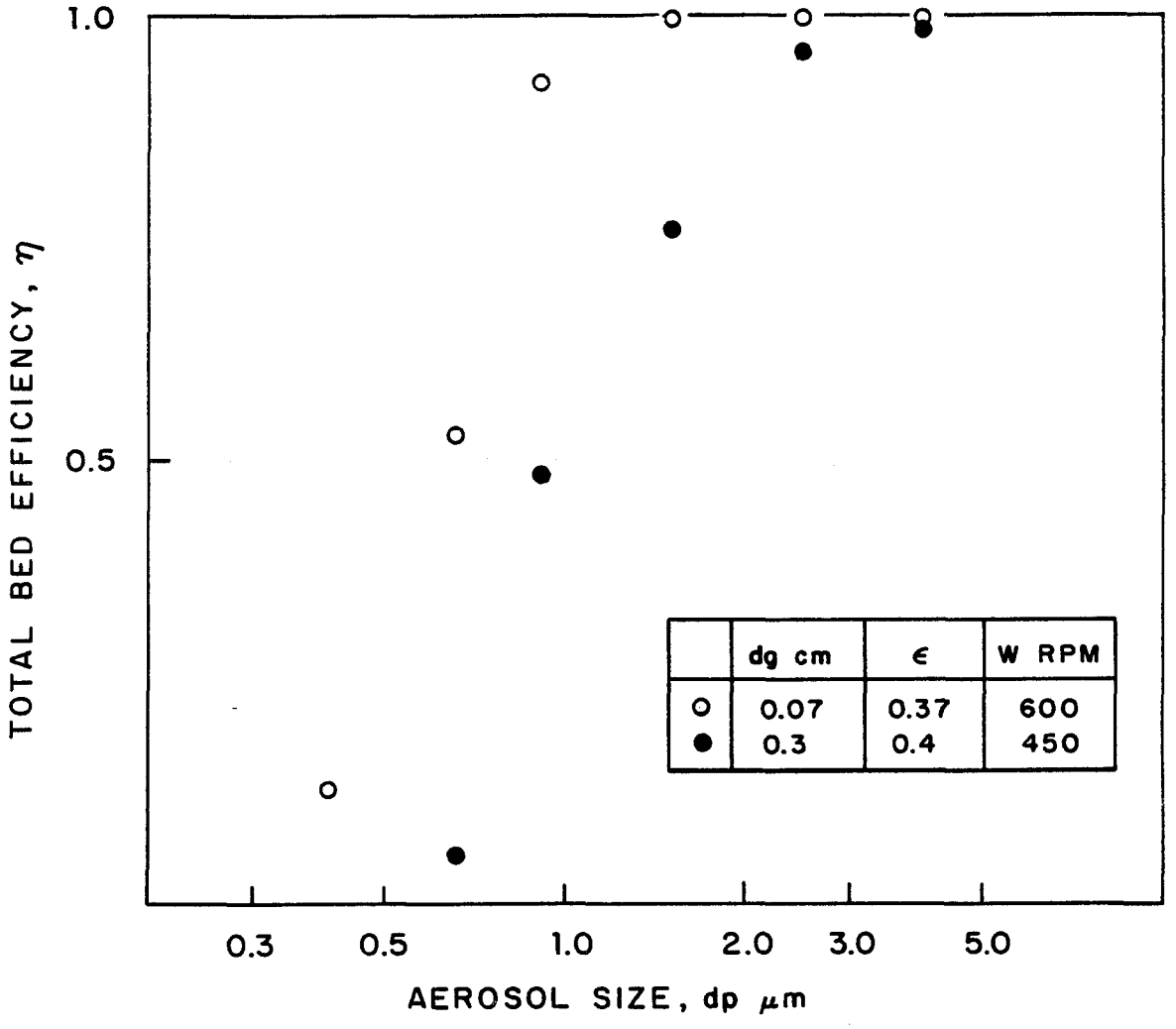

Figure 4.12: Total bed efficiency as a function of DOP aerosol particle size.
Bed thickness, L = 1.0 cm; Air velocity, Uo = 180 cm/sec; Relative humidity, RHu = 35-40%

The experiments described above show that the inertia mechanism in the RFBF acts similarly to that in other granular beds, i.e. an increase in air velocity, dust particle size and density increases efficiency while an increase in granular size decreases filtration efficiency. The combined effect of all the parameters discussed above is shown in Figures 4.13 and 4.14 where total bed efficiency, η and single sphere efficiency, E, are given as a function of the Stokes number, St. The efficiency shown in Figures 4.13 and 4.14 correspond mainly to inertial effects which are dominant in these experiments. The "tails" to the left in Figure 4.13 indicates the contribution of mechanisms other than inertia which become important at the low range of the Stokes number. In general the inertia mechanism does not contribute in the filtration of aerosol particles smaller then about 0.5μm even when high velocities and small bed granules are used. To obtain high filtration efficiency of small aerosol particles in granular bed filters mechanisms other than inertia should be utilized.

4.4.2. Direct interception, diffusion and gravity effects

Pfeffer and Hill (1978) calculated the effects of direct interception, diffusion and gravity settling on filtration efficiency in the rotating fluidized bed filter.

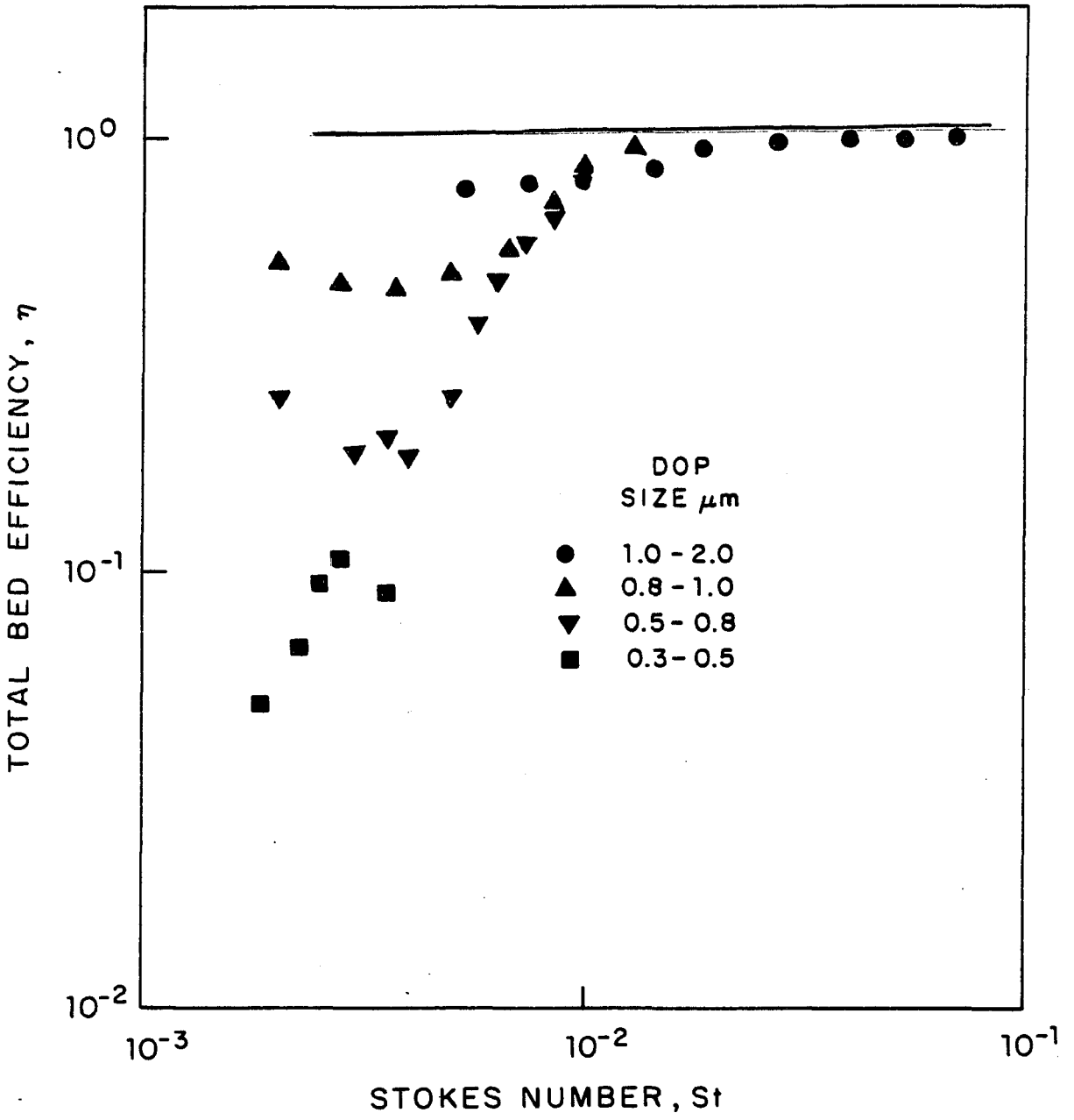

Figure 4.13: Total bed efficiency as a function of the Sto kes number, St, in the RFBF containing 0.07 cm diameter polystyrene granules.
Bed thickness, L = 1.0 cm; Bed porosity, ε = 0.37; Rotating speed, W = 600 RPM

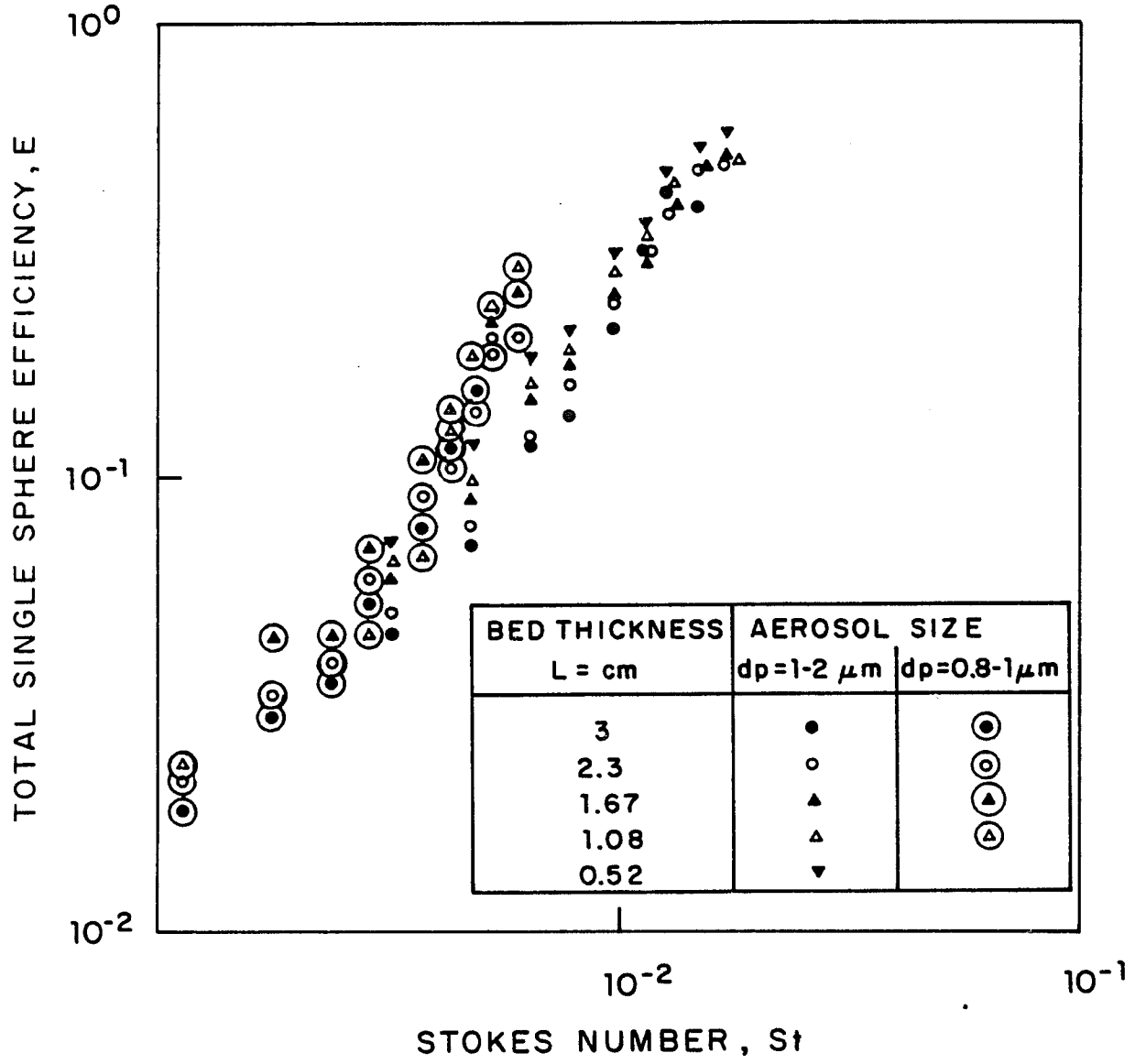

Figure 4.14: Single sphere efficiency as a function of the Stokes number, St, in the RFBF containing 0.3 cm diameter polyethylene granules.
Bed porosity, ε= 0.4; Rotating speed, W = 450 RPM; Relative Humidity, RHu = 25-40%

They used the single sphere approach to predict single sphere efficiency. Similar calculations are presented here. Diffusion and interception are assumed to be uneffected by the fluidization and the rotation. Gravity settling, on the other hand, is affected by the rotation since the settling forces in the RFBF depend on the radial acceleration rather then gravity.

To account for the rotation (assuming that the angular velocity of the dust particles inside the bed to be the same as the angular velocity of the bed) the acceleration of gravity, g, in equation 2.8 is replaced by the radial accelation, W^2r. With rotational speeds as high as 600 RPM (W^2r_o=40g's) gravity settling effects become somewhat more important. Figure 4.15 gives the combined predicted effect of interception, diffusion and gravity settling for DOP particles in the Stokes numbers range of the experiment for viscous flow, Re->0 (equations 2.5 (n=-2/3), 2.8 and 2.10), and for potential flow, Re->∞ (equations 2.5 (n=-1/2), 2.8 and 2.11) and for particle sizes 1-2μm, 0.8-1.0μm, 0.5-0.8μm and 0.3-0.5μm. The contribution of diffusion and interception to the combined efficiency for Re->0 is small and the efficiency is mainly due to gravity settling which is not affected by the type of flow. For Re->∞, diffusion and interception are more pronounced as shown by the difference between the full and dashed lines in Figure 4.15. In any case these mechanisms are negligible compare to inertia.

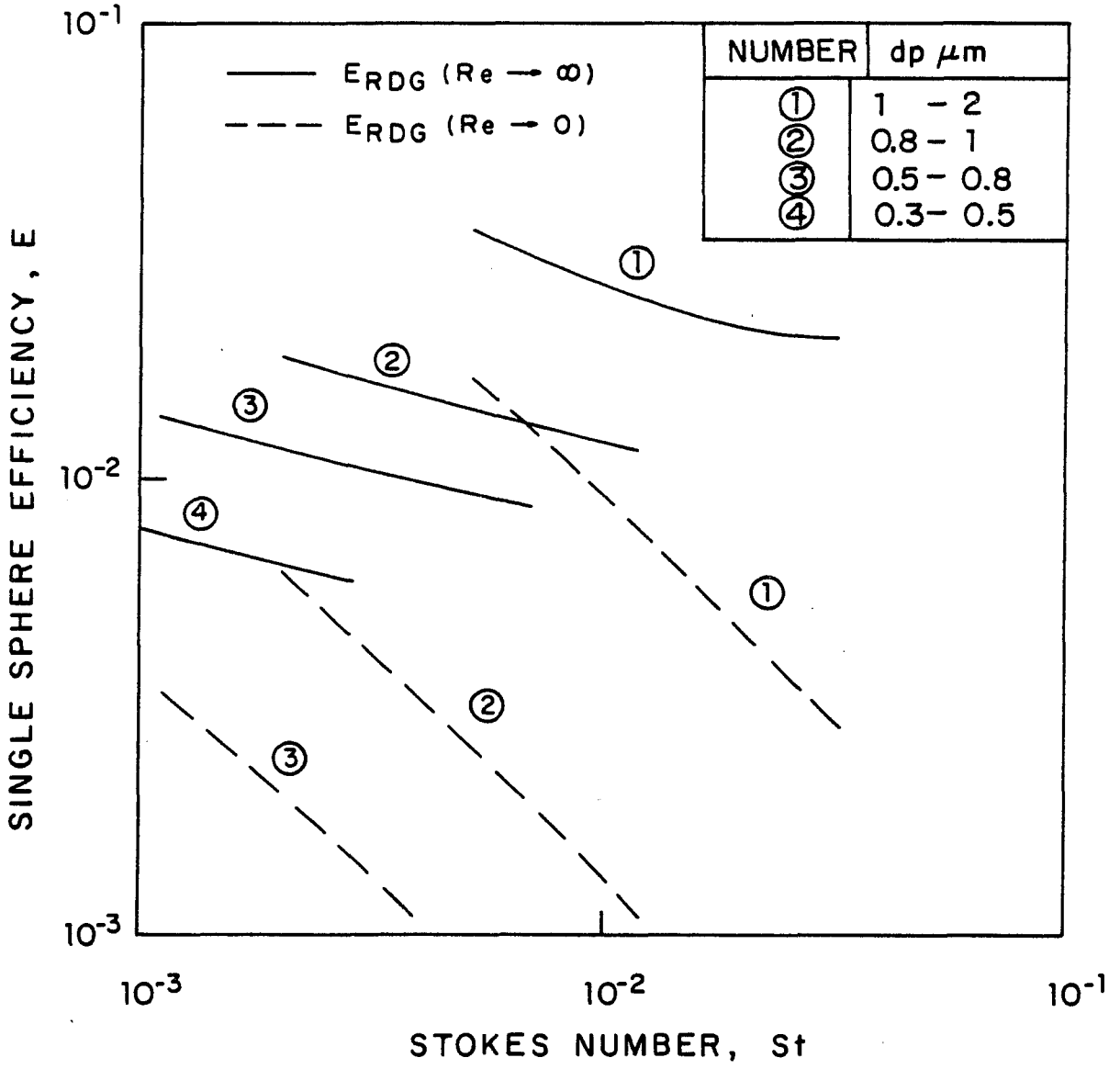

Figure 4.15: The combined effect of interception, diffusion and gravity settling on single sphere efficiency as a function of the Stokes number calculated for the experimental conditions in the RFBF.
Bed thickness, L = 1.0 cm; Bed porosity, ε = 0.37;
Granule diameter, d_g = 0.07 cm

4.4.3. The effect of rotating speed

In the rotating fluidized bed minimum fluidization may be obtained at almost any given velocity by adjusting the rotating speed of the bed within the mechanical limitations of the system. The effect of rotating speed on filtration efficiency is shown in Figure 4.16. In the fixed bed region filtration efficiency is not affected by the rotation. As the rotating speed decreases the bed changes from a fixed to a fluidized bed. The filtration efficiency at minimum fluidization conditions is about the same as the efficiency in the fixed bed region and drops slightly as the rotating speed decreases. Further decrease in rotating speed results in bubble formation which reduces filtration efficiency very rapidly. It is advantageous to operate the bed just above minimum fluidization velocity where the filtration efficiency is high and the bed material can continuously be introduced and discharged from the bed.

4.4.4. The Effect of Bed Thickness

As the bed thickness increases dust particle pass through more layers of bed material and the probability of them being captured increases. Assuming that each granule experiences the same filtration phenomena, one expects an exponential relationship between the total bed efficiency and the bed thickness. In Figures 4.17 and 4.18 total bed

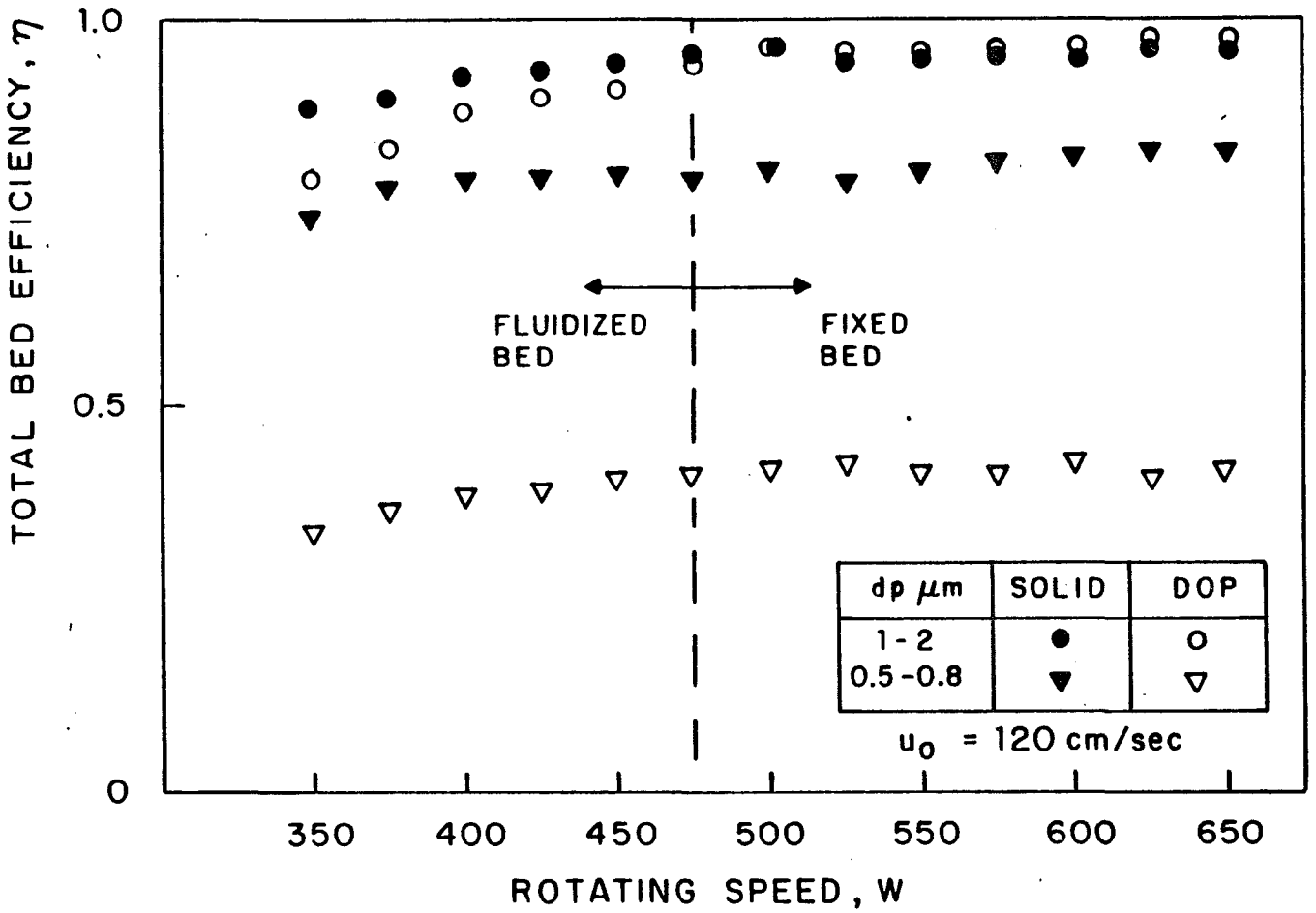

Figure 4.16; Total bed efficiency as a function of rotational speed of the RFBF containing polystyrene granules. Bed thickness, L = 1.0 cm; Bed porosity, ϵ = 0.37; Granule diameter, d_g = 0.07 cm; Relative humidity, RHu = 0.10%

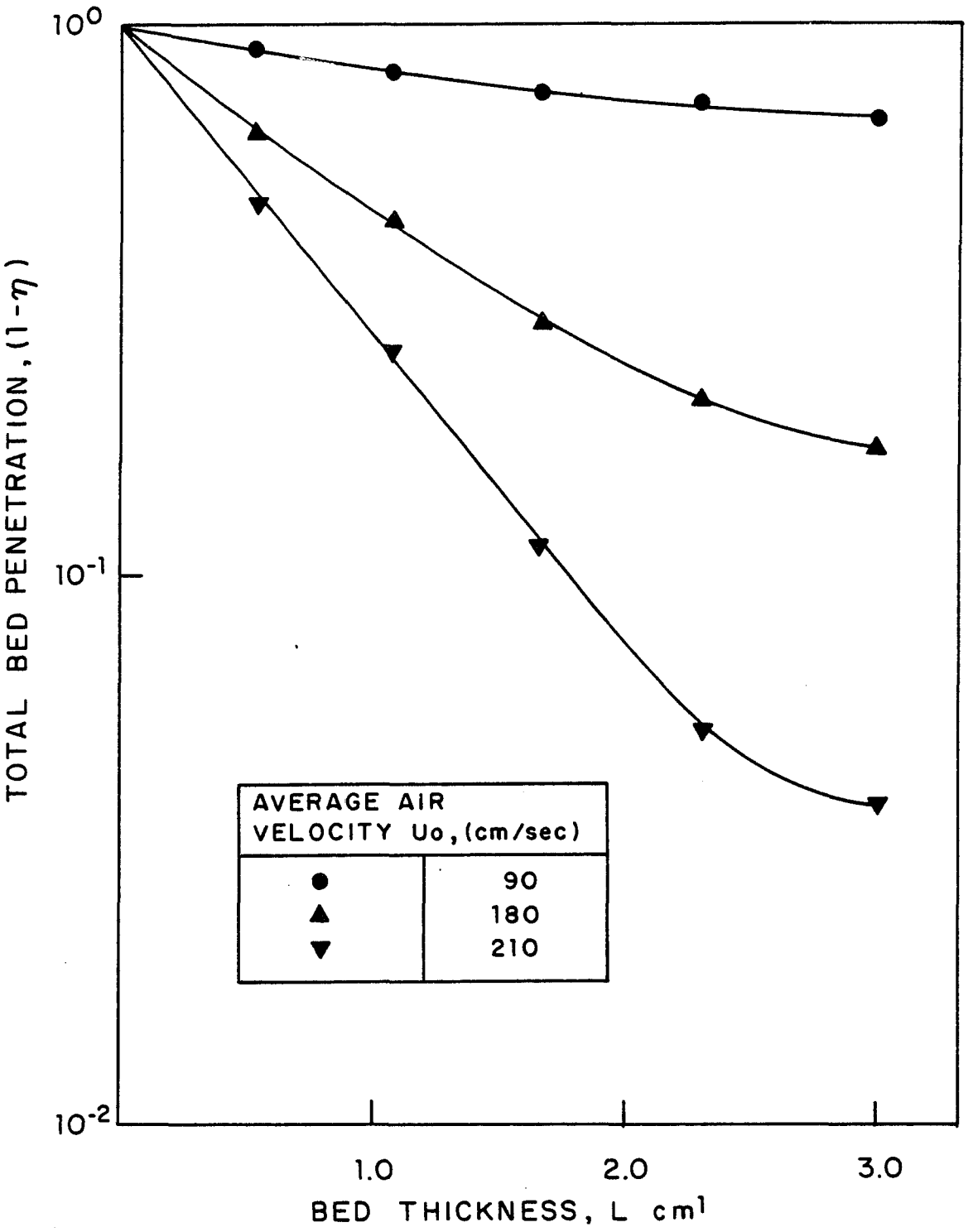

Figure 4.17: Total bed penetration as a function of bed thickness at different velocities in the RFBF containing polyethylene granules.
Granule diameter, d_g = Ø.3 cm; Bed porosity, ε = Ø.4; Relative humidity, RHu = Ø-1Ø%; Rotating speed, W = 45Ø RPM; DOP particles diameter, d_p = 1-2 μm

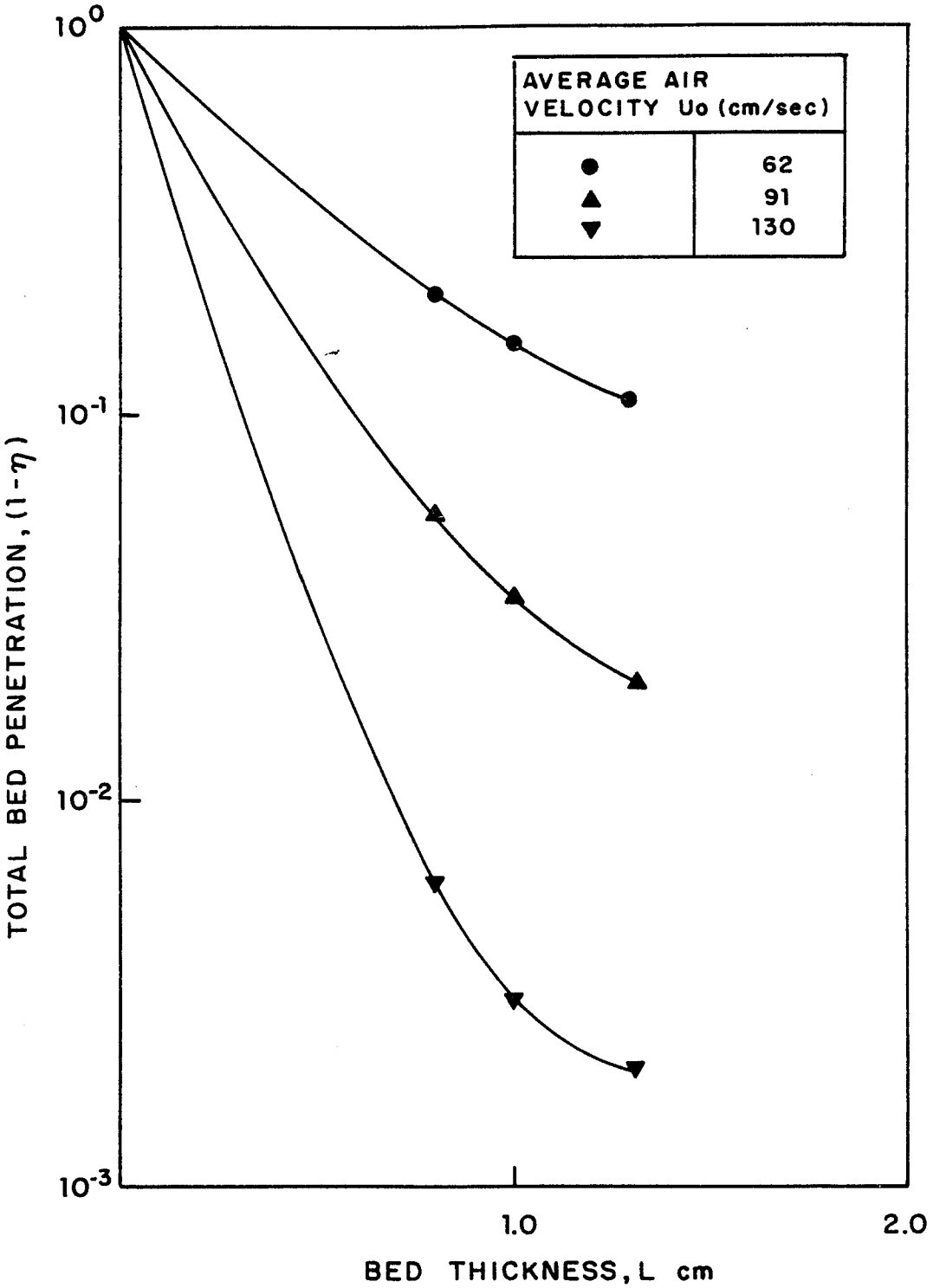

Figure 4.18: Total bed penetration as a function of bed thickness at different velocities in the RFBF containing polystyrene granules.
Granule diameter, d_g = Ø.Ø7 cm; Bed porosity, ε = Ø.37; Relative humidity, RHu = Ø-1Ø%; Rotating speed, W = 6ØØ RPM; DOP particles, d_p = 1-2 μm

penetration, which is defined as $1-\eta$, is shown as a function of bed thickness. The curves, in Figure 4.17 are linear as expected from equation 2.3 up to bed thickness of about 2-2.5 cm. The slopes changes somewhat as the thickness increases. This phenomena of lower than expected efficiency near the surface of a thicker bed, especially for high velocities and small granules can be explained by the nonuniformity of the fluidization in the existing rotating fluidized bed set-up. As the air flows radially inward through the bed, the cross sectional area becomes smaller and the average gas velocity increases. In addition, radial accelaration and centrifugal forces close to the surface are smaller than those close to the distributor adding to the nonuniformity of fluidization. Thus while the bed operates, on the average, near minimum fluidization velocity or even in the fixed bed region, the surface may be in bubbling conditions with much lower efficiency than the rest of the bed. The problem is more pronounced when operating the bed with small particles at lower granule Reynolds numbers. The Ø.3 cm polyethylene granules could be loaded in the bed to up to a thickness of 3 cm when elutriation started. The Ø.Ø7 cm polystyrene granules could only be loaded to up to 1.3 cm when particles start to flow out of the bed. Bubbles start even before elutriation is observed causing the decrease in the slope of the curves in Figures 4.17 and 4.18.

A solution to the nonuniformity of fluidization in the

existing rotating fluidized bed filter is proposed in the new design shown in section 4.7.

4.4.5. Efficiency measurments in the continuously operating sysytem

The rotating fluidized bed filter was operated continuously with granules fed and discharged from the system for periods of up to 3.25 hours with DOP and up to 1.75 hours with solid dust. In both cases runs stopped due to mechanical problems in the feeding system not related to the RFBF operation itself. No problems were observed as far as the bed itself was concerned. The 14 mesh (Ø.115 cm) screen remained almost clean and no increase in pressure drop was observed. Bed thickness could be maintained constant at up to 3 cm with no difficulties and DOP aerosol concentration was kept constant at about $1.5x1Ø^5$ particles/liter while the solid dust concentration varied somwhat in the range from $5x1Ø^4$ to $2x1Ø^5$ particles/liter due to the uneven operation of the dust feeder. Filtration efficiency could be maintained constant throughout the experiments and were by and large unaffected by variations in dust load as can be seen in Figure 4.19. Granules were fed continuously to the bed at a rate of about 1.Ø liter/hr so that the average residence time of granules in the bed was about Ø.5 hour and the dust load on the granules was somewhat less than 1.Ø gr/kg of bed.

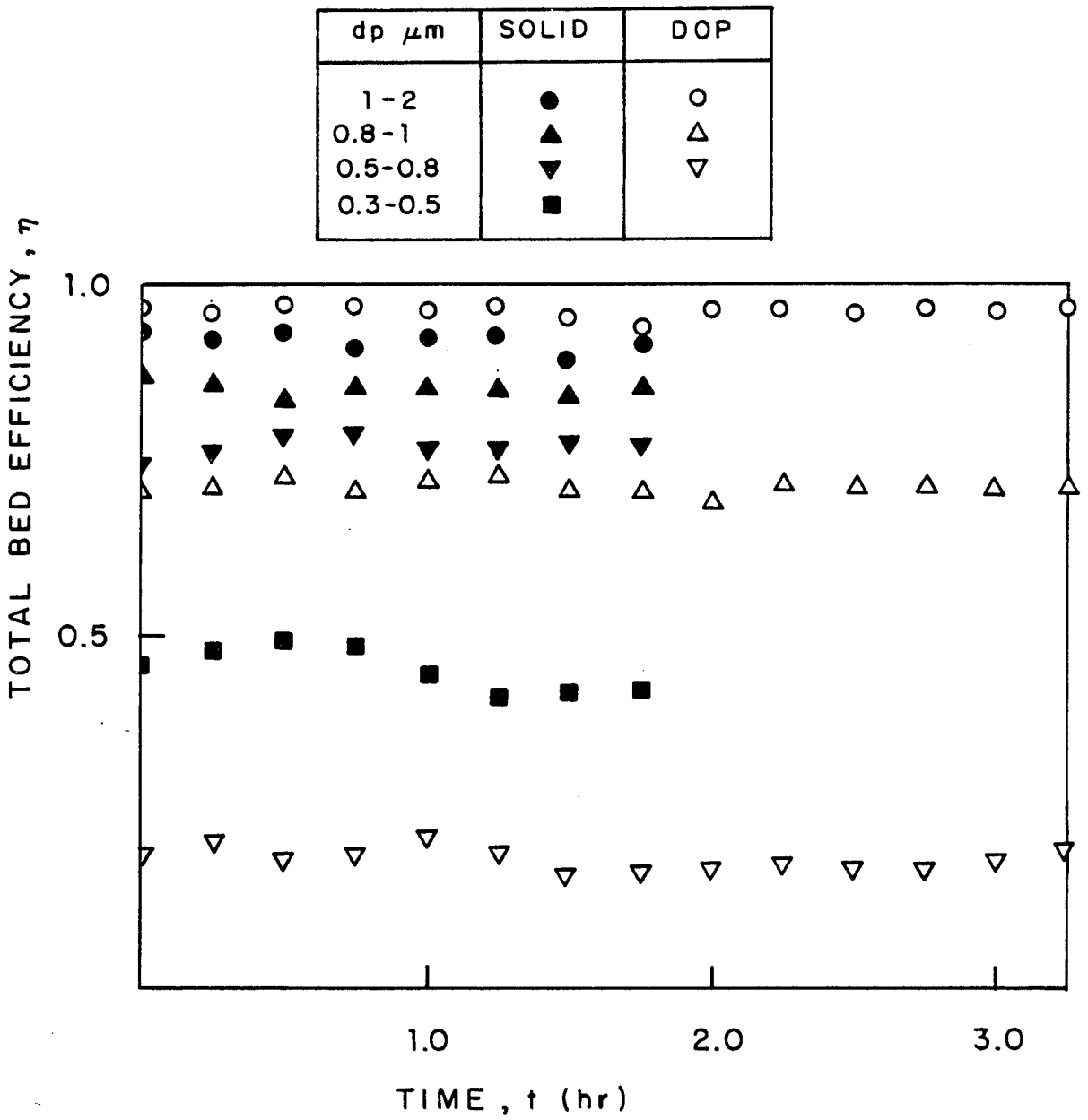

Figure 4.19: Total bed efficiency as a function of time for solid dust and DOP aerosol in the RFBF containing Ø.3 cm diameter polyethylene granules. Bed thickness, L = 3.Ø cm; Bed porosity, ε = Ø.4; Relative humidity, RHu = Ø-1Ø%; Rotating speed, W = 45Ø RPM; Air velocity, U_o = 28Ø cm/sec

4.5 Measurement of Electrostatic effects

Many experimental and theoretical studies (Thomas and Woodfin, 1959; Havelick, 1961; Walkenhorst, 1970; Kirsh, 1972; Neilsen and Hill, 1976; Dietz, 1981) have shown that electrical forces can significantly enhance the collection efficiency of fine particles in granular beds and fibrous filters. The electrical forces become considerably important in the range of low Stokes numbers (low velocity, small aerosol particles) where inertia effects are small and the filtration efficiency is low. A fluidized bed may be electrically charged by an external electric field or by triboelectrification. Triboelectrification is a well known phenomena described by Anderson and Silverman (1958), Ciborovsky and Wlodarsky (1962), Zahedi and Melcher (1976) and Tardos and Pfeffer (1980). It occurs in a fluidized bed due to collision between granules and between granules and the container wall during fluidization. The effect is more pronounced when the fluidized particles are nonconductors and the fluidization vessel is not grounded (Tardos and Pfeffer, 1980 and Tardos and Pfeffer, 1983). The electrostatic charge on the granules depends on the granule material and gas humidity which determine the rate of charge relaxation. Increasing the humidity increases conductivity (Zahedi and Melcher, 1976) and reduces the charge relaxation time.

Figures 4.20-23 clearly show that mechanisms other than inertia, interception,gravity settling and diffusion are involved in enhancing filtration efficiency especially that of small particles at low Stokes numbers. The filtration efficiency of small DOP particles, 0.3-0.5 μm and 0.5-0.8 μm at minimum fluidization velocity, Umf, is very low. It is about zero and 15% respecively in Figure 4.20 (polyethelene granules 0.3 cm in diameter) and 10% and 35% respectively in Figure 4.21 (polystyrene granules 0.07 cm in diameter). The filtration efficiency of the solid dust particles at Umf is much higher. It is about 45% and 80% for dust particles sizes of 0.3-0.5 μm and 0.5-0.8 μm respectively in Figure 4.20 and 90% and 95% for the same sizes respectively in Figure 4.21. Comparing single sphere efficiencies of DOP and solid dust as a function of the Stokes number, Figures 4.22 and 4.23 shows the same trend: a much higher filtration efficiency of the solid dust particles as compared with the DOP particles. Also, as the relative humidity increases the filtration efficiency of solid dust decreases and at a relative humidity of about 40-50% the filtration efficiency of the two types of aerosols, for equal Stokes numbers is almost the same as shown in Figures 4.23 and 4.24. Figure 4.24 shows the average results of many experiments conducted with a 3 cm thick bed of polyethylene granules at different relative humidities. The wide range of relative humidities

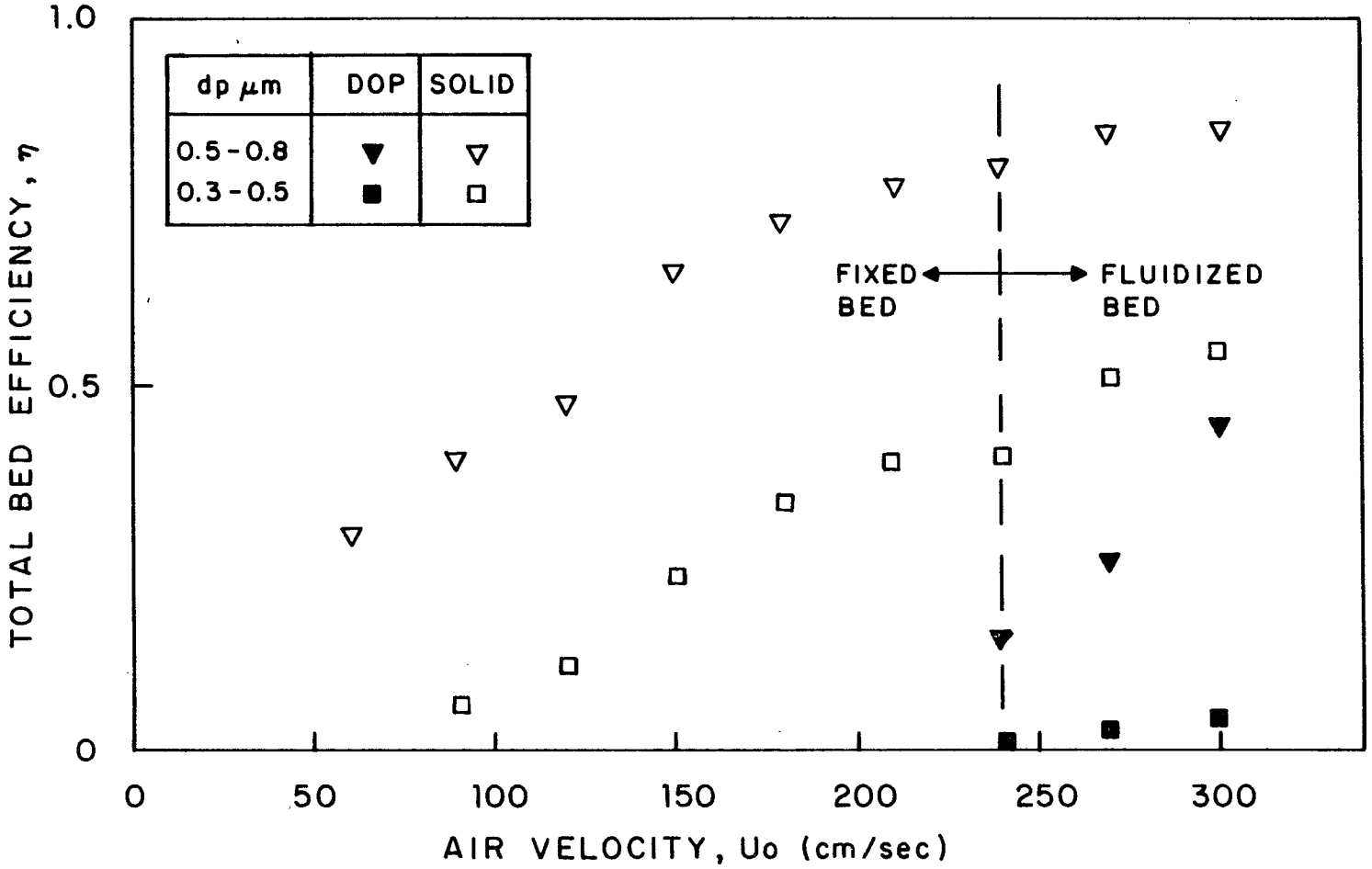

Figure 4.20: Total bed efficiency as a function of air velocity for DOP aerosol and solid dust in the RFBF containing 0.3 cm diameter polyethylene granules. Bed thickness, L = 3.0 cm; Bed porosity, ε = 0.4; Relative Humidity, RHu = 0-10%

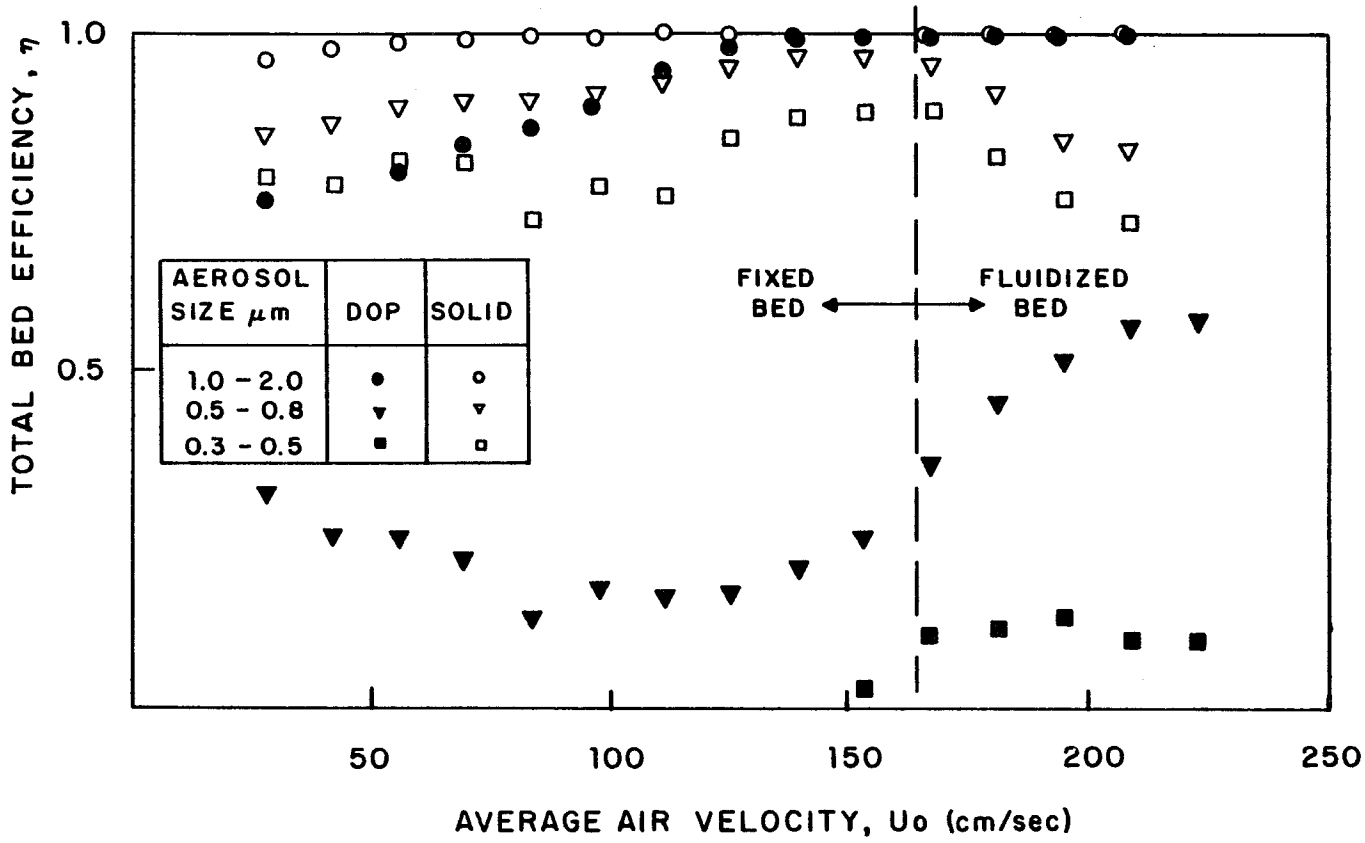

Figure 4.21: Total bed efficiency as a function of air velocity for DOP aerosol and solid dust in the RFBF containing Ø.Ø7 cm diameter polystyrene granules. Bed thickness, L = 1.Ø cm; Bed porosity, ε = Ø.37; Relative humidity, RHu = Ø-1Ø%

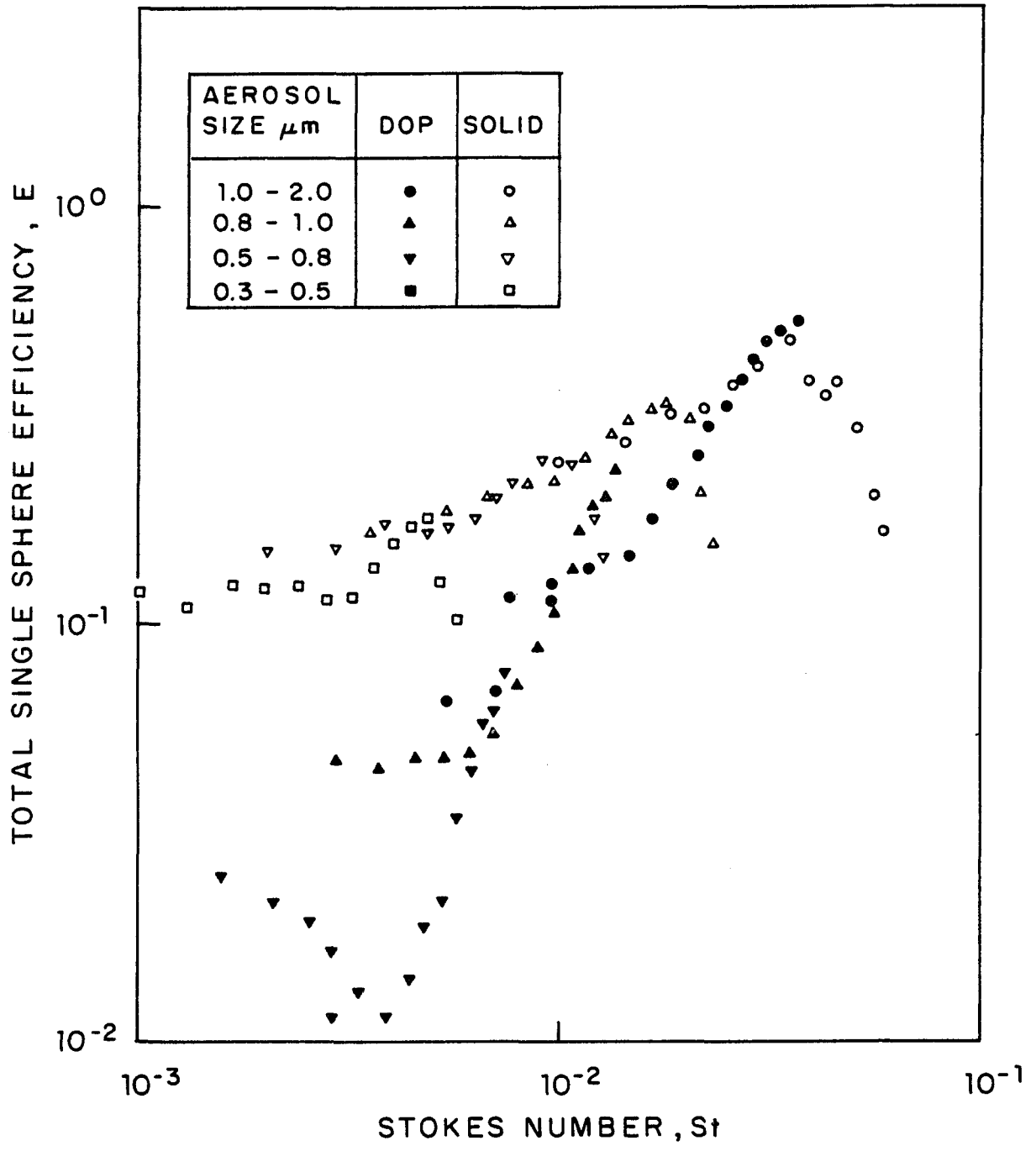

Figure 4.22: Single sphere efficiency as a function of the Stokes number for DOP aerosol and solid dust in the RFBF containing 0.07 cm diameter polystyrene granules. Bed thickness, L = 1.0 cm; Bed porosity, ε = 0.37; Relative humidity, RHu = 0-10%

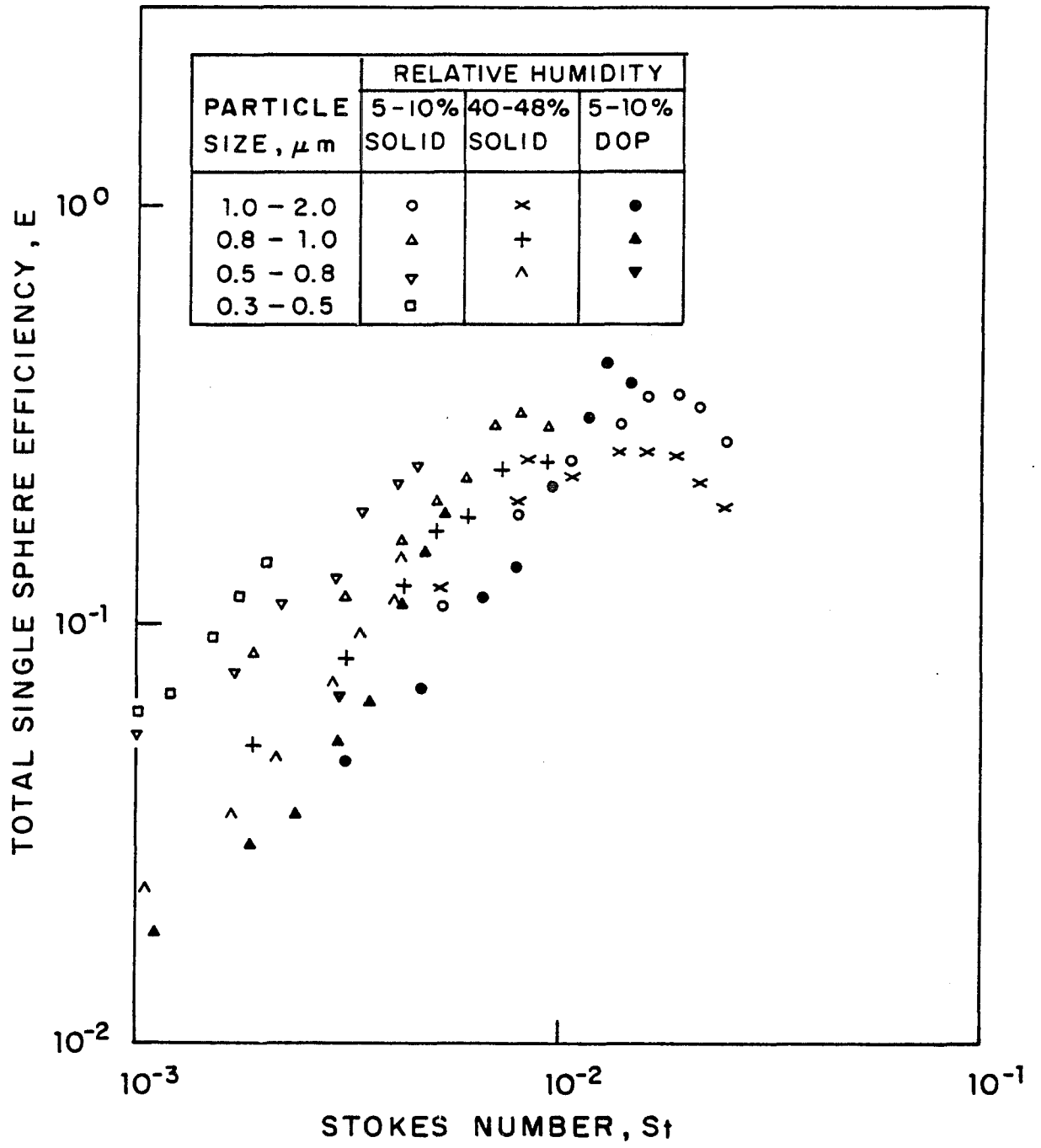

Figure 4.23: Single sphere efficiency as a function of the Stokes number for DOP aerosol and solid dust in the RFBF containing Ø.3 cm diameter polyethylene granules. Bed thickness, L = 3.Ø cm; Bed porosity, ε = Ø.4

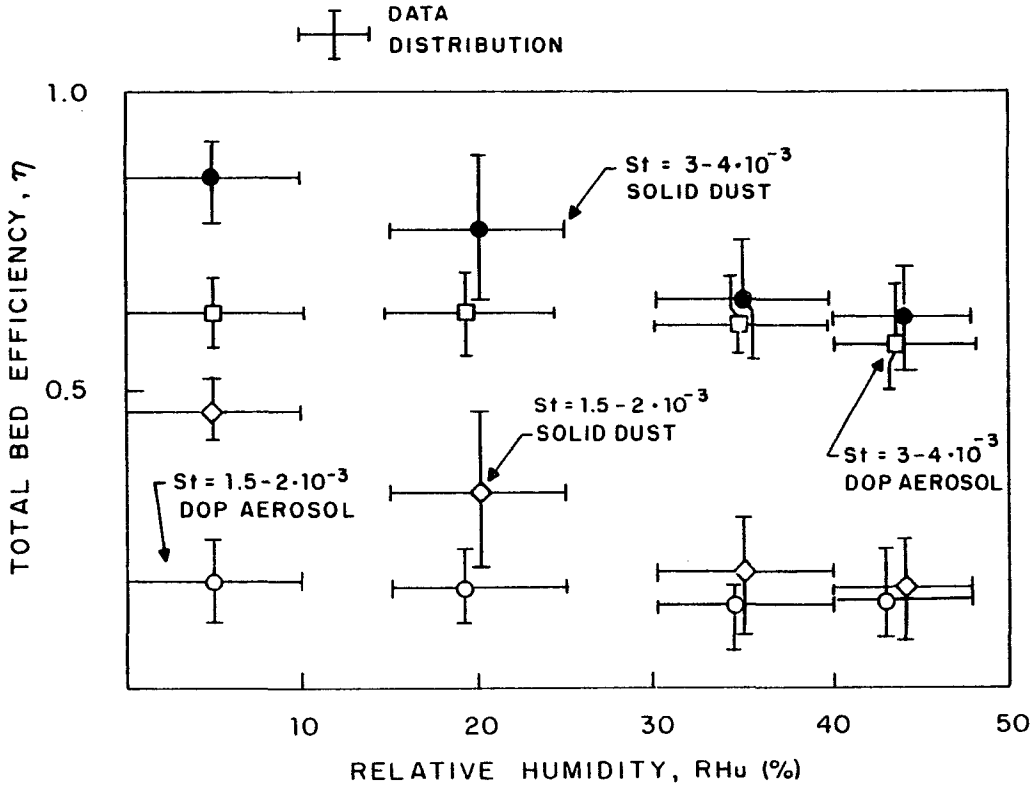

Figure 4.24: Total bed efficiency as a function of air relative humidity for solid dust and DOP aerosol at different Stokes numbers in the RFBF containing Ø.3 cm diameter polyethylene granules. Bed thickness, L = 3.Ø cm; Bed porosity, ε = Ø.4

is the average of many experiments performed during different days because relative humidity in these experiments is measured but is not controlled. As shown in the figure the filtration efficiency of the solid dust drops by about 25-30% as the relative humidity increases from 0-10% to 40-48% at low Stokes numbers ranging from $1.5\text{-}2\text{x}10^{-3}$ to $3\text{-}4\text{x}10^{-3}$. Similar phenomena is not observed for the filtration efficiency of the DOP aerosol which remains about constant as the relative humidity changes. At high relative humidity the filtration efficiency of the solid dust drops to the level of the efficiency of the DOP aerosol.

The fact that relative humidity and the type of granules and aerosol affect filtration efficiency is due mainly to electrostatic effects. Quantitative evalution of these effects, however is very difficult both theoretically and experimentally. Ciborvsky and Wlodarsky (1962), Tardos and Pfeffer (1980) and Tardos et al. (1983) measured the average net charge in fluidized beds by measuring the current generated when a grounded wire is submerged inside the fluidized bed or directly by collecting a bulk of granules in a Faraday cage. Measuring net average charge, is practically meaningless for a quantitative anlysis of the electrostatic effects since triboelectrification, by nature, produces positive and negative charges, and the magnitude of the electrical field in the voidage of the bed, hence the

filtration efficiency, depends on both. In fact, if the bed is electrically insolated and charge is not dissipated through the flowing air the net charge in the bed is expected to be zero.

Electrostatic charge on bed granules was measured simultanously with that of dust concentration. A side stream of out-going granules flows into the Teflon vessel inside a Faraday Cage as shown in Figure 4.4. If a granule entering the cage is electrically charged it produces an electric field inside the cage which induces an equal charge on the copper vessel which forms the cage. This charge is measured by the Keithly 610c electrometer and by the HP 3438A voltmeter. The data is also collected on a microcomputer for storage and analysis. Each one volt reading corresponds to 10^{-9} coulombs for the 0.3 cm polyethylene granules and 0.3×10^{-9} coulombs for the 0.07 cm polystyrene granules.

The electric potential reading is recorded continuously and each time a charged particle enters the cage there is a step change in the reading. The step change may be positive or negative according to the charge on the incoming particle. A similar procedure was earlier used by Tardos and Pfeffer (1980) for electrostatic charge measurments on bulk granules. Details and considerations regarding the precision of the method are described there. The number of step changes in the electric potential reading was compared to

the actual number of particles collected in the Teflon vessel and was found to be within a range of 85-100% in all experiments. Usually (but not always) the number of particles in the vessel was larger than the number of step changes. This may indicate the presence of electrically neutral particles. If the stream of granules is kept low enough so that particles are entering the Faraday cage one at a time one can obtain the electrostatic charge distribution on the granules. Such results on 0.3 cm in diameter polyethylene and 0.07 cm in diameter polystyrene granules are shown in Figures 4.25-27 for different relative humidities and with clean or contaminated air flowing through the bed. Each curve in Figures 4.25-27 represents the average charge from measurements on 500 to 1500 granules performed over several different runs. Since the relative humidity is not conrolled, the results are given within a range of humidities of about 10%. The results clearly show that both positive and negative charges exist in the bed. The charge is evenly distributed between negative and positive both in magnitude and in numbers of charged granules. The net average charge per particle, $\tilde{q}_c$, is defined as:

$$\tilde{q}_c = \sum_{i=1}^{n} q_i/n \qquad (4.8)$$

where n is the number of granules counted and q_i is the individual charge on each particle.(In Figures 4.21-23, $\tilde{q}_c$

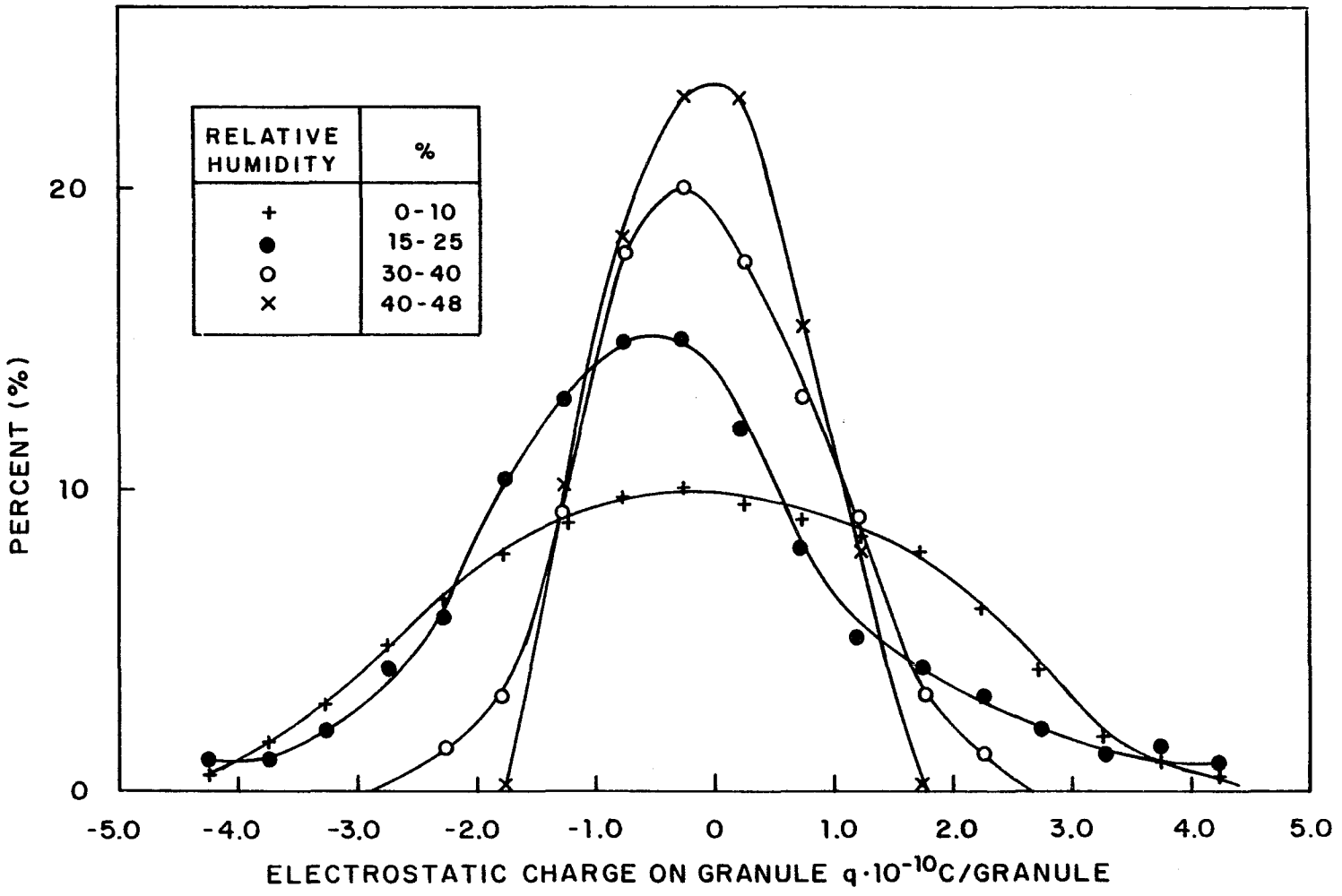

Figure 4.25: Electrostatic charge distribution on polyethylene granules Ø.3 in diameter in the RFBF.
Bed thickness, L = 3.Ø cm; Bed porosity, ε = Ø.4

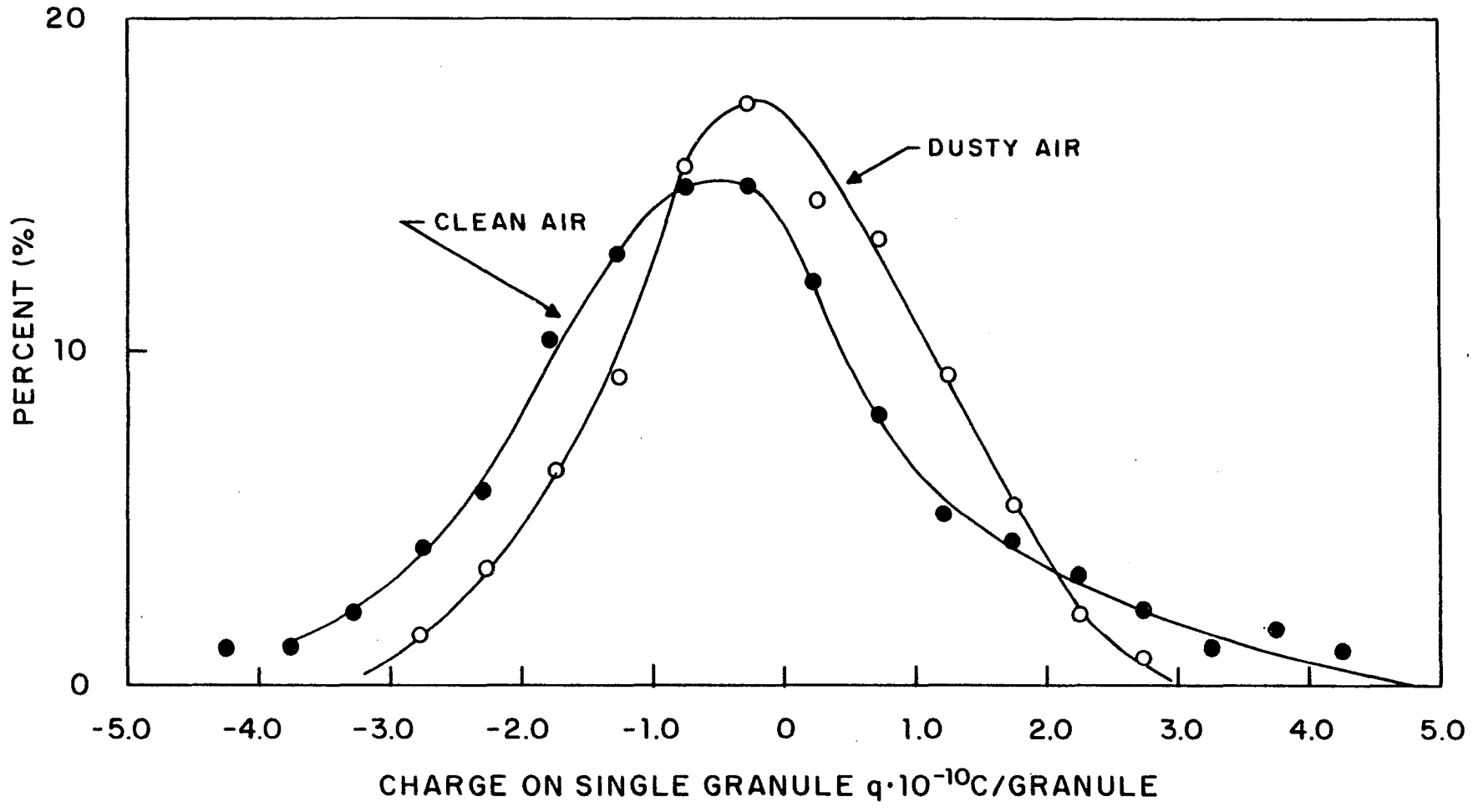

Figure 4.26: Electrostatic charge distribution on polyethylene granules Ø.3 cm diameter in the RFBF.
Bed thickness, L = 3.Ø cm; Bed porosity, ε = Ø.4;
Relative humidity, Rhu = 15-25%

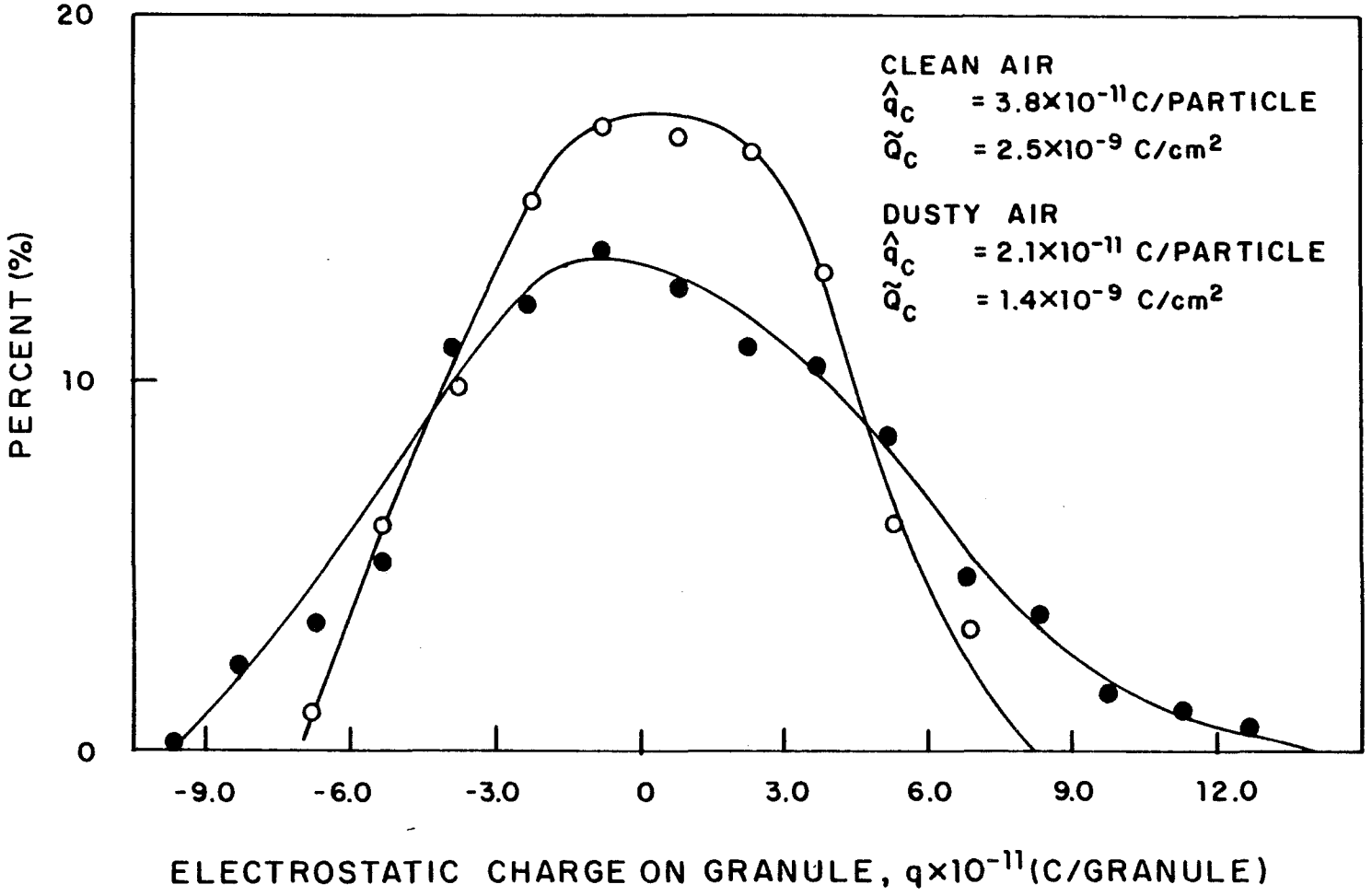

Figure 4.27: Electrostatic charge distribution on polystyrene granules 0.07 cm diameter in the RFBF.
Bed thickness, L = 1.0 cm; Bed porosity, ε = 0.37;
Relative humidity, RHu = 0-10%

is the value obtained by a line that devides the area under each curve into to equal parts). As seen the value of $\tilde{q}_c$ is very small and it fluctuates between positive and negative values. If one defines the absolute average charge as

$$\hat{q}_c = \sum_{i=1}^{m} |q_i| / n \qquad (4.9)$$

where $|q_i|$ is the absolute value of the charge on individual particle. The values found for $\tilde{q}_c$ are smaller by about an order of magnitude than the absolute average charge, $\hat{q}_c$. As relative humidity increases, the positive and negative branches of the distribution curves (see Figure 4.25) move closer to zero and the absolute average charge, q_c, becomes significantly smaller. This is shown in Figure 4.28 where $\hat{q}_c$ for relative humidity RHu=40-48% is only about 20% of $\hat{q}_c$ for RHu=0-10%.

When a charged aerosol particle is captured by a granule with opposite charge there is a reduction in the net charge of the granule. As charged aerosols flow through the roating fluidized bed the absolute average charge, $\hat{q}_c$, decreases as shown in Figures 4.26-28. The electrostatic charge on the granules becomes smaller and the tail coresponding to particles with high charges almost disappears. The drop in charge is about 25% for the experiments described in Figure 4.28 and about 45% for the experiments described in Figure

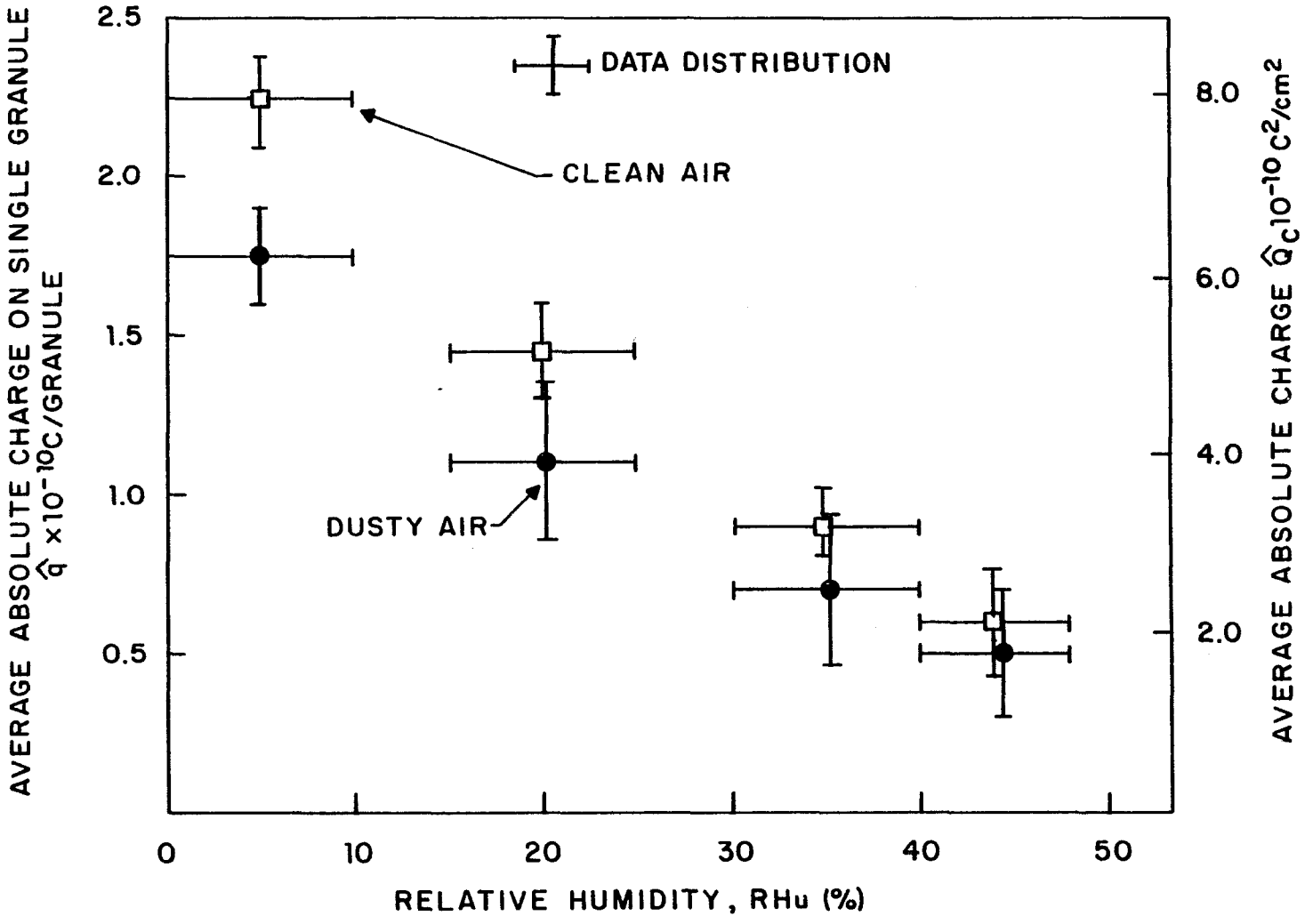

Figure 4.28: Average absolute electrostatic charge on polystyrene granules Ø.3 cm diameter in the RFBF as a function of relative humidity.
Bed thickness, L = 3.Ø cm; Bed porosity, ε = Ø.4;

4.27. There are many parameters effecting the charge distribution in Figures 4.26 and 4.27 including the magnitude and sign of charge on the aerosol particles, aerosol concentration, air flow rate, collection efficiency, granule material and the effect of aerosols coating the granules on their conductivity.

The general shape of the charge distribution curve for polyethylene and polystyrene is similar in Figures 4.25-27. The individual charge is different, however, due to the granule size and to differences in material composition. For the same humidity between Ø-1Ø% the absolute average charge $\hat{q}_c$=1.7-2.2x1Ø$^{-1Ø}$ C for poylethylene granules (see Figure 4.28) and it is 2.1-3.8x1Ø$^{-11}$ C for polystyrene granules (Figure 4.27). The average absolute charge per unit surface area is about 6-8x1Ø$^{-1Ø}$ C/cm^2 for polyethelene and 1.4-2.5x1Ø$^{-9}$ C/cm^2 for polystyrene.

The average electrostatic charge on dust particles is also measured simultanously with the filtration efficiency and the charge on the granules using a side stream of dusty air just before it enters the filter plenum, as shown in Figure 4.4. The flow rate of the side stream is kept equal to the flow rate of air to the particle analyzer so that the number of particles counted is also the number of particles in the side stream. The side stream of dusty gas flows through an absolute filter which is situated in a second

Farady cage as shown in Figure 4.29. The apparatus is the same as the one used and described earlier by Tardos and Snaddon (1983). All dust particles are assumed to be captured in the absolute filter which is grounded through an electrometer. From the measurement of the current produced, which is the net flow of all the charges on the dust particles, and the measuement of the number and size of all particles flowing per unit time one can find the average charge of these particles.

The reading obtained from the above measurement is the same as the total net absolute average charge, $\hat{q}_p$, when all charges have the same sign. If a significant number of particles have opposite charge than the average charge, $\tilde{q}_p$, is much smaller than $\hat{q}_p$. To find the net average charge on individual aerosol particle it is assumed that the magnitude of charge is proportional to its surface area so that the average charge on a particle of given size can be found according to:

$$\tilde{q}_{pj} = I \times P_j / N_j \qquad (4.1\emptyset)$$

where j is a certain size range measured by the Climet particle analyzer, I is the current measured by the Keithly electrometer as described above, P_j is the fraction of surface area of all particles in the size range j (see Figure 4.3) and N_j is the number of particles of size range

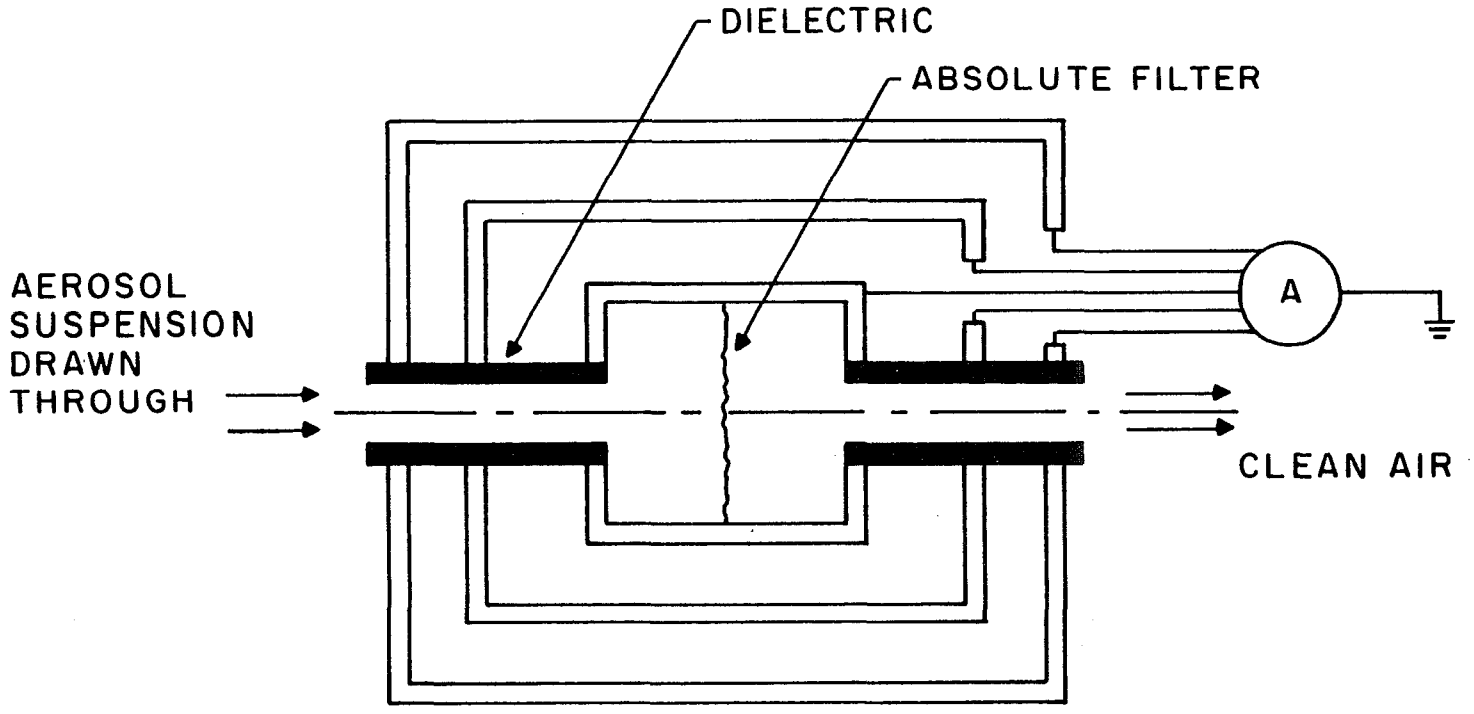

Figure 4.29: Faraday Cage for the measurement of electrostatic charge on dust particles.

j flowing through the Faraday cage per unit time. Similarly, the average charge per unit area, $\tilde{Q}_p$, can be found by

$$\tilde{Q}_p = I / \sum_{j=1}^{m} N_j x A_j \qquad (4.11)$$

where A_j is the average surface area of particles in the range j. The inacurracy in finding $\tilde{q}_{pj}$ and $\tilde{Q}_p$ is quite large due to the fact that the aerosol concentration is not stable, (especially in the experiments with solid dust) causing considerable fluctuations in the current I. The relative humidity is not controlled during the experiments and runs were performed over ranges of relative humidities rather than at a fixed value. Yet, it is possible to measure charge variation due to changes in relative humidity as shown in Figure 4.30.

The electrostatic charge on the solid dust particles is of the order of $+10^{-10}$ C/cm^2 while the charge on the DOP aerosol is of the order of $-0.1x10^{-10}$ C/cm^2. The results in Figure 4.30 clearly explain the much higher collection efficiency of solid dust as compared to DOP aerosol (See Figures 4.20 to 4.24). The magnitude of the charge on the naturally charged solid dust is about ten times as high as that of the naturally charged DOP at low relative humidities and about three times as high at high relative humidities. The electrostatic charge on the DOP aerosol is small and is not affected by humidity and consequently the filtration

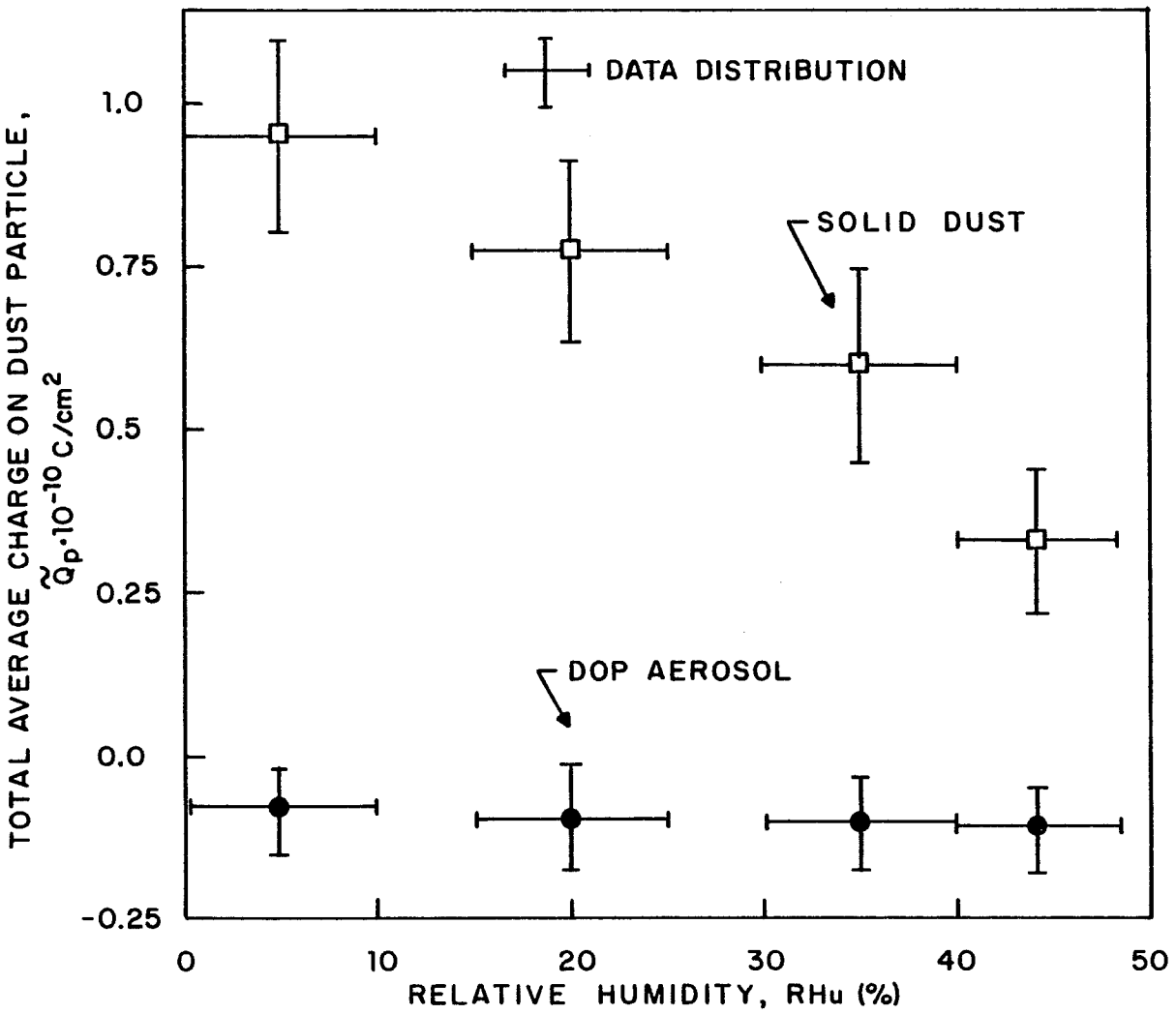

Figure 4.30: Total average charge on aerosol particles as a function of humidity.

efficiency of the DOP particles is independent of the relative humidity as shown in Figure 4.24. The differences in filtration efficiency between the DOP and the solid dust for the same Stokes numbers (See Figures 4.22 and 4.23) is the result of stronger electrostatic forces on the solid dust. The drop in the average absolute charge on granules when dusty air is flowing through the bed indicates that the charged dust particles are captured on granules with opposite charge hence reducing the total charge of the bed.

Since in the rotating fluidized bed experiments described above, both dust and bed granules are electrically charged the electrostatic effects are mainly due to Coulombic forces. The dimensionless parameter characteristic of Coulombic forces, K_c, is given by

$$K_c = Cq_c q_p / 24\,{}^{2}\epsilon_f r_p a^2 \mu U_o = 2Cr_p Q_c Q_p / 3\epsilon_f \mu U_o \qquad (4.12)$$

If one takes the charge Q_p to be the average charge $\tilde{Q}_p$ as defined by equation 4.11 and Q_c to be the total absolute average charge per unit area of granule, experimental values for K_c can be computed. Such values calculated for solid dust and polystyrene granules at a relative humidity of Ø-1Ø% as a function of the Stokes number is given in Figure 4.31. The values of K_c increase as the Stokes number decreases which is an indication of the importance of electrostatic effects in the low Stokes nubers range.

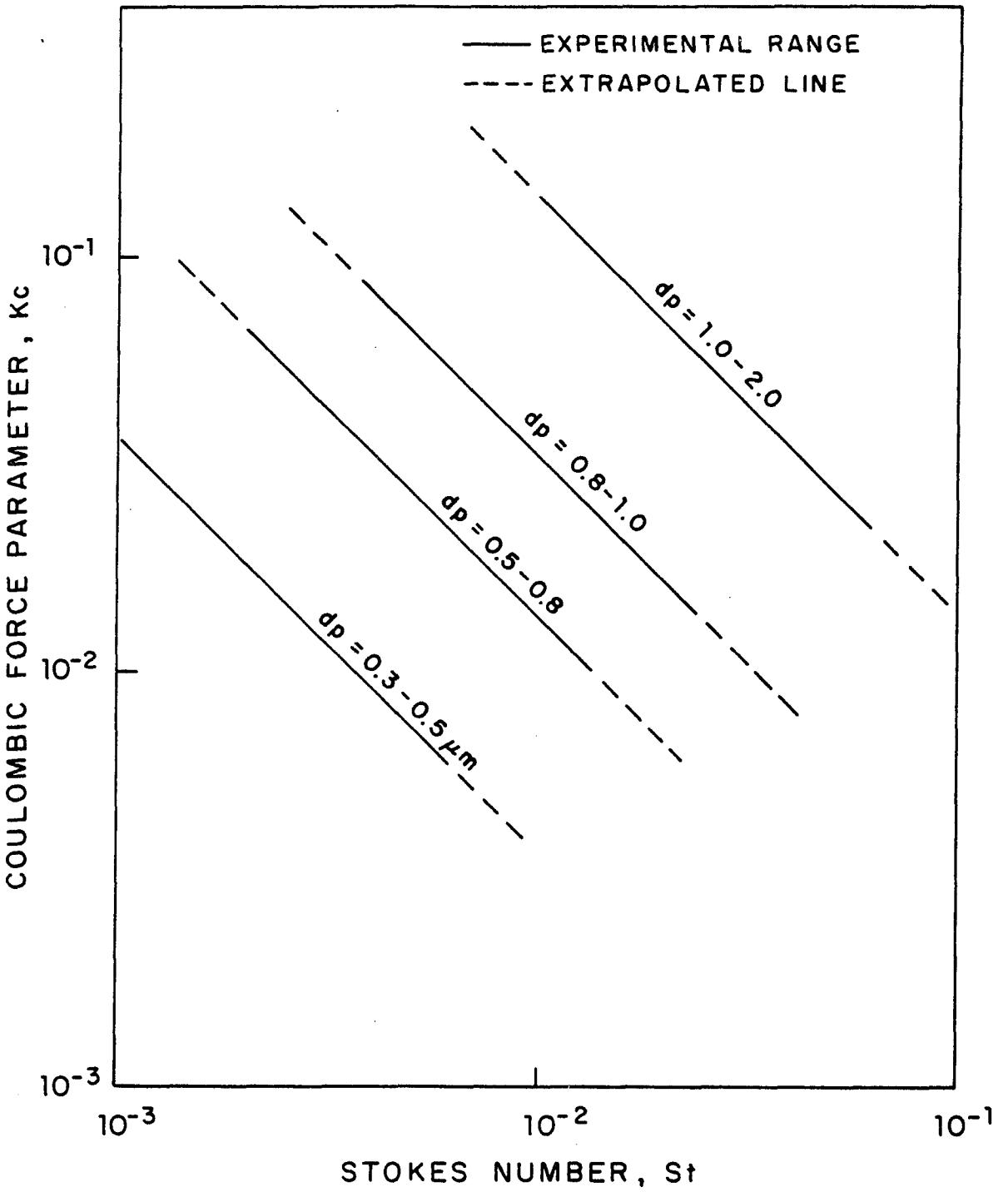

Figure 4.31: The coulombic force parameter K_c as a function of the Stokes number calculated for the Ø.Ø7 cm diameter polystyrene granules using equation 4.12. The electrostatic charges, Q_c and Q_p are found in figures 4.27 and 4.3Ø respectively.
Relative humidity, RHu = Ø-1Ø%

Comparison of the effect of electrical forces on the filtration efficiency of the RFBF is given in the following section.

4.6. Comparison of results with theoretical models

As shown in section 4.4 inertia is the most important filtration mechanism in the rotating fluidized bed filter for the filtration of DOP aerosol. Electrostatic effects become important in the filtration of naturaly charged solid dust at low relatively humidity as demonstrated in section 4.5. Direct interception, diffusion and gravity settling playes a minor roll in the range of Stokes numbers of about $0.001 < St < 0.01$.

Single sphere efficiency in the RFBF calculated using equation 2.3 with DOP aerosol filtered in a bed of 0.3 cm diameter polyethylene granules is compared in Figure 4.32 to the correlations derived by Goren (1978), Thambimuthu et al (1978), D'Ottavio and Goren (1983) and to the model for inertia in a fixed bed as derived in section 3. All the works mentioned above are derived for fixed bed conditions and compare poorly with the experimental results shown in Figure 4.32. D'Ottavio and Goren's correlation seems to underestimate the effect of Reynolds numbers. The correction factor to the Stokes number there depends on $Re^{0.5}$ so that the experimentally calculated St_{eff} are

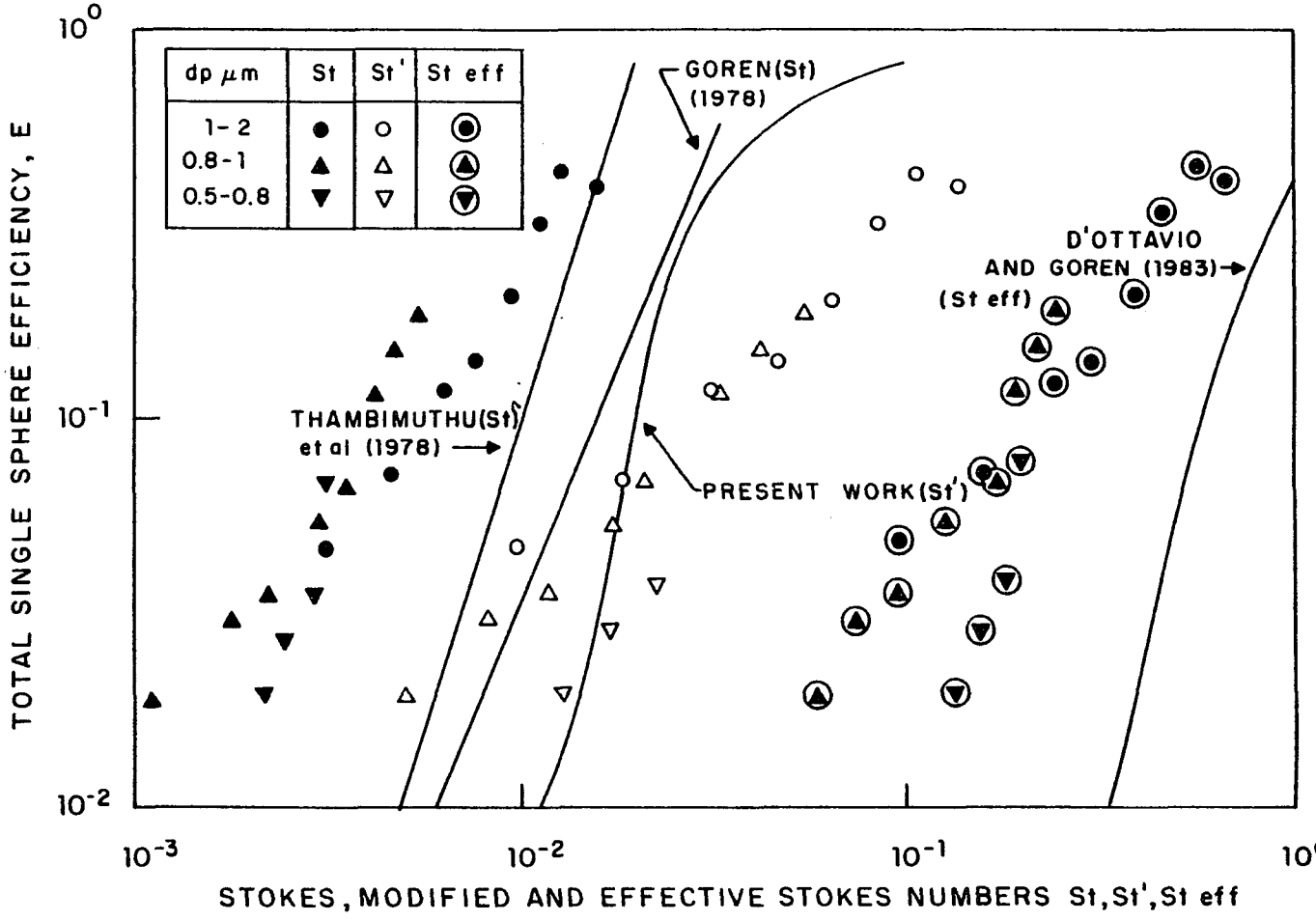

Figure 4.32: Single sphere efficiency as a function of Stokes, modified and effective Stokes numbers using polyethylene granules Ø.3 cm diameter. Bed porosity, ε= Ø.4; Relative humidity, RHu = 35%; Rotating speed, W = 45Ø RPM

smaller than the correlation predicts and all experimental points fall to the left of the correlation curve by a factor of Ø.3 to Ø.5 of St_{eff}. On the other hand in the theoretical correlation developed during the present work (equation 3.24) the correction factor containing the Stokes number depends linearly on Re. This linear dependence seems to overestimate the effect of the Reynolds number especially for high Re. The experimentally calculated modified Stokes numbers, St' are by a factor of 1.5 to 3.Ø larger than predicted by the model. For the lower range of Stokes and Reynolds numbers the model predicts the efficency somewhat better. The correlations by Thambimuthu et al (1978) and Goren (1978) also underestimate the efficiency as is shown in Figure 4.32.

DOP experiments using polystyrene granules of Ø.Ø7 cm in diameter were performed at lower Reynolds numbers and agree much better with the correlations mentioned above, as shown in Figures 4.33-35. The correlation by Thambimuthu et al (1978) agrees well with the experimental results at the lower range of Stokes numbers Ø.ØØ4<St<Ø.Ø12 in Figure 4.33 while Goren's (1978) correlation agrees better with the experimental results at the higher range of Stokes numbers, Ø.Ø15<St<Ø.Ø4. The slope predicted by Pendse and Tien's (1982) correlation is smaller than the experiments show. One reason for this is that the curves are drawn for a constant Reynolds number while the experimental values are in the

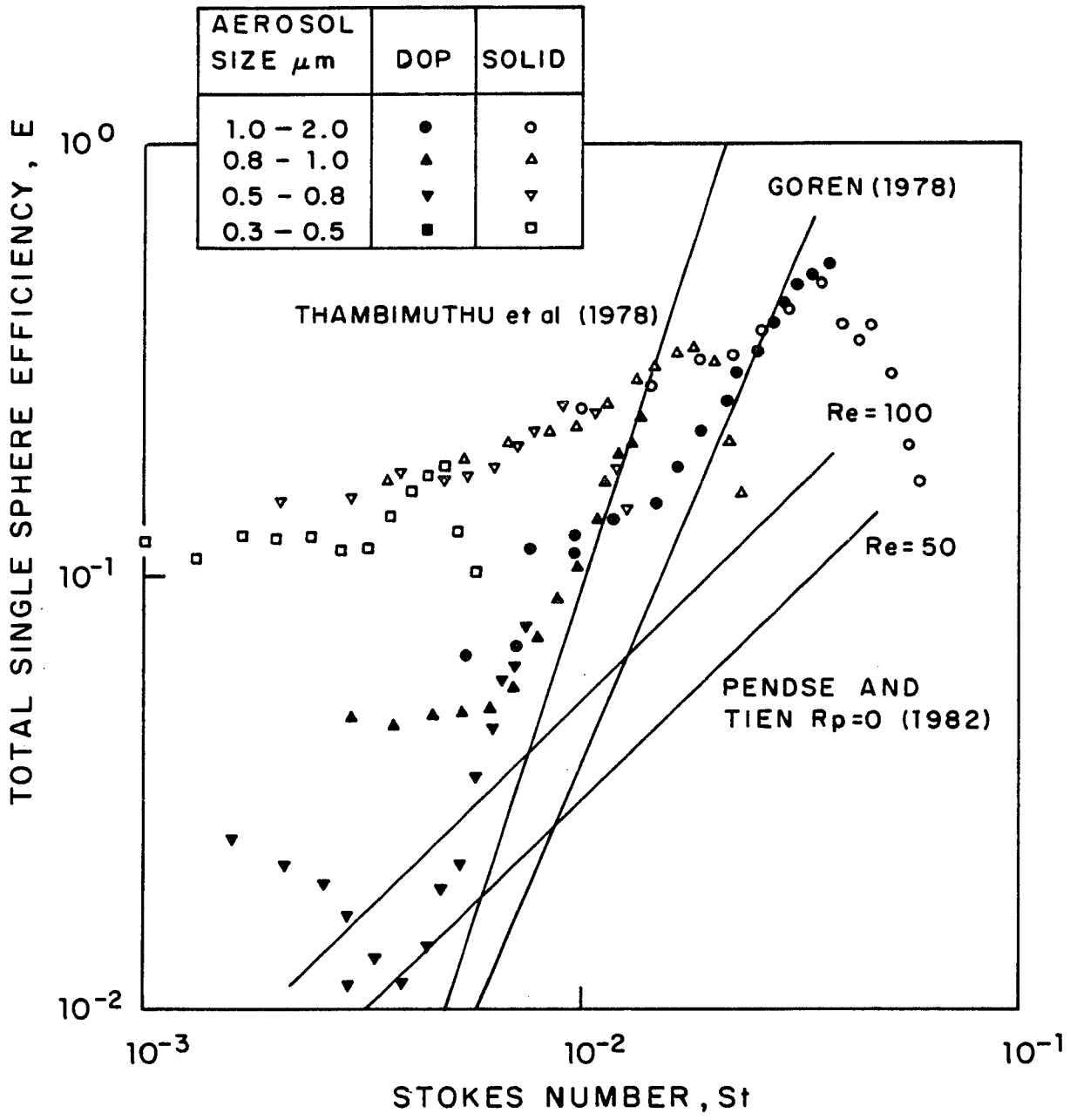

Figure 4.33: Single sphere efficiency as a function of the Stokes number using polystyrene granules Ø.Ø7 cm diameter. Relative humidity, RHu = Ø-1Ø%; Bed porosity, ϵ = Ø.37; Rotating speed W = 6ØØ RPM

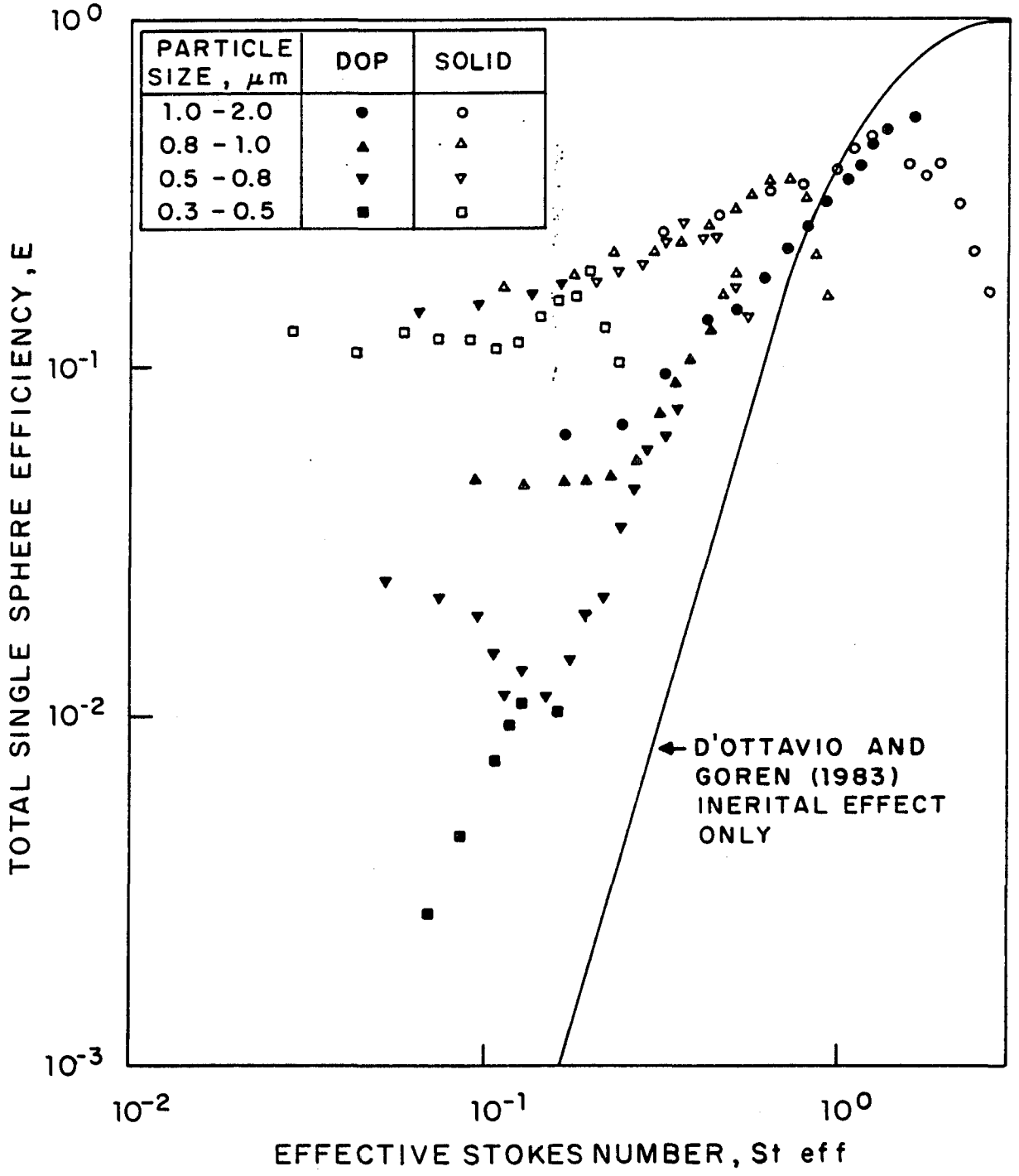

Figure 4.34: Single sphere efficiency as a function of the modified Stokes number using polystyrene granules 0.07 cm diameter. Relative humidity, RHu = 0-10%; Bed porosity, ε = 0.37; Rotating speed W = 600 RPM

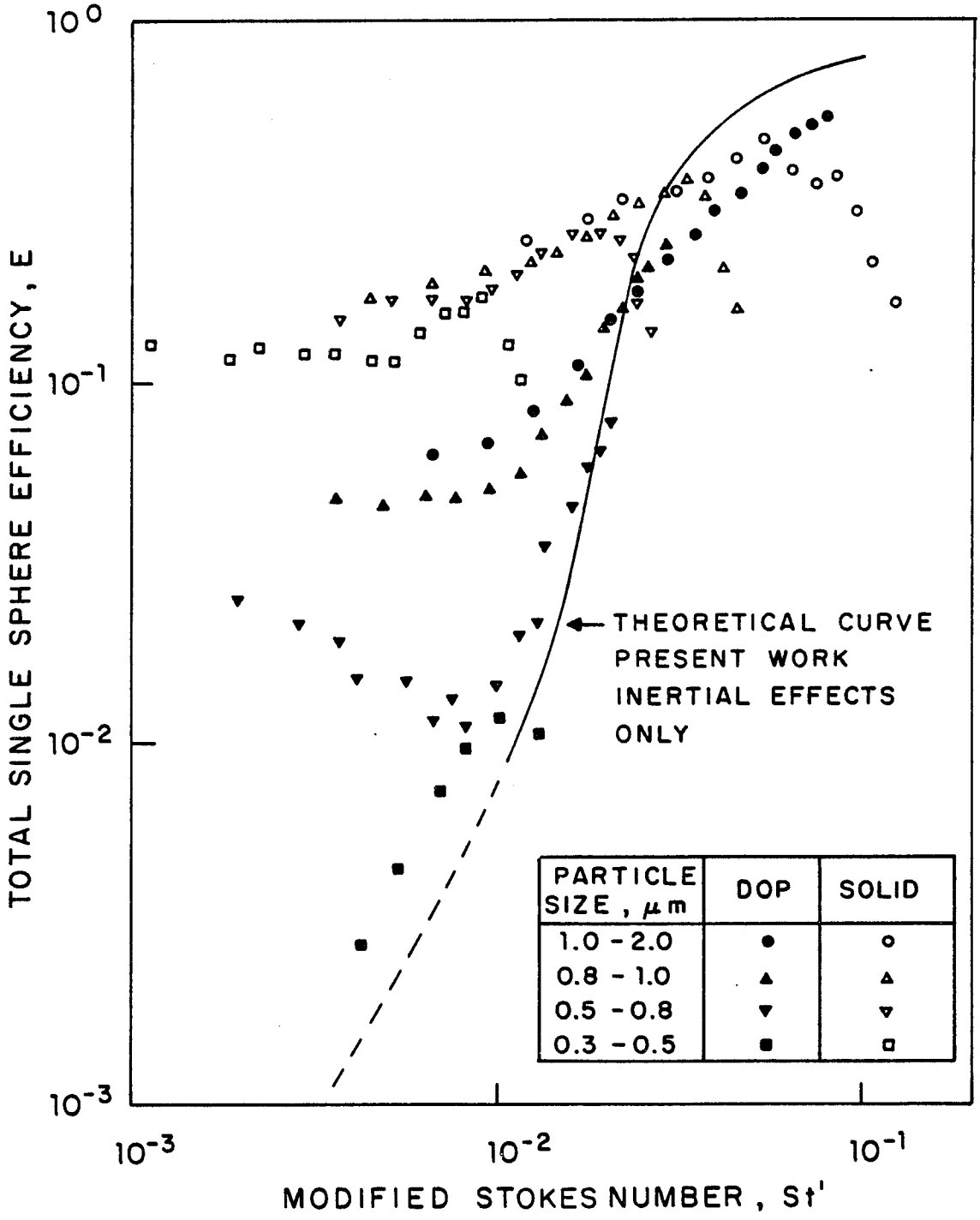

Figure 4.35: Single sphere efficiency as a function of the effective Stokes number using polystyrene granules 0.07 cm diameter. Relative humidity, RHu = 0-10%; Bed porosity, ε = 0.37; Rotating speed W = 600 RPM

Reynolds number range of 15-12Ø. The experiments with polystyrene are also compared to the D'Ottavio and Goren (1983) correlation, Figure 4.34, and the present work (inertia model) in Figure 4.35. The experimental results agree relatively well with the models. Still, D'Ottavio and Goren's correction factor underestimates the effect of the Reynolds number at the low range of Stokes numbers while the present inertia model overestimates the effect of Reynolds number at high Stokes values. The model agrees very well with the experimental results for St<Ø.Ø3.

The correlations discussed above, were derived for inertial impaction effects only. All the experimental points which are far right of the curves in figures 4.34 and 4.35 can be explained by either experimental error, bouncing effects for the solid dust or inaccuracies in the model for the DOP. All points which are significantly to the left of the curve represent the effects of filtration mechanisms other than inertia. Those effects are strong especially in the filtration of soild dust. The effect of diffusion, interception and gravity settling on filtration efficiency, as calculated in section 4.4.3 is shown in Figure 4.36. All values of the combined effect, E_{RDG} for potential and viscous flows are lower than the experimental results. The calculated E_{RDG} is negligble compared to the total single sphere efficiency, E, for solid dust. E_{RDG} at Re->Ø is also very small compared to E for DOP while E_{RDG}

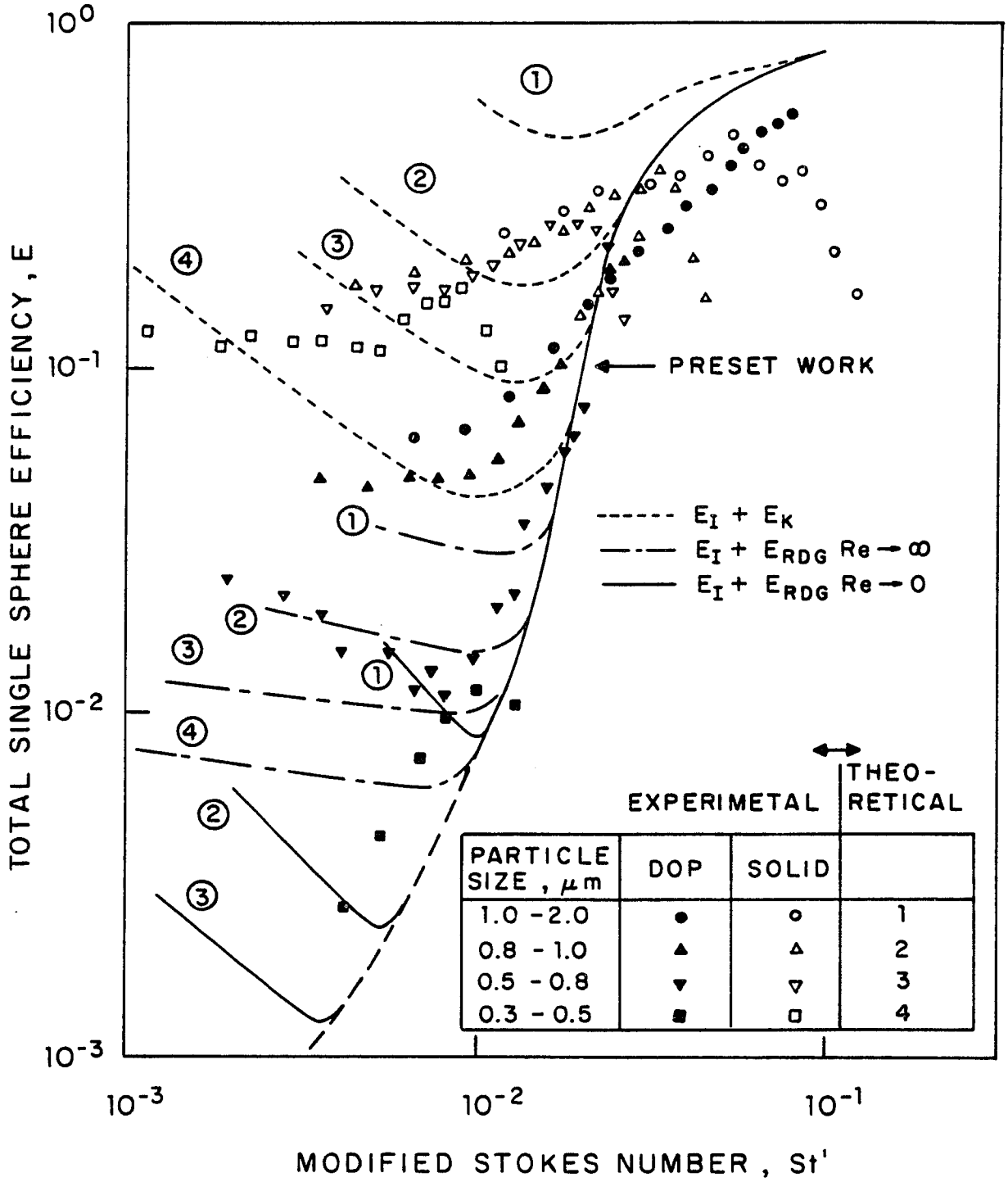

Figure 4.36: Single sphere efficiency as a function of the modified Stokes number using polystyrene granules 0.07 cm diameter. Relative humidity, RHu = 0-10%; Bed porosity, ε = 0.37; Rotating speed W = 600 RPM

at Re->∞ is smaller by a factor of 2-3 than the experimental values.

Electrostatic effects clearly play a major roll in improving filtration efficiency in the rotating fluidized bed filter at low Stokes values in the range $\emptyset.\emptyset\emptyset1<St<\emptyset.\emptyset1$. The value of the electrostatic parameter, K_c, for solid aerosol is shown in Figure 4.31. It is impossible however, with existing models to quantitatively predict the single sphere efficiency due to these effects, E_k, in the RFBF. Even if we ignore the experimental difficulties involved in the evaluation of K_c including the averaging of charge on the dust particles and we accept the value found for K_c there is still a basic unresolved problem. The single sphere efficiency approach assumes all granules in the bed experience the same filtration phenomena. While in the case of inertia, diffusion, interception and gravity settling this is to a large extent true, it is not so for the case of electrostatic effects in a naturally charged bed where positive and negative charges exist. A charged aerosol particle entering the bed experiences attraction and repulsion forces as it approaches different granules. The net effect is an increase in filtration efficiency as shown in figure 4.36. Thus the existing theoretical models are not likely to predict the affect of electrostatic charge in a granular bed filter such as RFBF. With the reservation mentioned above the value of the single sphere efficiency,

E_k, is computed as shown in Figure 4.36 using the solution of Nielsen and Hill (1976) for a single charged particle and a single charged granule:

$$E_k = 4K_c \qquad (4.13)$$

While the experimental values of the single sphere efficiency supposedly caused by electrostatics $E-E_I-E_{RDG}$ (Figure 4.36) decrease slightly as the Stokes number decreases in the narrow range of Ø.1-Ø.2 the values of the computed E_k from equation 4.13 increases much more in the range of Ø.Ø6-Ø.6. This discrepancy only shows that the single sphere model for electrostatic deposition which is due to triboelectrification effects is far to simplistic to enable accurate computation of this effect. A new model is clearly necessary to explain the results obtained in the RFBF. This task, however is not talked in this work.

4.7 New Design of a pilot RFBF

A main problem in the existing roatting fluidized bed filter is the nonunoformity of fluidization as explained in section 4.4.5. Fluidization starts close to the surface of the bed where the gas velocity is relatively high and centrifugal forces are relatively weak. While the region close to the surface may be under fluidization conditions the region close to the distributor may still experience

fixed bed conditions. The bed becomes unstable when the bed is thick especially when the granules are small.

A new system is proposed to solve the nonuniform fluidization problem and is shown in Figure 4.37. The rotating cylinder is divided into four separate equal sections where the air flow rate to each is the total flow rate F divided by four. If h is the hieght of the cylinder the cross section area in each section is $A(r)=h2\pi r\theta$ and the velocity is $U=F/h8\pi r\theta$. The differential form of the Ergun correlation for the arrangement in Figure 4.37 for a fixed bed is given by:

$$dp/dr = k_1/r\theta + k_2/r^2\theta^2 \qquad (4.14)$$

where: $k_1 = 150\mu(1-\varepsilon)F / d_g^2 \varepsilon^3 h8\pi$

$$k_2 = 1.75\rho_l(1-\varepsilon)F^2 / d_g \varepsilon^3 h^2 64\pi^2$$

and the differential pressure drop for fluidization is given by the equation:

$$dp/dr = (1-\varepsilon)\rho_g W^2 r = k_3 r \qquad (4.5)$$

At minimum fluidization the differential pressure drop in equations 4.14 and 4.5 is equal so that

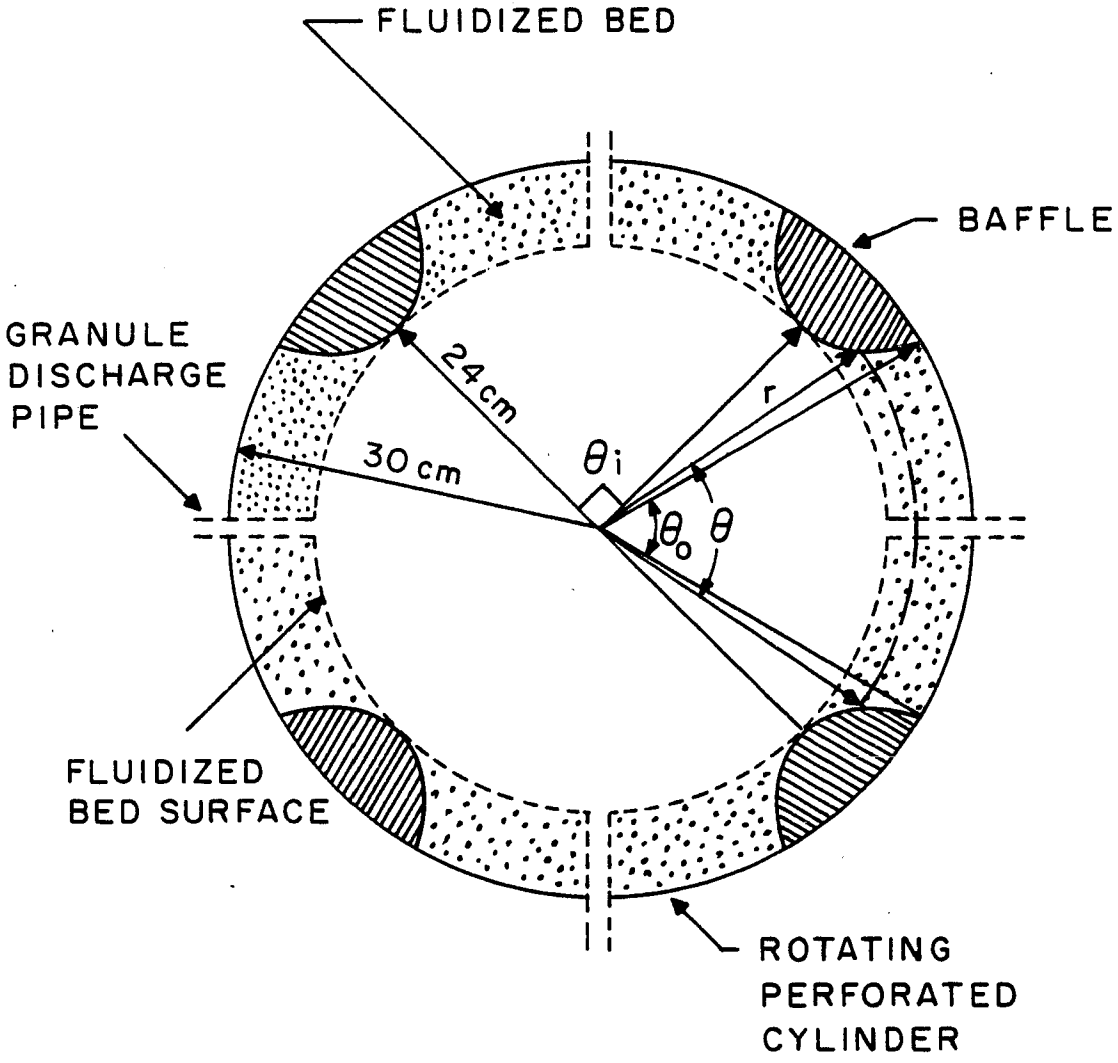

Figure 4.37: A design for a pilot size rotating fluidized bed filter. Top view.

$$k_1/r\theta + k_2/r^2\theta^2 = k_3 r \qquad (4.15)$$

At Re->Ø equation 4.15 reduces to

$$k_1/r\theta = k_3 r \qquad (4.16)$$

so that

$$\theta/\theta_o = (r_\emptyset/r)^2 \qquad (4.17)$$

at Re-> ∞ equation 4.15 reduces to

$$k_2/r^2\theta^2 = k_3 r \qquad (4.18)$$

so that

$$\theta/\theta_o = (r_\emptyset/r)^{1.5} \qquad (4.19)$$

The fluidization in the rotating fluidized bed filter will be uniform if the radii ratios suggested by equation 4.17 for low Reynolds numbers, or equation 4.19 for high Reynolds numbers, is used. The above solution also indicates that the existing RFBF is more difficult to control when it operates with small granules because the granule's Reynolds number is small and the ratio of angles required for uniform fluidization is closer to that of equation 4.17 than to that of equation 4.19. In a rotating fluidized bed filter with a

distributor radius of $r_{\emptyset}$=30cm, a maximum bed thickness of L=6 cm (r_i=24 cm) and an opening angle of $\theta_i(r_i=24\ cm)=90^{\circ}$ about 36% of the distributor should be blocked ($\theta_{\emptyset}=58^{\circ}$) at Re->0. At Re->$\infty$ only 28% of the distributor should be blocked ($\theta_{\emptyset}=65^{\circ}$). For a larger bed diameter and moderately thick bed the angle difference is not significant.

A 30 cm radius bed with baffles as shown in figure 4.37, will be easy to controll and to operate. Elutriation should not be a problem if working conditions are kept within the range of 20-30% of minimum fluidization.

The granules' feeding system used in the existing RFBF is similar to the one used by Levy et al (1978) and should work well if a proper air lock is installed.

The granules discharge system should be replaced, so that granules are discharged through the plenum as shown in figure 4.38. The plennume should be an outer cyclone used both as a housing for the filter and a separator for large aerosol particles. Dirty granules will be discharged through small pipes penetrating through the distributor. The pipe's penetration into the cylinder should be adjustable so as to determine the required bed thickness, as shown in figure 4.38. The granules will be discharged to the cyclone and be collected at its bottom, where they can be removed through the lock hopper.

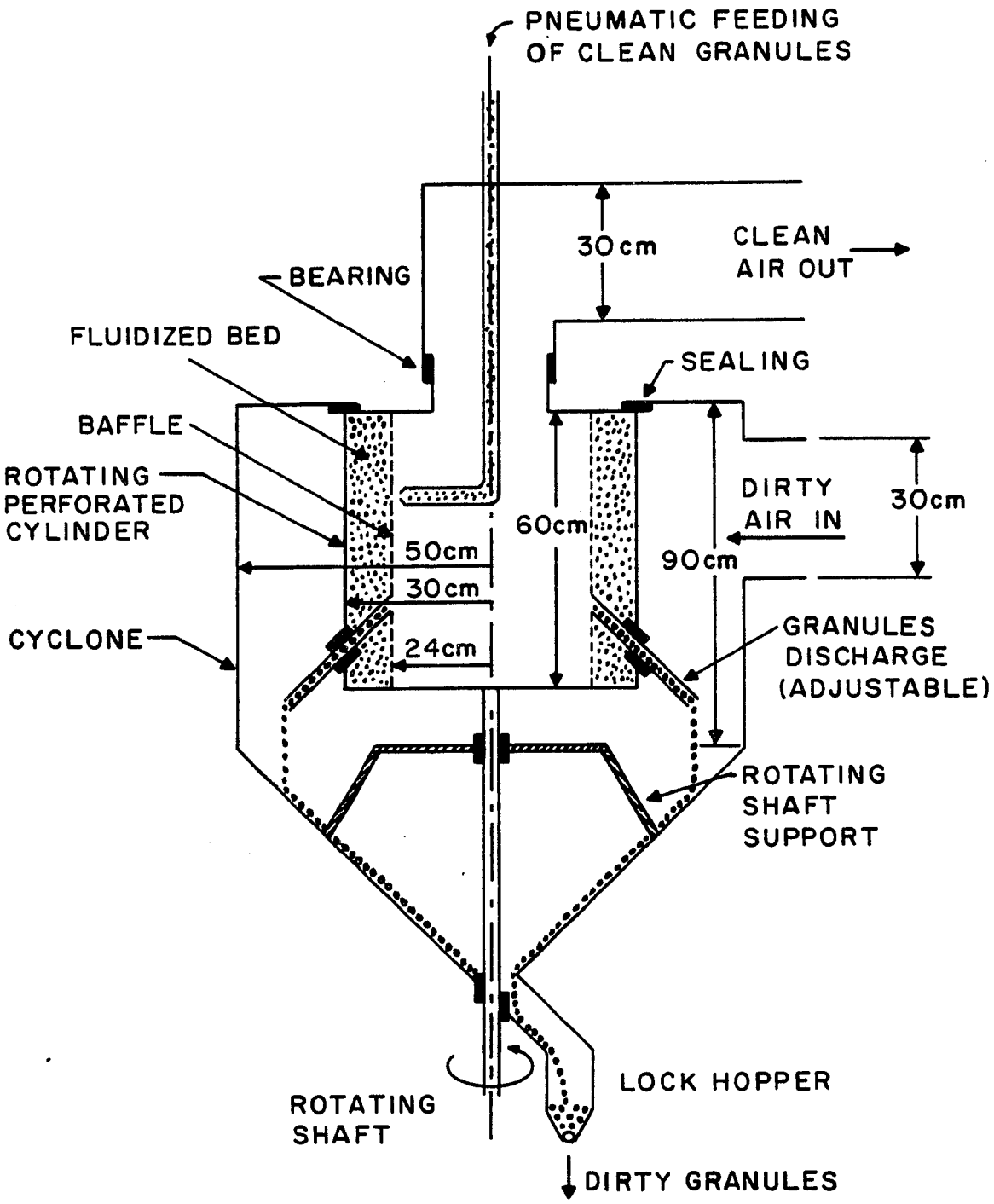

Figure 4.38: A design for a pilot size rotating fluidized bed filter. Side view.

The thickness of the bed should be adjustable with a maximum thickness of 6 cm. Based on the experiments performed, it is believed that such a bed will have efficiencies as high as 99.9% for all charged dust particles Ø.3 μm and larger.

The radius of the bed is chosen to be 3Ø cm according to the recomendations of Levy et al (1981). These authors found that at a radii ratio $r_i/r_Ø$ smaller than Ø.75 the radial velocity is not uniform and depends on the height of the bed height. At $r_i/r_Ø$=Ø.8 as suggested here the radial velocity, hence fluidization will be uniform.

4.8 Conclusions and Recomendations

The experimental rotating fluidized bed filter (RFBF) set-up is the first such device that has ever been tested, and as such has many design problems as discussed previously. The experience accumulated through the running of the device is important and is used as a base for the design of a new pilot size RFBF as suggested in section 4.6. In spite of many operational and design problems, the existing RFBF experimental set-up proved to be a very efficient filter device for micron and submicron particles with efficiencies of 99.9% for particles in the 1-2 μm range and 9Ø% for particles in the Ø.3-Ø.5 μm range. These high efficiencies were obtained in shallow (1.Ø cm) beds with

granules and particles naturally charged.

The high efficieny obtained in the RFBF is due mainly to inertia and electrostatic effects. The inertia effects are strong because of the high gas velocity (up to 300 cm/sec) which is used. These effects are stronger when the granule's diameter is small. Even at high velocity using small granules the inertia effects, which decrease as a function of the particle radius squared r_p^2, are not sufficient for collecting particles smaller than about 0.5μm. These particles are collected mainly due to the electrostatic effects. Granules in the RFBF are naturally charged by triboelectrification which is strong because of the intense fluidization. Dust particles are also charged by triboelectrification or may be charged by a corona charger. Coulombic forces between granules and particles in such a system are strong causing high collection efficiency for all submicron particles.

The efficiency of the RFBF may be increased significantly above the collection efficiency of the current system if deeper beds are used and if the dust particles are charged in a corona charger before entering the filter. With charged particles the RFBF works in a similar way as an electrostatic precipitator with the advantage of a large surface area for particle collection and significant inertia effects. The RFBF is worth further investigation and

it is recomended that a pilot size RFBF should be built as described in section 4.7 with the addition of a corona to charge aerosol particles. The RFBF should also be tested at high temperature (up to 500°C) with granules which are high temperature and corrosion resistent.

APPENDIX A

The Snyder and Stewart (1966) flow model including the computer programs used for the computation of the improved flow field

The flow field and pressure in dense cubic packing (Snyder 1965), is given by:

$$v_j = \sum_{i=1}^{N} C_{ji} \chi \phi_{ji} \qquad j=1,2,3 \qquad [1A]$$

$$P = (Z+\sqrt{2})/2\sqrt{2} + \sum_{i=1}^{N} C_{pi} \phi_{pi} \qquad [2A]$$

The function χ satisfies the no-slip condition on M neighboring spherical surfaces and is given by:

$$\chi = \prod_{k=1}^{M} \{1-[Q_k+0.0001(Q_k^2-1)^{16}]^{-1}\} \qquad [3A]$$

where Q_k is the distance of any point (x,y,z) in the void from the center of the k'th sphere given by:

$$Q_k=[(x-x_k)^2+(y-y_k)^2+(z-z_k)^2]^{1/2} \qquad [4A]$$

The value of Q_k is 1.0 on the surface of the k'th sphere and larger elsewhere in the void. Consequently χ is zero on the surface of the k'th sphere and larger in the void. In the

solution M=18 is used. Increasing M to 19 makes a difference of only 10^{-8} in the value of χ .

The functions χ , $\frac{\partial \chi}{\partial X_j}$, $\frac{\partial^2 \chi}{\partial X_j^2}$ j=1,2,3 are evaluated by Subroutine XXX.

The functions ϕ_{ji} and ϕ_{pi} are trigonometric functions satisfying the symmetry conditions and they are given by:

$$\phi_{zi}=\cos(a_i\pi X)\cos(b_i\pi Y)\cos(c_i\pi Z/\sqrt{2}) \quad [5A]$$

$$\phi_{xi}=\sin([a_i+1]\pi X)\cos(b_i\pi Y)\sin([c_i+1]\pi Z/\sqrt{2}) \quad [6A]$$

$$\phi_{yi}=\cos(a_i\pi X)\sin([b_i+1]\pi Y)\sin([c_i+1]\pi Z/\sqrt{2}) \quad [7A]$$

$$\phi_{pi}=\cos(a_i'\pi X)\cos(b_i'\pi Y)\sin([c_i'+1]\pi Z/\sqrt{2}) \quad [8A]$$

The indices $a_i,b_i,c_i,a_i',b_i',c_i'$ are positive integers which may be varied independently within the restrictions:

$$a_i+b_i+c_i = \text{an even number} \quad [9A]$$

$$a_i'+b_i'+c_i' = \text{an odd number} \quad [10A]$$

Equations [1A] and [2A] are used in the volumetric integral form of the continuity and momentum equations at Re=Ø. The equations have the form:

$$Cx_iF1_{ij}+\ Cy_iF2_{ij}+\ Cz_iF3_{ij} = Ø \quad [11A]$$

$$Cx_iF4_{ij} + Cp_iF7_{ij} = Ø \quad [12A]$$

$$Cy_iF5_{ij}+ Cp_iF8_{ij} = Ø \quad [13A]$$

$$Cz_i + Cp_iF9_{ij} = -\ F10_j \quad [14A]$$

where:

$$F1_{ij}=\int_V \frac{\partial \alpha \phi_{xi}}{\partial x} w_j' dV \qquad [15A]$$

$$F2_{ij}=\int_V \frac{\partial \alpha \phi_{yi}}{\partial y} w_j' dV \qquad [16A]$$

$$F3_{ij}=\int_V \frac{\partial \alpha \phi_{zi}}{\partial z} w_j' dV \qquad [17A]$$

$$F4_{ij}=\int_V \nabla^2(\alpha \phi_{xi}) w_j dV \qquad [18A]$$

$$F5_{ij}=\int_V \nabla^2(\alpha \phi_{yi}) w_j dV \qquad [19A]$$

$$F6_{ij}=\int_V \nabla^2(\alpha \phi_{zi}) w_j dV \qquad [20A]$$

$$F7ij=\int_V \frac{\partial \phi_{pi}}{\partial X} w_j dV \qquad [21A]$$

$$F8_{ij}=\int_V \frac{\partial \phi_{pi}}{\partial y} w_j dV \qquad [22A]$$

$$F9_{ij}=\int_V \frac{\partial \phi_{pi}}{\partial z} w_j dV \qquad [23A]$$

$$F10_{ij}=\int_V \frac{1}{2\sqrt{2}} w_j dV \qquad [24A]$$

and w_j and w_j' are weight functions given by:

$$w_j=\cos(a_j \pi X)\cos(b_j \pi Y)\cos(c_j \pi Z/\sqrt{2}) \qquad [25A]$$

$$w_j'=\cos(a_j'\pi X)\cos(b_j'\pi Y)\cos(c_j'\pi Z/\sqrt{2}) \qquad [26A]$$

In equations [5A-26A] i=1,2,....N and j=1,2,....N

The set of equations [11A-14A] is a set of 4N linear equations with 4N unknowns. From symmetry considerations $v_x(X,Y,Z)=v_y(Y,X,Z)$ which requires (see Snyder 1965) that an i^*th term in the trial function defined by:

$$a_i=b_i^*,\ b_i=a_i^*,\ c_i=c_i^*,\ a_i'=b_i'^*,\ b_i'=a_i'^*,\ c_i'=c_i'^* \qquad [27A]$$

exists such that:

$$Cx_i=Cy_i^* \qquad [28A]$$

The number of unknowns can therefor be reduced to 3N and the number o: reduced system that should be solved simultaneously is:

$$Cxi(F1_{ij}+F2^*_{ij})+\ Cz_iF3_{ij} = \emptyset \qquad [29A]$$

$$Cx_iF4_{ij} + Cp_iF7_{ij} = \emptyset \qquad [30A]$$

$$Cz_iF6_{ij}+\ Cp_iF9_{ij} = -\ F1\emptyset_j \qquad [31A]$$

$F1_{ij}$,$F2^*_{ij}$,$F3_{ij}$,$F4_{ij}$,$F6_{ij}$,$F7_{ij}$,$F9_{ij}$ and $F1\emptyset_j$ are evaluated by Subroutine PHE. The volumetric integral of equations [15A-24A] is calculated over 1/8 of the void volume contained in $\emptyset<X<1.\emptyset$, $\emptyset<Y<1.\emptyset$, $\emptyset<Z<\sqrt{2}$ using 2Øx2Øx2Ø Gausian points. For i=j=68 Subroutine XXX and the inner loop in

Subroutine PHE should run approximately 3.7×10^7 times. Once all the F's are evaluated the linear system

$$\begin{bmatrix} F1_{ij}+F2^{*}_{ij} & F3_{ij} & \emptyset \\ F4_{ij} & \emptyset & F7_{ij} \\ \emptyset & F6_{ij} & F9_{ij} \end{bmatrix} \begin{bmatrix} Cx_i \\ Cz_i \\ Cp_i \end{bmatrix} = \begin{bmatrix} \emptyset \\ \emptyset \\ -F10_j \end{bmatrix} \qquad [32A]$$

$i=1,2,\ldots N \qquad j=1,2,\ldots N$

is solved for the 3N unknowns Cx_i, Cz_i, Cp_i using Subroutine Gausel from Villadsen and Michelsen (1978). Cy_i is evaluated using equation [28A]. These constants are used in Subroutine VEL (see appendix B) to evaluate the flow field given by equation [1].

The computer program given below is the one used for the computation of the matrix F of equation (32A) the program contains the subroutines PHE that calculates the F's values as given in equations (15A-24A) and subroutine XXX that evaluate the value of the functions $\mathcal{C}$, $\frac{\partial \mathcal{C}}{\partial X_j}$, $\frac{\partial^2 \mathcal{C}}{\partial X_j^2}$.

Computer program for the evaluation of the F matrix

```
IMPLICIT REAL*8(A-H,O-Z)
READ N M
DO 1 J=1,N
```

```
      DO 2 I=1,N
      CALL PHE(I,J,F1,F3,F4,F6,F7,F9,F1Ø)
      WRITE(6,1Ø) F1,F3,F4,F6
   1Ø FORMAT(4F19.16)
      WRITE(6,12) F7,F9,F1Ø
   12 FORMAT(3F19.16)
    2 CONTINUE
    1 CONTINUE
      STOP
      END

      SUBROUTINE PHE(I,J,F1,F3,F4,F6,F7,F9,F1Ø)
      IMPLICIT REAL*8(A-H,O-Z)
      DIMENSION A(86),B(86),C(86),AP(86),BP(86),CP(86)
      READ A,B,C,AP,BP,CP
      T=3.1415927DØ
      R=1.4142135624DØ
      M=2Ø
      MM=M/2
      BB=M
      DX=1.ØDØ/BB
      DZ=R/BB
      Z=Ø.ØDØ
      DO 3 I1=1,MM
      Y=Ø.ØDØ
      DO 4 I2=1,M
      X=Ø.ØDØ
      DO 5 I3=1,M
      RR1=X**2+Y**2+Z**2
      RR2=(X-1.ØDØ)**2+(Y-1.ØDØ)**2+(Z-R)**2
      IF(RR1.LE.1.ØØØ1DØ) GOTO 6
      IF(RR2.LE.1.ØØØ1DØ) GOTO 6
      CALL XXX(X,Y,Z,CH,DXX1,DXY1,DXZ1,DXX2,DXY2,DXZ2)
      T1=T*X
      T2=T*Y
      T3=T*Z/R
```

```
 T4=T*T
 E1=DCOS(A(I)*T1)
 E2=DCOS(B(I)*T2)
 E3=DCOS(C(I)*T3)
 E11=DCOS(A(J)*T1)
 E12=DCOS(B(J)*T2)
 E13=DCOS(C(J)*T3)
 E4=DSIN((A(I)+1.ØDØ)*T1)
 E5=DSIN((B(I)+1.ØDØ)*T2)
 E6=DSIN((C(I)+1.ØDØ)*T3)
 E7=DCOS(AP(I)*T1)
 E71=DCOS(AP(J)*T1)
 E8=DCOS(BP(I)*T2)
 E81=DCOS(BP(J)*T2)
 E9=DCOS(CP(J)*T3)
 E1Ø=DSIN((CP(I)+1.ØDØ)*T3)
 EZPJ=E71*E81*E9*DX*DX*DZ
 EZJ=E11*E12*E13*DX*DX*DZ
 EX=E4*E2*E6
 EY=DCOS(B(I)*T1)*DSIN((A(I)+1.ØDØ)*T2)*E6
 EZ=E1*E2*E3
 EP=E7*E8*E1Ø
 EXX=(A(I)+1.ØDØ)*T*DCOS((A(I)+1.ØDØ)*T1)*E2*E6
 EZX=-A(I)*T*DSIN(A(I)*T1)*E2*E3
 EPX=-AP(I)*T*DSIN(AP(I)*T1)*E8*E1Ø
 EXY=-B(I)*T*DSIN(B(I)*T2)*E4*E6
 EYY=(A(I)+1.ØDØ)*T*DCOS((A(I)+1.ØDØ)*T2)*E6
@*DCOS(B(I)*T1)
 EZY=-B(I)*T*DSIN(B(I)*T2)*E1*E3
 EXZ=(C(I)+1.ØDØ)*T/R*DCOS((C(I)+1.ØDØ)*T3)*E4*E2
 EZZ=-C(I)*T/R*DSIN(C(I)*T3)*E1*E2
 EPZ=(CP(I)+1.ØDØ)*T/R*DCOS((CP(I)+1.ØDØ)*T3)
@*E7*E8
 EXXX=-(A(I)+1.ØDØ)**2*T4*EX
 EZXX=-A(I)**2*T4*EZ
 EXYY=-B(I)**2*T4*EX
```

```
      EZYY=-B(I)**2*T4*EZ
      EXZZ=-(C(I)+1.ØDØ)**2*T4/2.ØDØ*EX
      EZZZ=-C(I)**2*T4/2.ØDØ*EZ
      F1=F1+(CH*(EXX+EYY)+DXX1*EX+DXY1*EY)*EZPJ
      F3=F3+(CH*EZZ+DXZ1*EZ)*EZPJ
      F4=F4+(2.ØDØ*(EXX*DXX1+EXY*DXY1+EXZ*DXZ1)+EX*(DXX2+
     @DXY2+DXZ2)+CH*(EXXX+EXYY+EXZZ))*EZJ
      F6=F6+(2.ØDØ*(EZX*DXX1+EZY*DXY1+EZZ*DXZ1)+EZ*(DXX2+
     @DXY2+DXZ2)+CH*(EZXX+EZYY+EZZZ))*EZJ
      F7=F7+EPX*EZJ
      F9=F9+EPZ*EZJ
      F1Ø=Ø.3535533DØ*EZJ+F1Ø
    6 X=X+DX
    5 CONTINUE
      Y=Y+DX
    4 CONTINUE
      Z=Z+DZ
    3 CONTINUE
      RETURN
      END

      SUBROUTINE XXX(X,Y,Z,CH,DXX1,DXY1,DXZ1,DXX2,DXY2,DXZ2)
      IMPLICIT REAL*8(A-H,O-Z)
      DIMENSION XX(18),YY(18),ZZ(18)
      READ XX,YY,ZZ
      CH=1.Ø
      DO 1Ø I=1,18
      SX=X-XX(I)
      SY=Y-YY(I)
      SZ=Z-ZZ(I)
      SQ=SX*SX+SY*SY+SZ*SZ
      BR=SQ**Ø.5+Ø.ØØ1*(SQ-1.Ø)**16
      G=1.Ø-1.Ø/BR
      PAR=1/SQ**Ø.5+Ø.Ø32*(SQ-1.Ø)**15
      PARM=-1.ØDØ/SQ**1.5+Ø.96*(SQ-1.ØDØ)**14
      C1=PAR/G/BR/BR
```

```
      C2=C1*PARM/PAR
      C3=C1**2*(2.ØDØ*BR-1.ØDØ)
      DU=SX*C1
      DW=SY*C1
      DS=SZ*C1
      DXU=DU+DXU
      DXW=DW+DXW
      DXS=DS+DXS
      DXUA=C1+C2*SX**2-C3*SX**2
      DXWA=C1+C2*SY**2-C3*SY**2
      DXSA=C1+C2*SZ**2-C3*SZ**2
      DXUB=DXUB+DXUA
      DXWB=DXWB+DXWA
      DXSB=DXSB+DXSA
      CH=CH*G
   1Ø CONTINUE
      DXX1=DXU*CH
      DXY1=DXW*CH
      DXZ1=DXS*CH
      DXX2=CH*DXU**2+CH*DXUB
      DXY2=CH*DXW**2+CH*DXWB
      DXZ2=CH*DXS**2+CH*DXSB
      RETURN
      END
```

Appendix B

Computer program for the solution of the trajectory equation in a dense cubic bed

The trajectory equation in the dense packed bed is given by equation 3.18 with the initial conditions given by equations 3.18a and 3.18b

$$\frac{d^2\vec{X}}{dT^2} = \frac{1}{St'}\left(\vec{U} - \frac{d\vec{X}}{dT}\right) \qquad (3.18)$$

$$\vec{X}(T=\emptyset) = (X_\emptyset, Y_\emptyset, -\sqrt{2}) \qquad (3.18a)$$

$$d\vec{X}/dT(T=\emptyset) = \vec{U} \qquad (3.18b)$$

The vectorial equation (3.18) is solved as a three dimensional system where the unknown are the X,Y,Z location vectors of a particle for any given time T. The system is solved using subroutine STIFF3 (Villadsen and Michelsen, 1978). The velocity profile $\vec{U}$ in equation (3.18) is computed in subroutine VEL. The main program and the subroutines STIFF3 and VEL are given below.

Main program and the subroutines used for the solution of equation (3.18)

```
      IMPLICIT REAL*8(A-H,O-Z)
      DIMENSION XTAB(1ØØ),IP(3Ø),Y(3Ø),YOLD(3Ø),YOLD1(3Ø),
     @YA(3Ø),F(3Ø),FOLD(3Ø),YK1(3Ø),YK2(3Ø),DF(3Ø,3Ø),
     @DFOLD(3Ø,3Ø),W(3Ø),YK3(3Ø),
```

```
  @CX(68),CY(68),CZ(68)
   COMMON /STOCK/ST
   COMMON /XYZ/CX,CY,CZ
   EXTERNAL FUN,DFUN,OUT
   DO 12 I=1,68
   READ(5,11) CX(I),CY(I),CZ(I)
11 FORMAT(3F18.10)
12 CONTINUE
   ST=0.020D0
   WRITE(6,71) ST
71 FORMAT('  STOCK NUMBER =',1F10.5)
   RP=0.0001D0
   CON=68.0D0
   WRITE(6,72) RP
   WRITE(6,73) CON
72 FORMAT('    RP =',1F10.5)
73 FORMAT(' CONSTANTS=',1F10.5)
   NCOM=6
   IF(ST.LT.0.001D0) NCOM=3
   NTAB=60
   NPRINT=60
   DYY=0.01D0
   DXA=0.01D0
   XA=0.53D0
   DO 101 KJ=1,1
   YB=0.0D0
   XA=XA+DXA
   DO 100 KI=1,1
   YB=YB+DYY
   A1=0.0D0
   DO 30 I=1,NCOM
   W(I)=1.0D0
30 CONTINUE
   WRITE(6,74)
74 FORMAT('******************************')
   RAD=(1.0D0-XA)**2+(1.0D0-YB)**2
```

```
      IF(RAD.LE.1.ØDØ) GOTO 1Ø1
      XTAB(1)=Ø.ØDØ
      DO 1Ø3 I=2,NTAB
1Ø3   XTAB(I)=XTAB(I-1)+Ø.5ØDØ
      Y(1)=XA
      Y(2)=YB
      Y(3)=-2.ØDØ**Ø.5
      CALL VEL(1.ØDØ,Y(1),Y(2),Y(3),VX,VY,VZ,DVXX,DVXY,
     @DVXZ,DVYX,DVYY,DVYZ,DVZX,DVZY,DVZZ)
      Y(4)=VX
      Y(5)=VY
      Y(6)=VZ
      EPS=1.ØD-3
      XST=Ø.ØDØ
      HØ=1.ØD-3
      IF(EPS.EQ.Ø.DØ)GOTO 1ØØ
 51   X1=XST
      DO 5Ø I=1,NTAB
      X2=XTAB(I)
      CALL STIFF3(NCOM,3Ø,NPRINT,FUN,DFUN,OUT,X1,X2,HØ,
     @EPS,W,Y,YOLD,YOLD1,IP,YA,YK1,YK2,YK3,DF,DFOLD,F,
     @FOLD)
      IF(Y(7).EQ.1.ØDØ) GOTO 1Ø4
 5Ø   X1=X2
1Ø4   IF((Y(8).EQ.1.ØDØ).OR.(Y(9).EQ.1.ØDØ)) GOTO 1ØØ
      IF(Y(12).EQ.1.ØDØ) Y(3)=Y(3)-2.8284271248DØ
      A1=A1+Y(12)
      WRITE(6,62) A1
 62   FORMAT(1F1Ø.5)
      IF(A1.GE.4.ØDØ) GOTO 1ØØ
      GOTO 51
1ØØ   CONTINUE
1Ø1   CONTINUE
      STOP
      END
```

```
      SUBROUTINE STIFF3(N,ND,NPRINT,FUN,DFUN,OUT,XØ,X1,
     @HØ,EPS,W,Y,YOLD,YOLD1,IP,YA,YK1,YK2,YK3,DF,DFOLD,
     @F,FOLD)
      IMPLICIT REAL*8(A-H,O-Z)
      DIMENSION IP(ND),Y(ND),YOLD(ND),YOLD1(ND),YA(ND),
     @YK1(ND),YK2(ND),YK3(ND),W(ND),F(ND),FOLD(ND),
     @DF(ND,ND),DFOLD(ND,ND)
      COMMON/STOCK/ST
      ICON=Ø
      NOUT=Ø
      X=XØ
      H=HØ
      IF(XØ+2.*H.LT.X1) GOTO 1
    2 H=(X1-X)/2
      ICON=1
    1 IF(ICON.EQ.Ø.AND.X+4*H.GT.X1) H=(X1-X)/4
      CALL FUN(Y,F,ST)
      IF(Y(7).EQ.1.ØDØ) GOTO 188
      CALL DFUN(Y,DF,ST)
      IHA=-1
      DO 3Ø I=1,N
      YOLD(I)=Y(I)
      FOLD(I)=F(I)
      DO 3Ø J=1,N
   3Ø DFOLD(I,J)=DF(I,J)
   37 CALL SIRK3(N,ND,FUN,IP,F,Y,YK1,YK2,YK3,DF,2*H)
      IF(Y(7).EQ.1.ØDØ) GOTO 188
      DO 35 I=1,N
      YA(I)=Y(I)
      Y(I)=YOLD(I)
      F(I)=FOLD(I)
      DO 35 J=1,N
   35 DF(I,J)=DFOLD(I,J)
   38 IHA=IHA+1
      CALL SIRK3(N,ND,FUN,IP,F,Y,YK1,YK2,YK3,DF,H)
      CALL FUN(Y,F,ST)
```

```
      CALL DFUN(Y,DF,ST)
      DO 4Ø I=1,N
   4Ø YOLD1(I)=Y(I)
      CALL SIRK3(N,ND,FUN,IP,F,Y,YK1,YK2,YK3,DF,H)
      IF(Y(7).EQ.1.ØDØ) GOTO 188
      E=Ø.
      DO 41 I=1,N
      ES=W(I)*DABS(YA(I)-Y(I))/(1.+DABS(Y(I)))
      IF(ES.GT.E) E=ES
   41 CONTINUE
      Q=E/EPS
      QA=(4.*Q)**.25
      IF(Q.LE.1.) GOTO 48
      DO 45 I=1,N
      YA(I)=YOLD1(I)
      F(I)=FOLD(I)
      Y(I)=YOLD(I)
      DO 45 J=1,N
   45 DF(I,J)=DFOLD(I,J)
      H=H/2
      ICON=Ø
      GOTO 38
   48 DO 49 I=1,N
   49 Y(I)=Y(I)+(Y(I)-YA(I))/7.ØDØ
      X=X+2*H
      QA=1./(QA+1.D-1Ø)
      IF(QA.GT.3.) QA=3.
      H=QA*H
      NOUT=NOUT+1
      IF((NOUT/NPRINT)*NPRINT.EQ.NOUT.OR.ICON.EQ.1) CALL
     @OUT(X,Y)
      IF(ICON.EQ.1) GOTO 187
      HØ=H
      IF(X+2.*H.LT.X1) GOTO 1
      GOTO 2
  187 RETURN
```

```
188 CALL OUT(X,Y)
    RETURN
    END

    SUBROUTINE BACK(ND,N,IPIV,A,V)
    IMPLICIT REAL*8(A-H,O-Z)
    DIMENSION IPIV(ND),A(ND,ND),V(ND)
    N1=N-1
    DO 1Ø I=1,N1
    I1=I+1
    K=IPIV(I)
    IF(K.EQ.I) GOTO 11
    X=V(I)
    V(I)=V(K)
    V(K)=X
 11 DO 1Ø J=I1,N
 1Ø V(J)=V(J)+A(J,I)*V(I)
    V(N)=V(N)/A(N,N)
    DO 15 II=2,N
    I=N+1-II
    I1=I+1
    DO 16 J=I1,N
 16 V(I)=V(I)-A(I,J)*V(J)
 15 V(I)=V(I)/A(I,I)
    RETURN
    END

    SUBROUTINE LU (ND,N,IPIV,A)
    IMPLICIT REAL*8(A-H,O-Z)
    DIMENSION IPIV(ND),A(ND,ND)
    IPIV(N)=N
    N1=N-1
    DO 1Ø I=1,N1
    X=A(I,I)
    IF(X.LT.Ø.) X=-X
    IPIV(I)=I
```

```
      II=I+1
      DO 11 J=II,N
      Y=A(I,J)
      IF(Y.LT.Ø.) Y=-Y
      IF(Y.LE.X) GOTO 11
      X=Y
      IPIV(I)=J
   11 CONTINUE
      IF(IPIV(I).EQ.I) GOTO 14
      K=IPIV(I)
      DO 12 J=I,N
      X=A(I,J)
      A(I,J)=A(K,J)
   12 A(K,J)=X
   14 DO 1Ø J=II,N
      X=-A(J,I)/A(I,I)
      A(J,I)=X
      DO 1Ø K=II,N
   1Ø A(J,K)=A(J,K)+X*A(I,K)
      RETURN
      END

      SUBROUTINE SIRK3 (N,ND,FUN,IPIV,F,Y,YK1,YK2,YK3,
     @DF,H)
      IMPLICIT REAL*8(A-H,O-Z)
      DIMENSION F(ND),Y(ND),YK1(ND),YK2(ND),YK3(ND),
     @IPIV(ND),DF(ND,ND),R(4)
      COMMON/STOCK/ST
      DATA A,R/.4358665215Ø84589DØ,1.Ø376Ø9496131859DØ,
     @.8349Ø4838526377DØ,-.63Ø2Ø2Ø887244523DØ,
     @-.2423378912ØØ452DØ/
      DO 5 I=1,N
      DO 6 J=1,N
      DF(I,J)=-H*A*DF(I,J)
      IF(DABS(DF(I,J)).LT.1.D-12) DF(I,J)=Ø.
    6 CONTINUE
```

```
 5 DF(I,I)=DF(I,I)+1.
   CALL LU(ND,N,IPIV,DF)
   CALL BACK(ND,N,IPIV,DF,F)
   DO 8 I=1,N
   YK1(I)=H*F(I)
 8 YK2(I)=Y(I)+.75DØ*YK1(I)
   CALL FUN(YK2,F,ST)
   IF(Y(7).EQ.1.ØDØ) GOTO 17
   CALL BACK(ND,N,IPIV,DF,F)
   DO 9 I=1,N
   YK2(I)=H*F(I)
   Y(I)=Y(I)+R(1)*YK1(I)+R(2)*YK2(I)
 9 YK2(I)=R(3)*YK1(I)+R(4)*YK2(I)
   CALL BACK(ND,N,IPIV,DF,YK2)
   DO 1Ø I=1,N
1Ø Y(I)=Y(I)+YK2(I)
17 RETURN
   END

   SUBROUTINE FUN(Y,F,ST)
   IMPLICIT REAL*8(A-H,O-Z)
   DIMENSION Y(3Ø),F(3Ø)
   Y(7)=Ø.ØDØ
   CALL VEL(1.ØDØ,Y(1),Y(2),Y(3),VX,VY,VZ,DVXX,DVXY,DVXZ,
  @DVYX,DVYY,DVYZ,DVZX,DVZY,DVZZ)
   IF(VZ.EQ.Ø.ØDØ) GOTO 1Ø
   IF(ST.LT.Ø.ØØ1DØ) GOTO 11
   F(4)=(VX-Y(4))/ST
   F(5)=(VY-Y(5))/ST
   F(6)=(VZ-Y(6))/ST
   F(1)=Y(4)
   F(2)=Y(5)
   F(3)=Y(6)
   RETURN
1Ø Y(7)=1.ØDØ
   RETURN
```

```
11 F(1)=VX
   F(2)=VY
   F(3)=VZ
   RETURN
   END

   SUBROUTINE DFUN(Y,DF,ST)
   IMPLICIT REAL*8(A-H,O-Z)
   DIMENSION Y(3Ø),DF(3Ø,3Ø)
   CALL VEL(Ø.ØDØ,Y(1),Y(2),Y(3),VX,VY,VZ,DVXX,DVXY,
  @DVXZ,DVYX,DVYY,DVYZ,DVZX,DVZY,DVZZ)
   IF(ST.LT.Ø.ØØ1DØ) GOTO 12
   DO 1Ø I=1,6
   DO 11 J=1,6
   DF(I,J)=Ø.ØDØ
11 CONTINUE
   DF(I,I)=1.ØDØ
1Ø CONTINUE
   DF(4,1)=DVXX/ST
   DF(4,2)=DVXY/ST
   DF(4,3)=DVXZ/ST
   DF(4,4)=-1.ØDØ/ST
   DF(5,1)=DVYX/ST
   DF(5,2)=DVYY/ST
   DF(5,3)=DVYZ/ST
   DF(5,5)=-1.ØDØ/ST
   DF(6,1)=DVZX/ST
   DF(6,2)=DVZY/ST
   DF(6,3)=DVZZ/ST
   DF(6,6)=-1.ØDØ/ST
   DF(1,4)=1.ØDØ
   DF(2,5)=1.ØDØ
   DF(3,6)=1.ØDØ
   RETURN
12 DF(1,1)=DVXX
   DF(1,2)=DVXY
```

```
      DF(1,3)=DVXZ
      DF(2,1)=DVYX
      DF(2,2)=DVYY
      DF(2,3)=DVYZ
      DF(3,1)=DVZX
      DF(3,2)=DVZY
      DF(3,3)=DVZZ
      RETURN
      END

      SUBROUTINE OUT(X,Y)
      IMPLICIT REAL*8(A-H,O-Z)
      DIMENSION Y(3Ø)
      CALL VEL(1.ØDØ,Y(1),Y(2),Y(3),VX,VY,VZ,DVXX,DVXY,DVXZ,
     @DVYX,DVYY,DVYZ,DVZX,DVZY,DVZZ)
      U=DABS(Y(1))
      V=DABS(Y(2))
      W=DABS(Y(3))
      RR1=(U**2+V**2+W**2)**Ø.5DØ
      RR2=((U-1.ØDØ)**2+(V-1.ØDØ)**2+
     @(W-1.4142135624DØ)**2)**Ø.5DØ
      WRITE(6,5) X,Y(1),Y(2),Y(3),VX,VY,VZ,RR1,RR2
    5 FORMAT(1X,9F1Ø.6)
      IF((U.GE.1.ØDØ).OR.(V.GE.1.ØDØ).OR.(Y(3).GE.
     @1.414213DØ)) GOTO 6
      IF(RR1.LT.1.ØØ1DØ) GOTO 6
      IF(RR2.LT.1.ØØ1DØ) GOTO 6
      IF(VZ.LE.Ø.ØDØ) GOTO 6
      RETURN
    6 Y(8)=Ø.ØDØ
      Y(9)=Ø.ØDØ
      Y(12)=Ø.ØDØ
      Y(7)=1.ØDØ
      IF(RR1.LT.1.ØØ1DØ) Y(8)=1.ØDØ
      IF(VZ.LT.ø.ØDØ) Y(8)=1.ØDØ
      IF(RR2.LT.1.ØØ1DØ) Y(9)=1.ØDØ
```

```
 IF(Y(1).GT.1.ØDØ) Y(1)=Y(1)-2.ØDØ
 IF(Y(1).LT.-1.ØDØ) Y(1)=Y(1)+2.ØDØ
 IF(Y(2).GT.1.ØDØ) Y(2)=Y(2)-2.ØDØ
 IF(Y(2).LT.-1.ØDØ) Y(2)=Y(2)+2.ØDØ
 IF(Y(3).GE.+1.414213DØ) Y(12)=1.ØDØ
 RETURN
 END

 SUBROUTINE VEL(BB,X,Y,Z,VX,VY,VZ,DVXX,DVXY,DVXZ,
@DVYX,DVYY,DVYZ,DVZX,DVZY,DVZZ)
 IMPLICIT REAL*8(A-H,O-Z)
 DIMENSION A(68),B(68),C(68),CX(68),CY(68),CZ(68)
 COMMON /XYZ/CX,CY,CZ
 READ A,B,C
 T=3.1415927DØ
 R=1.4142135624DØ
 R8=R+Ø.ØØØØ1DØ
 VØ=Ø.ØØØ258DØ
 DA=1.ØDØ
 DB=1.ØDØ
 DC=1.ØDØ
 IF(X.LT.Ø.ØDØ) DA=-1.ØDØ
 IF(Y.LT.Ø.ØDØ) DB=-1.ØDØ
 IF(Z.LT.Ø.ØDØ) DC=-1.ØDØ
 U=X
 V=Y
 W=Z
 X=DABS(X)
 Y=DABS(Y)
 Z=DABS(Z)
 RR1=(X**2+Y**2+Z**2)**Ø.5DØ
 RR2=((X-1.ØDØ)**2+(Y-1.ØDØ)**2+(Z-R)**2)**Ø.5DØ
 IF(RR1.LE.1.ØØØ1DØ) GOTO 6
 IF(RR2.LE.1.ØØØ1DØ) GOTO 6
 IF((X.GT.1.ØDØ).OR.(Y.GT.1.ØDØ).OR.(Z.GT.R8))
@ GOTO 6
```

```
      CALL XXX(BB,X,Y,Z,CH,DXX1,DXY1,DXZ1,DXX2,DXY2,DXZ2)
      DO 8Ø I=1,68
      E1=DCOS(A(I)*T*X)
      E2=DCOS(B(I)*T*Y)
      E3=DCOS(C(I)*T*Z/R)
      E4=DSIN((A(I)+1.ØDØ)*T*X)
      E5=DSIN((B(I)+1.ØDØ)*T*Y)
      E6=DSIN((C(I)+1.ØDØ)*T*Z/R)
      EX=E4*E2*E6
      EY=E1*E5*E6
      EZ=E1*E2*E3
      VX=VX+CX(I)*CH*EX
      VY=VY+CY(I)*CH*EY
      VZ=VZ+CZ(I)*CH*EZ
      IF(BB.EQ.1.ØDØ) GOTO 8Ø
      EXX=(A(I)+1.ØDØ)*T*DCOS((A(I)+1.ØDØ)*T*X)*E2*E6
      EYX=-A(I)*T*DSIN(A(I)*T*X)*E5*E6
      EZX=-A(I)*T*DSIN(A(I)*T*X)*E2*E3
      EXY=-B(I)*T*DSIN(B(I)*T*Y)*E4*E6
      EYY=(B(I)+1.ØDØ)*T*DCOS((B(I)+1.ØDØ)*T*Y)*E1*E6
      EZY=-B(I)*T*DSIN(B(I)*T*Y)*E1*E3
      EXZ=(C(I)+1.ØDØ)*T/R*DCOS((C(I)+1.ØDØ)*T*Z/R)*E4*E2
      EYZ=(C(I)+1.ØDØ)*T/R*DCOS((C(I)+1.ØDØ)*T*Z/R)*E5*E1
      EZZ=-C(I)*T/R*DSIN(C(I)*T*Z/R)*E1*E2
      DVXX=DVXX+CX(I)*(EX*DXX1+CH*EXX)
      DVXY=DVXY+CX(I)*(EX*DXY1+CH*EXY)
      DVXZ=DVXZ+CX(I)*(EX*DXZ1+CH*EXZ)
      DVYX=DVYX+CY(I)*(EY*DXX1+CH*EYX)
      DVYY=DVYY+CY(I)*(EY*DXY1+CH*EYY)
      DVYZ=DVYZ+CY(I)*(EY*DXZ1+CH*EYZ)
      DVZX=DVZX+CZ(I)*(EZ*DXX1+CH*EZX)
      DVZY=DVZY+CZ(I)*(EZ*DXY1+CH*EZY)
      DVZZ=DVZZ+CZ(I)*(EZ*DXZ1+CH*EZZ)
8Ø    CONTINUE
      X=U
      Y=V
```

```
      Z=W
      VX=VX*DA*DC/VØ
      VY=VY*DB*DC/VØ
      VZ=VZ/VØ
      IF(BB.EQ.1.ØDØ) GOTO 7
      DVXX=DVXX*DC/VØ
      DVXY=DVXY*DA*DB*DC/VØ
      DVXZ=DVXZ*DA/VØ
      DVYX=DVYX*DA*DB*DC/VØ
      DVYY=DVYY*DC/VØ
      DVYZ=DVYZ*DB/VØ
      DVZX=DVZX*DA/VØ
      DVZY=DVZY*DB/VØ
      DVZZ=DVZZ*DC/VØ
    7 RETURN
    6 X=U
      Y=V
      Z=W
      RETURN
      END
      SUBROUTINE
XXX(BB,X,Y,Z,CH,DXX1,DXY1,DXZ1,DXX2,DXY2,DXZ2)
      IMPLICIT REAL*8(A-H,O-Z)
      DIMENSION XX(18),YY(18),ZZ(18)
      READ XX,YY,ZZ
      CH=1.Ø
      DO 1Ø I=1,18
      SX=X-XX(I)
      SY=Y-YY(I)
      SZ=Z-ZZ(I)
      SQ=SX*SX+SY*SY+SZ*SZ
      BR=SQ**Ø.5+Ø.ØØ1*(SQ-1.Ø)**16
      G=1.Ø-1.Ø/BR
      CH=CH*G
      IF(BB.EQ.1.ØDØ) GOTO 1Ø
      PAR=1/SQ**Ø.5+Ø.Ø32*(SQ-1.Ø)**15
```

```
      PARM=-1.ØDØ/SQ**1.5+Ø.96*(SQ-1.ØDØ)**14
      C1=PAR/G/BR/BR
      C2=C1*PARM/PAR
      C3=C1**2*(2.ØDØ*BR-1.ØDØ)
      DU=SX*C1
      DW=SY*C1
      DS=SZ*C1
      DXU=DU+DXU
      DXW=DW+DXW
      DXS=DS+DXS
      DXUA=C1+C2*SX**2-C3*SX**2
      DXWA=C1+C2*SY**2-C3*SY**2
      DXSA=C1+C2*SZ**2-C3*SZ**2
      DXUB=DXUB+DXUA
      DXWB=DXWB+DXWA
      DXSB=DXSB+DXSA
   1Ø CONTINUE
      IF(BB.EQ.1.ØDØ) GOTO 7
      DXX1=DXU*CH
      DXY1=DXW*CH
      DXZ1=DXS*CH
      DXX2=CH*DXU**2+CH*DXUB
      DXY2=CH*DXW**2+CH*DXWB
      DXZ2=CH*DXS**2+CH*DXSB
    7 RETURN
      END
```

Appendix C

Computer programs for data collecrtion and analysis in the RFBF experiments and sample result

The following two programs are written in Basic and they are used by the Digital Mincll microcomputer for data collection and analysis. The data is stored on a disc as file #1.

The command CIN receives the signal from the Climet 21Ø multi channel monitor. The vector received contains 32Ø characters for the number of particles in 16 channels where each channel represents the size range of dust particles given in table C.1.

The input and output concentration of dust in the air is given by Channels 1-8 and 9-16 respectively.

The command RECIEVE receives volt signals representing electrostatic charge in the Faraday cage. The signals are coming at a rate of 21Ø signals/minute. The reading may increase or decrease according to the charge entering the Faraday cage.

Table C.1: Size range of dust particles

Channel number	Dust particle diameter μm
1,9	Ø.3-Ø.5
2,1Ø	Ø.5-Ø.8
3,11	Ø.8-1.Ø
4,12	1.Ø-2.Ø
5,13	2.Ø-3.Ø
6,14	3.Ø-5.Ø
7,15	5.Ø-1Ø.Ø
8,16	>1Ø

```
PRINT 'NUMBER OF CLIMET RUNS',\INPUT N
PRINT 'NUMBER OF CHARGE READINGS',\INPUT N1
PRINT 'AIR FLOW RATE',\INPUT Q
PRINT 'ROTATING SPEED',\INPUT R
PRINT 'PRESSURE DROP',\INPUT P
PRINT 'RELATIVE HUMIDITY',\INPUT H
PRINT 'TYPE  OF AEROSOL',\INPUT G1$
PRINT 'FILE NAME',\INPUT D$
PRINT D$
OPEN D$ FOR OUTPUT AS FILE #1
PRINT #1,N
PRINT #1,N1
PRINT #1,Q
PRINT #1,R
PRINT #1,P
```

```
  PRINT #1,L
  PRINT #1,H
  PRINT #1,D$
  IF N=Ø THAN GOTO 1
  J=Ø
3 CIN('RETRIEVE',S$,172)
  S$=SEG$(S$,31,17Ø)
  J=J+1
  PRINT #1,S$
  CIN('RETRIEVE',S$,144)
  T$=SEG$(T$,1,14Ø)
  PRINT #1,T$
  IF J=N THEN GOTO 2
  GOTO 3
2 IF N1=Ø THEN GOTO 4
1 I=1
5 RECEIVE(V$,1,1)
  RECEIVE(A$,,1,2Ø3)
  A$=SEG$(A$,1,LEN(A$)-2)
  A=VAL(A$)
  PRINT #1,A
  IF I>N1 THEN GOTO 4
  I=I+1
  GOTO 5
4 CLOSE #1
  END
```

The program above collect the data and the program below analyzes the results. The Climet readings with the experimental conditions are used for evaluating the filtration efficiency, the Stokes number and the modified Stokes number. The electrostatic charge distribution is also analyzed. Each two consequtive readings are compared. When the difference is larger than the level of noise in the system (the level noise depends on humidity) the difference is count as the charge on the incoming granule. The number

of counts is compared with the number of granules in the Faraday cage and the difference does not exceed 5%.

```
510 LINPUT #1,U1$
520 J=J+1
530 PRINT J
540 LINPUT #1,T$
550 LINPUT #1,W$
560 LINPUT #1,W1$
570 PRINT
580 A(1)=VAL(SEG$(S$,7,11)&'E'&SEG$(S$,12,12))
590 A(2)=VAL(SEG$(S$,24,28)&'E'&SEG$(S$,29,29))
600 A(3)=VAL(SEG$(S$,41,45)&'E'&SEG$(S$,46,46))
610 A(4)=VAL(SEG$(S$,58,62)&'E'&SEG$(S$,63,63))
620 A(5)=VAL(SEG$(U$,7,11)&'E'&SEG$(U$,12,12))
630 A(6)=VAL(SEG$(U$,24,28)&'E'&SEG$(U$,29,29))
640 A(7)=VAL(SEG$(U$,41,45)&'E'&SEG$(U$,46,46))
650 A(8)=VAL(SEG$(U$,58,62)&'E'&SEG$(U$,63,63))
660 A(9)=VAL(SEG$(T$,7,11)&'E'&SEG$(T$,12,12))
670 A(10)=VAL(SEG$(T$,24,28)&'E'&SEG$(T$,29,29))
680 A(11)=VAL(SEG$(T$,41,45)&'E'&SEG$(T$,46,46))
690 A(12)=VAL(SEG$(T$,58,62)&'E'&SEG$(T$,63,63))
700 A(13)=VAL(SEG$(W$,7,11)&'E'&SEG$(W$,12,12))
710 A(14)=VAL(SEG$(W$,24,28)&'E'&SEG$(W$,29,29))
720 A(15)=VAL(SEG$(W$,41,45)&'E'&SEG$(W$,46,46))
730 A(16)=VAL(SEG$(W$,58,62)&'E'&SEG$(W$,63,63))
740 FOR K=1 TO 8
750 B(K)=B(K)+A(K)
760 B(K+8)=B(K+8)+A(K+8)
770 NEXT K
780 PRINT 'FILTRATION EFFICIENCY'
790 PRINT 'SIZE','INPUT','OUTPUT','EFFICIENCY'
800 FOR I=1 TO 7
810 IF A(I)=0 GO TO 830
820 S=1-A(I)/A(I+8)
830 PRINT E1(I),A(I+8),A(I),S
840 NEXT I
850 PRINT
860 GO TO 470
870 PRINT
875 IF N=0 THEN  GO TO 965
880 PRINT 'AVERAGE EFFICIENCY'
890 PRINT 'SIZE','INPUT','OUTPUT','EFFICIENCY'
900 FOR I=1 TO 7
910 B(I)=B(I)/J
920 B(I+8)=B(I+8)/J
930 IF B(I)=0 THEN  GO TO 950
940 S=1-B(I)/B(I+8)
950 PRINT E1(I),B(I+8),B(I),S
960 NEXT I
965 IF N1=0 THEN  GO TO 1225
970 OPEN 'SY1:OREN.DAT' FOR OUTPUT AS FILE #2
980 DIM #2,D(2000)
990 K=0
1000 I=0
```

```
10 DIM A(16),B(16),E1(8),C1(8)
20 E1(1)=.4
30 E1(2)=.65
40 E1(3)=.9
50 E1(4)=1.5
60 E1(5)=2.5
70 E1(6)=4
80 E1(7)=7.5
90 PRINT 'FILE NAME' \ INPUT X$
100 C1(1)=1.45
110 C1(2)=1.25
120 C1(3)=1.15
130 C1(4)=1.1
140 C1(5)=1.06
150 C1(6)=1.03
160 C1(7)=1
170 Y$='SY1:'&X$
180 OPEN Y$ FOR INPUT AS FILE #1
190 J=0
200 INPUT #1,X
210 INPUT #1,N
220 INPUT #1,N1
230 IF X=0 GO TO 460
240 INPUT #1,Q
250 INPUT #1,R
260 INPUT #1,P
270 INPUT #1,L
280 INPUT #1,H
290 V=Q*30.4^3/60/3.14/20/12
300 PRINT 'AIR FLOW RATE FT3/MIN',Q
310 PRINT 'AIR VELOCITY CM/SEC',V
320 R1=.3*V/.15
330 PRINT 'GRANULE RE NUMBER',R1
340 PRINT 'ROTATING SPEED RPM',R
350 PRINT 'PRESSURE DROP',,P
360 PRINT 'BED THICKNESS CM',L
370 PRINT 'RELATIVE HUMIDITY %',H
380 INPUT #1,G1$
390 PRINT 'TYPE OF AEROSOL',G1$
400 PRINT
410 PRINT 'PARTICLE SIZE',,'ST NUMBER'
420 FOR I=1 TO 7
430 S5=2.058/100000*C1(I)*V*E1(I)^2
440 PRINT E1(I),,S5
450 NEXT I
460 M=0
470 IF M=N GO TO 870
480 M=M+1
490 LINPUT #1,S$
500 LINPUT #1,U$
```

```
1010 INPUT #1,B1
1020 IF END #1 GO TO 1220
1030 IF I>N1 THEN  GO TO 1220
1040 INPUT #1,B
1050 I=I+1
1060 C=B-B1
1070 B1=B
1080 IF ABS(C)<.02 THEN  GO TO 1020
1090 IF ABS(C)>1.1 THEN  GO TO 1020
1100 K=K+1
1110 D(K)=C
1120 IF K=1 THEN  GO TO 1020
1130 FOR M=K TO 2 STEP -1
1140 IF C<=D(M-1) GO TO 1200
1150 D(M)=D(M-1)
1160 NEXT M
1170 M=M+1
1180 D(M-1)=C
1190 GO TO 1020
1200 D(M)=C
1205 PRINT I,D(M)
1210 GO TO 1020
1220 CLOSE #1
1225 IF N1=0 THEN  GO TO 1410
1230 P=0
1240 N=0
1250 FOR I=1 TO K
1260 IF D(I)>0 THEN P=P+D(I)
1270 IF D(I)>0 THEN P1=P1+1
1280 IF D(I)<0 THEN N=N+D(I)
1290 IF D(I)<0 THEN N2=N2+1
1300 PRINT D(I),P1,P,N2,N
1310 NEXT I
1320 PRINT 'SUM OF POSITIVE CHARGE 10-9C',P
1330 PRINT 'NUMBER OF POSITIVE PARTICLES',P1
1340 PRINT 'SUM OF NEGATIVE CHARGE 10-9C',N
1350 PRINT 'NUMBER OF NEGATIVE PARTICLES',N2
1360 PRINT 'AVERAGE POSITIVE CHARGE',P/P1
1370 PRINT 'AVERAGE NEGATIVE CHARGE',N/N2
1380 V=(P+N)/(P1+N2)
1390 PRINT 'NET AVERAGE CHARGE',V
1400 CLOSE #2
1410 END
```

SY1:STY31

AIR FLOW RATE FT3/MIN	17Ø
AIR VELOCITY CM/SEC	1Ø2
GRANULE RE NUMBER	52
ROTATING SPEED RPM	6ØØ
PRESSURE DROP	6
BED THICKNESS CM	1
RELATIVE HUMIDITY 5	1
TYPE OF AEROSOL	SOLID

PARTICLE SIZE	ST NUMBER	MODIFIED ST
.4	4.62E-4	8.41E-4
.65	1.Ø7E-3	1.94E-3
.9	1.87E-3	3.39E-3
1.5	5.Ø1E-3	9.1ØE-3
2.5	1.35E-2	2.45E-2
4	3.35E-2	6.Ø8E-2
7.5	1.14E-1	2.Ø7E-1

FILTRATION EFFICIENCY

SIZE	INPUT	OUTPUT	EFFICIENCY
.4	1Ø45ØØ	36Ø8Ø	.654737
.65	61190	5524	.9Ø9724
.9	57990	1328	.977Ø99
1.5	62Ø3Ø	196	.99684
2.5	7Ø98	14	.998Ø28
4	757	9	.988111
7.5	2Ø	2	.9

FILTRATION EFFICIENCY

SIZE	INPUT	OUTPUT	EFFICIENCY
.4	99310	24190	.756419
.65	51000	3369	.933941
.9	43140	862	.980019
1.5	40730	94	.997692
2.5	4510	13	.997118
4	646	10	.98452
7.5	65	1	.984615

FILTRATION EFFICIENCY

SIZE	INPUT	OUTPUT	EFFICIENCY
.4	89010	15160	.829682
.65	35680	1973	.944703
.9	24990	456	.981753
1.5	20020	62	.996903
2.5	3031	13	.995711
4	649	2	.996918
7.5	17	1	.941176

FILTRATION EFFICIENCY

SIZE	INPUT	OUTPUR	EFFICIENCY
.4	76330	11930	.843705
.65	27870	1485	.946717
.9	19290	360	.981337
1.5	16130	62	.996156
2.5	3299	14	.995756
4	782	3	.996164
7.5	24	2	.916667

FILTRATION EFFICIENCY

SIZE	INPUT	OUTPUT	EFFICIENCY
.4	63440	8555	.865148
.65	21800	1094	.949817
.9	15010	300	.980013
1.5	14500	79	.994552
2.5	3751	8	.997867
4	1003	7	.993021
7.5	30	1	.966667

AVERAGE EFFICIENCY

SIZE	INPUT	OUTPUT	EFFICIENCY
.4	86518	19183	.778277
.65	39508	2689	.931938
.9	32084	661.2	.979392
1.5	30682	98.6	.996786
2.5	4337.8	12.4	.997141
4	767.4	6.2	.991921
7.5	31.2	1.4	.955128

REFERENCES

Amdure M. and Corn M., Am. Ind. Hy. Assoc. J. 24, 326 (1963).

Balusubramanian M. et al, Cana. J. of Che. Eng. 56, 298 (1978).

Beal K.S., J. Aerosol Sci. 9, 455 (1978).

Black G.H. and Boubel R.W., IEC Proc. Dsign Dev. 8, 573 (1969).

Chao B.T., J. Heat Transfer, Trans. ASME, 91, 273, (1969).

Ciboroski J. and Wlodarsky A., Chem. Eng. Sci., 17, 23 (1962).

Clift R. and Thambimuthu K.V., Paper Presented at "Symp. on Removal of Fine Particulates from Gas Streams" IChE, London (1976).

Clift R., Ghadiri M. and Thambimuthu K.V., Filtration of gases in fluidized beds. In 'Progress in filtration and separation', Vol. 2, p 75-123,ed. R.J. Wakeman, Elsvier , Amsterdam.

Clift R. 'fundamental processes in gas filtration' The inst of eng. Australia p 181-191. (1984).

Colberg D.R. and Liu Y.A. Paper No. 36d AIChE ann. Meeting Los Angeles, CA. Nov. (1982).

Cookson J.T., Environ. Sci. Tech., 17, 348 (1970).

Coury J.R., 'Electrostatic effects in granular bed filtration of gases' Ph.D. Diss. Univ of Cambridge (1983).

Degani D.D. and Tardos I.G., APCA J. 31, 9, 981 Sep. (1981).

Dietz P.W., J. Aerosol Sci. 12, 27 (1981).

Doganoglu Y. and Clift R., Ann. Meet. of Can. Soc. of Ch.E., Ottawa, Can. (1974).

Doganoglu, Y. Jog, V., Thambimuthu K.V., and Clift R., Trans. IChemE., 56, 293, (1978)

Doganoglu Y. PhD Thesis, McGill univ. Montreal (1975).

Dorman R.G., in 'Aerodynamic capture of particles' ed. E.G. Richardson, Pergamon, London p 112-122 (1960).

D'Ottavio T. and Goren S., Aerosol Sci. and Tech. 2, 91 (1983).

EFB, Inc. 'Electrified Bed Particulate Control System Test' Final Report, Jan (1979).

Fan K.C. and Gentry J.W., Ind. Eng. Chem. Fundam., 18, 4, 3Ø6 (1979).

Fedkiew P. and Newman J., AIChE J. 23, 255 (1977).

Gal E., Tardos G.I. and Pfeffer R. Proc. to World Filtration Congress III, Downingtown, Pa. Sept. (1982).

George H.F. and Poehlein G.W., Envi. Sci. & Tech. 8, 46 Jan. (1974).

Goren S. Paper presented at the "Symp. on the Transfer and Utilization of Particulate Control Technology." Denver 24-28 July (1978).

Geffken J. et al, Paper presented at the 1st Int. Symp. on Particle Tech. Denver (1978).

Gutfinger C. et al, Proceeding of the 5th Confference on Fluidized Beds Combustion, Washington D.C. Dec. 1Ø-12 (1977).

Gutfinger C. and Tardos G.I., Atmos. Envi. 13, 553 (1979).

Happel J., AIChE J., 4, 197, (1958).

Havlick V., Int. J. Air Water Pollut. 4, 225, (1961).

Ishii T. and Johnson A.I., Can. J. Chem. Eng. 48. 56. (197Ø).

Jackson M., AIChE Symp. Ser., 141, 82, (1974).

Jackson S. and Calvert S., AIChE J. 12, 6, 1Ø75, (1966).

Johnson T.W. and Melcher J.R., Ind. Eng. Chem. Fund., 14, 146, (1975).

Kalen B. and Zenz F.A., Chem. Eng. Prog. 69, 5, 67, (1973).

Kallio G.A. and Dietz P.W. in 'Gas borne particles' pp 1Ø1-11Ø Instn. Mech. Engrs. London (1981).

Kirsh A.A., J. Aerosol Sci., 3, 25 (1972).

Knetting P. and Beekman J. M., Canad. J. Chem. Eng. 52, 7Ø3 (Dec. 1974).

Krupp-Kopper, British Patent 1921684 (1974).

Kuabara S., J. Phys. Soc. Japan, 14, 527, (1959).

Kunii D. and Levenspiel O., Fluidization Engineering, Wiley, New York (1969).

Lamb H., Hydrodynamics, 6th ed., Cambridge Univ. Press, Cambridge (1932).

Lee K. W. and Gieseke J. A., Envi. Sci. & Tech. 13, 4, 466 (Apr. 1979).

Lee K.C., Ph.D. Dissertation, City University of N.Y.,(1975).

Levich V.G. Physiochemical Hydrodynamics, Prentice-Hall Englwood Cliffs, NJ (1962).

Levy E.K. and Chen J.C., Paper presented at Int. Powder and Bulk Solid Handling and Proceesing Conf., Rosmont Il. (1977).

Levy E.K. et al, Fluidization, J. Davidson and D.L. Kearins, Editores Cambridge Univesity Press (1978).

Levy E.k, Shakespeare W.J., Tabatabaie A. R. and Chen J.C., in AIChe Sym. Ser., 77, 205, (1981)

Lindauer G.C. et al, BNL 5ØØ13 (T-435), (1966).

Mahar H. and Zimmerman N. Mitre Corp. interim report. EPA cont. 68-Ø2-1859 (1975).

Martin J.J., McCabe W.L. and Monrad C.C., Chem. Eng. Prog. 47, 2, 91 (Feb. 1951).

McCarthy D. et al, Ind. Eng. Chem., Process Des. Dev., 15, 2, 266, (1976).

McElroy M.W. et al, Science 215, 4528, 13 (Jan. 1981).

Meisen A. and Mathur K.B., Inst. Chem. Engrs. Symp. Ser. 38 Paper K3, (1974).

Metcalf C. I. and Howard J. R., App. Energy 3, 65 (1977).

Meltcher J.R. et al, Final Report to eseer Corp. 89, (1978).

Neal G.H. and Nader W.K., AIChE J. 2Ø, 3, 53Ø (1974).

Niera A.M. and Payatakes A.C. AIChE J. 24, 1, 43 (1978).

Nielsen K.A. and Hill J.C., I&EC Fund. 15, 149, (1976).

Paretsky L. C., "Filtration of Aerosol by Granular Beds" Ph.D. Dissertation, The City Univ. Of N.Y., N.Y. (1972).

Paretsky L.C. et al J., Air Poll. Cont. Ass., 21 2Ø4 (1971).

Patterson, R. G. and Jackson M. L., AIChE Symp. Ser.161, 73, 64 (1977).

Payatakes A.C., Tien C. and Turian R.M., AIChE J. 19, 1, 58 (1973).

Payatakes A.C., Tien C. and Turian R.M., AIChE J. 20, 5, 889 (1974).

Pendse H. and Tien C., AIChE J. 28, 4, 677 (1982).

Petersen E. E., AIChE J. 4, 3, 343 (1958).

Pfeffer R., Tardos G.I. and Piesman L., I&EC Fundamentals 20, 2, 168, (1981).

Pilat M.J. and Perm A., Atmos. Envi. 10, 13 (1976).

Rajagopalan R. and Tien C., AIChE J. 22, 523 (1976).

Rajagopalan R. and Tien C,. "The Theory of Deep Bed Filtration pp. 179-269 in Progress in Filtration and Seperation" Vol, 1, Wakeman, R. J. (Ed.), Elsevier, Amsterdam, (1979).

Rajagopalan R. et al, AIChE J. 28, 5, 871, (1982).

Rosensweig R.E., Siegel J.H., Lee W.K. and Mikus T. AIChE 72nd Annual Meeting, San Francisco, CA, Nov. (1979).

Sangani A.S. and Acrivos A., Int. J. Multipase Flow 8, 4 343 (1982).

Schmidt et al, APCA J. 28, 2, 143 (Feb. 1978).

Scott D. S. and Guthrie D. A., Canad. J. of Chem. Eng. p 200 (Oct. 1959).

Shapiro M., Laufer G. and Gutfinger C., Atms. Envi. 17,3, (1983).

Snaddon R. W. L. and Dietz P. W., General Electric Internal Report no. 80CRD290 Dec. (1980).

Snaddon R.W.L, G.E. Internal rep. 124-833-81 (1981).

Snyder L. J., "An Analytical Study of Transport Processes in Packed Beds" Ph.D. Dissertation, Univ. of Wisconsin (1965).

Snyder L. J. and Stewart W. E. AIChE J. 12, 1, 167 (1966).

Sorensen J.P. and Stewart W.E., Chem. Eng. Sci. 29, 819 (1974).

Spielman L.A. and FitzPatrick J.A., J. Coll. Interface Sci., 42, 607, (1973).

Squire A.M. Pfeffer R., JAPCA, 20, 534, (1970).

Stairmand G.J., The Chemical Engineer, (Dec. 1965).

Tam C.K.W., J. Fluid Mech., 38, 537 (1969).

Tardos G.I. and Pfeffer R., Prceeddings, Second World Filtration Congress 239, London (1979).

Tardos G.I. et al, Israel J. Tech., 12, 184 (1974).

Tardos G.I. et al, JAPCA , 28, 4, 354, (1978).

Tardos G.I., "The Granular Bed Filter - Theory and Experiments" Ph.D. Dissertation, Technion-Israel Institute of Technology (1977).

Tardos G.I. et al, J. Colloid. Interface Sci., 71, 616 (1979).

Tardos G.I. and Pfefer R., AIChE J. 26, 4, 698, (198Ø).

Tardos G.I. et al, Atmos. Environ. 1Ø, 389 (1976).

Tardos G.I. and Pfeffer R., Chem. Eng. Commun. 4, 665 (198Ø).

Tardos G.I., Snaddon R.W.L. and Dietz P.W. 'Electrical Charge Measurements on Fine Airborne Particles' General Electric internal Rep. (1982).

Tardos G.I. and Snaddon R.W.L. 'Separation of charged Aerosol in Granular Beds With Imposed Electric Field' General Electric internal Rep. (1982).

Tardos G.I., Pfeffer R., Peters M. and Sweeney T. I&EC Fundamentals, 22,445, (1983).

Thumbimuthu K.V., Dogaanoglu Y., Farrokhalaee T.,and Clift R., Symposium of Deposition and Filtration of Particles from Gases and Liquids, Society of Chemical Industry, London, 1Ø7 (1978)

Thomas J.W. and Woodfin E.J., A.I.E.E.J. 78, 276 (1959).

Tien C. and Payatakes A. C., AIChE J. 25, 5, 739 (1979).

Tien C. in privat letter (1984).

Villadsen J. and Michelsen M. L., Solution of differential equation models by polynomial Approximation, Prentice-Hall, Inc Englewood Cliffs, NJ (1978).

Venhateson M. and Rajagopalan R., AIChE J. 26, 694 (198Ø).

Walkenhorst W., J. Aerosol Sci., 1, 225 (197Ø).

Zehedi K. and Melcher J.R., JAPCA 26, 345 (1976).

Zehedi K. and Melcher J.R., Annual Meeting, APCA, Boston Mass., Paper 75-57.8 (1975).

Zenz F.A. and Krockta L., Brit. Chem. Eng. and Proc. Tech. 17, 224 (1972).

Zick A.A. and Homsy G.M., J. Fluid Mech. 115, 13 (1982).